Investigating biomechanical determinants of endothelial permeability in a hollow fibre bioreactor

Department of Bioengineering,
Imperial College London

Stephen Gerard Gray

A thesis submitted in fulfilment of the requirements for the degrees of: Doctor of Philosophy & Diploma of Imperial College

Declaration

I, Stephen Gerard Gray declare that this thesis and the research to which it refers is a product of my own work. The experimental research for this thesis was carried out between May 2011 and January 2016, under the supervision of Professor Peter Weinberg in the Department of Bioengineering at Imperial College London. Information derived from other sources and work carried out with the assistance of others has been appropriately cited and acknowledged.

Acknowledgements

"Life should not be a journey to the grave with the intention of arriving safely in a pretty and well-preserved body, but rather to skid in broadside in a cloud of smoke, thoroughly used up, totally worn out, and loudly proclaiming "Wow! What a Ride!" — *Hunter S. Thompson, The Proud Highway: Saga of a Desperate Southern Gentleman, 1955-1967- Seen beside the door of Professor Roger Kamm's office at MIT.*

"It had long since come to my attention that people of accomplishment rarely sat back and let things happen to them. They went out and happened to things."– *Leonardo Da Vinci*

"Many of life's failures are people who did not realize how close they were to success when they gave up."– *Thomas A. Edison*

"It is impossible to escape the impression that people commonly use false standards of measurement — that they seek power, success and wealth for themselves and admire them in others, & that they underestimate what is of true value in life."– *Sigmund Freud*

"Your time is limited, so don't waste it living someone else's life. Don't be trapped by dogma – which is living with the results of other people's thinking."– *Steve Jobs*

"Only true champions come out and show their worth after defeat- and I expect us to do that." - Sir Alex Ferguson

**It isn't the mountains ahead to climb that wear you out; it's the pebble in your shoe."
"Braggin' is when a person says something and can't do it. I do what I say." "Impossible is just a big word thrown around by small men who find it easier to live in the world they've been given than to explore the power they have to change it. Impossible is not a fact. It's an opinion. Impossible is not a declaration. It's a dare. Impossible is potential. Impossible is temporary. Impossible is nothing."**- Muhammad Ali

"Imagination was given to man to compensate him for what he is not, and a sense of humour was provided to console him for what he is."– *Oscar Wilde*

To hell with circumstances; I create opportunities. Having no limitation as limitation. If you love life, don't waste time, for time is what life is made up of."- *Bruce Lee*

"I think perhaps education doesn't do us much good unless it is mixed with sweat."-
Barak Obama from the book Dreams From My Father. It is also my father Gerard Gray's view on academia and life from leaving school as a teenager to lecturing on electrical engineering. A lot of the quotes came from parents inspiration when I was a child.

"In order to write about life first you must live it."– *Ernest Hemingway*

Abstract

The effect of haemodynamic stresses on endothelial permeability to macromolecules is important to normal physiology and in the pathogenesis of atherosclerosis. I developed and applied novel methods to evaluate effects on such transport of acute or chronic exposure to flow along and across cultured endothelium. Porcine aortic endothelial cells were isolated and cultured at passage 1-3 within the porous capillaries of a FiberCell bioreactor. At confluence they were exposed to acute (4 h) or chronic (3-10 day) steady or pulsatile luminal flow (mean shear 3.75 dyne/cm^2), with or without transendothelial flow (4 x 10^7 cm/s). Permeability to rhodamine-labelled albumin was assessed by fluorimetry. Confluence of monolayers was confirmed by confocal and scanning electron microscopy and by demonstrating established effects of vasoactive agents on permeability: 10 U/ml thrombin increased permeability, as did 500 μM N$^\omega$-nitro-L-arginine methyl ester, compared to controls. Permeability was increased by acute pulsatile shear and decreased by chronic pulsatile shear compared to static controls. A decrease in PECAM-1 expression under chronic pulsatile flow was demonstrated by flow cytometry. Steady flow gave higher permeability than pulsatile flow. The introduction of transendothelial flow increased apparent permeability more than could be explained by the addition of the convective transport itself. Preliminary studies suggested that albumin transport may partially be an active process and demonstrated the potential for engineered fibre walls that would allow effects of cyclic strain to be investigated. In conclusion, the hollow fibre bioreactor allowed endothelial permeability to be measured with or without exposure to luminal flow and transendothelial flow over 30 days, permitting the investigation of effects of mechanical stresses. Effects of shear stress varied with duration, pulsatility and direction relative to the endothelial surface.

Table of Contents

<u>List of Figures</u>

List of Tables

Chapter 1: Introduction and Background

1.1 Introduction

A striking feature of atherosclerosis is its non-uniform distribution within the arterial system, which implies the existence of powerful local risk factors. Much attention has consequently been paid to effects on endothelial cells of mechanical stresses, particularly haemodynamic wall shear stress, which can vary considerably from site to site. The effect of mechanical stresses on endothelial permeability to circulating lipoproteins is likely to be a key factor since (a) the earliest lesions are characterized by an accumulation of lipid, (b) sites of high permeability are prone to lesions, and (c) permeability can be flow dependent *in vivo* [1, 2]. The influence of mechanical stresses on permeability is also of relevance to normal physiology.

Unfortunately, mechanisms linking mechanical stress and endothelial permeability are difficult to study. The most reliable information comes from in vivo studies [2, 3] but there are practical limits to the measurement and manipulation of mechanical stress in vivo and costs are high. For this reason, many investigators use endothelial monolayers in 2-D culture (particularly Transwells) but only some of the relevant stresses can be applied and only for a limited duration. Thus, there is a need for improved in vitro systems that can be used rigorously to investigate relevant mechanisms.

The present study aimed to provide a reproducible system giving approximately physiological conditions that could assess the influence of pulsatile flow, pressure, stretch, and transendothelial flux of water on endothelial permeability, or could be modified to do so. The project developed novel three-dimensional cell culture methods based on modifications to the FiberCell Systems hollow fibre bioreactor. The developed

bioreactor was validated by examining established effects of pharmacological agents and was then used to examine the effects on endothelial cell permeability of: (i) acute and chronic axial flow; (ii) pulsatile and steady flow; (iii) axial flow combined with transmural flow and (iv) active transport. Furthermore, development and investigation of novel biomaterial fabrication techniques - including the use of methods such as polymerization, electrospinning, and 3D bioprinting - were explored for future studies along similar lines but with distensible substrates.

1.2 Background

1.2.1 Atherosclerosis

Cardiovascular disease (CVD) is the primary cause of death worldwide, with 17.1 million deaths recorded by the World Health Organization (WHO) in 2004. It is estimated that by 2030 the number of CVD-related deaths will rise to 23.6 million. The high and increasing prevalence of CVD-related deaths is due to a complex combination of genetic, environmental, population, and clinical factors [4, 5].

Atherosclerosis, the predominant underlying cause of cardiovascular diseases such as myocardial infarction and stroke [6, 7], is the result of a multifactorial process with complicated aetiology. It is a chronic, inflammatory vessel disorder. Inflammation is thought to be initiated following entrance and accumulation of cholesterol-rich lipoproteins into the wall of arteries. This facilitates the infiltration of monocytes that differentiate into macrophages, and which are then transformed into foam cells [6, 7]. The continued deposition of lipids and other materials in the presence of coronary risk factors results in a lesion raised above the intima.

These fibrous plaques or raised lesions lead to chronic occlusion of the lumen causing local ischemia [8]. In acute cases the lesions may increase in size and/or rupture, thus exposing the underlying collagen and lipid-rich necrotic debris to blood, which triggers thrombus formation within the vessel. Thrombus formation can completely occlude the artery at the site of rupture or smaller thrombi may break off and embolise

downstream, blocking smaller vessels; either case will precipitate acute vascular events[8].

Hyperlipidaemia has been investigated as a contributing factor to atherosclerosis since the studies carried out by Anitschkow and colleagues on cholesterol-rich diets in rabbits in 1913 [6, 9, 10]. Systemic risk factors such as obesity, hypertension, and smoking have also been strongly linked to the development of the disease. However, none of these factors can account for the highly localized atherosclerotic plaque formation in regions of curvature and branching of the arterial system. For example, in the human carotid bifurcation, lesions occur preferentially on the lateral walls rather than the flow divider [9].

Since 1971 the low wall shear stress (WSS) model established by Caro and colleagues[11] has become the accepted theory for localized atherosclerotic plaque formation. Briefly, plaque formation was found at sites on the arterial wall that were thought to have been exposed to low wall shear stress[11]. The emergence of this theory led to the belief that the systemic risk factors are responsible for the overall rate of disease development but the site specific distribution of the disease is due to local haemodynamics. Subsequent studies suggest the multidirectional nature of the flow is also importantO'Donnell Jr [9, 12]. Much attention has consequently been paid to the physiological and molecular effects on endothelial cells (EC) of mechanical stresses, particularly WSS, and their role in the pathogenesis of atherosclerosis. In the next sections I summarise relevant aspects of research on the endothelium, the influence on the endothelium of WSS, and the particular importance of endothelial permeability.

1.2.2 Shear stress and the Endothelium

The endothelium is an important regulator of vascular homeostasis, exerting a number of vasoprotective effects[13]. As the endothelium acts as a barrier at the interface between blood flow and the vascular wall, it transduces physical and biological stimuli into physiological responses[14]. Endothelial cells sense and integrate humoral and hemodynamic stimuli, which results in the secretion of molecules and mediator proteins [13, 15]. For example, the activation of these molecular pathways facilitates the anticoagulant, and fibrinolytic properties of ECs along with the inhibition of inflammatory responses, and vasodilatory effects [13, 15]

Endothelial dysfunction involves alteration of the normal homeostatic effects of the endothelium. This increases the permeability of the endothelium, alters regulation of vessel tone (e.g. due to reduction in NO production), and increases adhesiveness to leukocytes or platelets [16]. It is theorized that it is the endothelial dysfunction caused by effects of local shear stress that is responsible for the influence of shear on atherosclerosis [14, 17]. The effect of mechanical stresses on endothelial function and permeability to circulating lipoproteins is likely to be a key local risk factor since, as noted in the introduction, (a) the earliest lesions are characterized by an accumulation of lipid, (b) sites of high permeability are prone to lesions, and (c) permeability can be flow dependent in vivo [1, 2].

In the arterial system, endothelial cells are exposed to mechanical forces arising from the action of the heart on the blood. Cyclical stress acting normal to the endothelium due to blood pressure fluctuations, leading to circumferential stretch

(strain), and hemodynamic shear stress acting tangential to the wall as a result of frictional forces exerted by blood flow over the endothelial cell apical surface, are the main biomechanical influences [15, 18]. The pathologist Virchow first observed the influence of extracellular forces on the endothelium more than 150 years ago when he demonstrated how the morphology of the endothelium varied in correlation with the different types of blood flow [19]. His observation was the precursor of modern studies of the biomechanical forces to which the endothelium is exposed and how they modulate morphology, structure and function, including permeability and repair [19].

Haemodynamic wall shear stress is probably the more significant, based on its stimulation of vasoactive substances in the control of vascular tone, cell metabolism, cell morphology, arterial structure and remodeling, alteration of gene expression, and putative localization of atherosclerotic lesions [15, 18]. (Nevertheless, it should be emphasized that there are fewer studies on the influence of cyclical stretch and its role may therefore have been underestimated.) Expressed in dimensions of force per unit area (units of N/m^2 – i.e. Pascals – or $dyne/cm^2$), it is determined by the product of the viscosity and the near wall shear rate (velocity gradient); the latter depends in turn on the mean flow rate of the blood and the geometry of the vessel (including the distance of the measuring site from the entrance to the arterial system), amongst other factors [20, 21].

The Reynolds number (Re) determines whether fluid flow will be laminar or turbulent. It describes the ratio of inertial forces to viscous forces. If viscous forces dominate the behavior of the fluid, there will be no turbulence even at high flow rates in complex geometries because disturbances tend to be damped out. A sufficiently high

Reynolds number will indicate that the flow is turbulent, because inertia means that disturbances will propagate. More specifically, in long straight tubes laminar flow occurs where the Re value is below 2,000, and any Re value above this means that the flow is likely to be turbulent [21]. Flow in arteries of human subjects (and smaller mammals) is mainly subcritical, although turbulence can occur in the proximal aorta in some of the larger species during late systole since decelerating flow is less stable than accelerating flow[22]. Even at subcritical values of Re, flow recirculation, circumferential swirling, or flow separation along with other forms of reversed flow can occur, and flow can change direction during the cardiac cycle, if the geometry is complex (curved, tapered or branched) – in the biological literature such behavior is loosely termed disturbed laminar flow [20, 21].

In general, the flow near the wall of the tube will be slower than the centre. Indeed it is axiomatic that the fluid in contact with the wall has a velocity of zero; this is the "no-slip condition," and has been experimentally validated. When the flow is steady and laminar in a straight rigid tube then after a sufficient length – termed the entrance length – the distribution of velocities across the tube – termed the velocity profile – becomes parabolic. Such flow is called Poiseuille flow.

Poiseuille's law can be used to derive the endothelial shear stress (τ) value at the vessel wall under such conditions; it takes into consideration the fluid flow rate (Q), the radius (r) and the fluid viscosity (η) as follows [20]:

$$\tau = 2Q\eta/\pi r^3$$

Under *in vivo* conditions, the situation is more complex due to the complex geometry, pulsatility of flow, distensible vessel walls, and non-Newtonian

characteristics of blood. As noted above, haemodynamic wall shear stress is proportional to the viscosity of blood, and contrary to the situation in Newtonian fluids this tends to increase at low blood velocities due to an aggregation of cellular elements [20]. The direction and magnitude of the shear stress patterns is mainly determined by the pulsatile blood flow in combination with vessel geometry; distensible walls and non-Newtonian viscosity can be ignored to a first approximation. In arteries the wall shear stress magnitude is highly variable. According to reference 21, it ranges from 15 to 70 dynes/cm^2. However, the range of values varies depending on the species (increasing in animals of smaller size[23]) and location in the circulatory system, and lower levels of shear stress certainly occur, at least instantaneously, when forward movement of the blood ceases or at stagnation points, such as occur upstream of stenoses, in areas of vessel curvature, and at arterial bifurcations or branch points [21].

1.2.3 The effect of shear stress on endothelial signal transduction

Variation in the characteristics of blood flow, and consequent variation in the wall shear stress that is generated, has a direct impact on endothelial responses whether or not the region is at risk of developing atherosclerosis.

Most studies of these phenomena have been conducted *in vitro*. Such studies have analyzed the effects of acute or chronic shear stress. In the present work, the term chronic shear stress is used to described cultures that are continuously exposed to shear stress for days or weeks whereas acute shear stress is used to refer to the application of force for up to a few hours after being cultured under static conditions. Endothelial cells

are continuously exposed to chronic shear stress *in vivo*; they only experience acute shear stress in newly formed blood vessels, at areas of injured endothelium, or after a temporary occlusion in a blood vessel [20], so chronic exposure is preferred but rarely used. (Some researchers have argued, however, that acute application of shear stress is akin to situations where endothelium is exposed *in vivo* to shear stresses that are constantly changing in magnitude and/or direction and therefore has difficulty in adapting[24].)

The mechanical coupling of endothelial cells to shear stress is not entirely understood. Some of the first studies [25] involved the investigation of endothelial cell early responses to shear stress. They successfully demonstrated that the forces generated by blood flow are transmitted at regions where intracellular structures are connected to the extracellular environment. In particular, cell deformation occurs when stress is applied and distorts intracellular structures through the integrins that are connected to the cell cytoskeleton and to the extracellular matrix [20, 25]. The link between the mechanically induced signaling of stress at the luminal surface to the junctions and focal adhesions was demonstrated by live imaging of filament displacement [26, 27]. Muller and colleagues demonstrated that flow-induced vasodilatation could be halted with blocking antibodies or peptides that act on the intergrins, supporting their importance in endothelial cell responses to shear stress [19, 28].

As the endothelial cell contains interconnected cytoskeletal actin, myosin, intermediate filaments and microtubules, the physical deformation of the monolayer enables the transmission of the forces through each cellular structure. This suggests that

the coupling of force to biochemical signaling can occur simultaneously at multiple locations within each cell. The exertion of shear stress on the cell or entire endothelium can alter the mobility, separation or conformation of membrane and junctional proteins, have a direct effect on luminal ion channel activation, or cause deformation of caveolae, cleavage of membrane phospholipids, protein phosphorylation, and alteration of integrin dynamics, all of which lead to the activation of secondary cell signaling [27].

Other mechanisms are also possible. Indeed, it is highly unlikely that a single hemodynamic mechanosensor exists within the endothelium. A decentralized model for endothelial mechanotransduction proposes that the entire cell is an assembly of structural sites [27]. It accommodates experimental findings that demonstrate direct biochemical signaling occurring though initial luminal deformation of the glycocalyx as well as transduction of signals at subcellular areas that are distant from the apical surface of the endothelial cell [27]. It is now widely accepted that the glycocalyx functions as a fluid shear-stress sensor. It is a coat of proteoglycans, glycosaminoglycans and absorbed plasma proteins that projects 0.5 µm (or perhaps more) from the luminal surface of the endothelial plasma membrane [27, 29, 30].

Primary cilia are an additional structure that may have a role in mechnaotransduction as they are more prevalent in regions of disturbed flow or at sites of atherosclerotic lesions. A study by Iomini and colleagues demonstrated that exposing endothelium to steady shear stress *in vitro* resulted in the disassembly of cilia after 2 h [27, 31].

The vessel wall's ability to sense and transduce mechanical forces with numerous receptors, integrins, and extracellular matrix remains a key topic in mechanobiology[32]. The topic has become so large that a comprehensive review is not practicable here.

Figure 1 demonstrates the importance of endothelial surface receptors and nuclear sensors in the activation of several signalling pathways[32] . For example, the deformation of integrins in response to shear stress occurs through pathways that are modulated by Platelet Endothelial Cell Adhesion Molecule-1 PECAM-1; Vascular Endothelial cell (VE)-cadherin; and Vascular Endothelial Growth Factor receptor 2 (VEGF2) [32]. As the nuclear membrane is also subject to the distribution of forces acting on the endothelium it is possible that mechanotransduction has a direct role in the mechanical regulation of gene expression [27, 33].
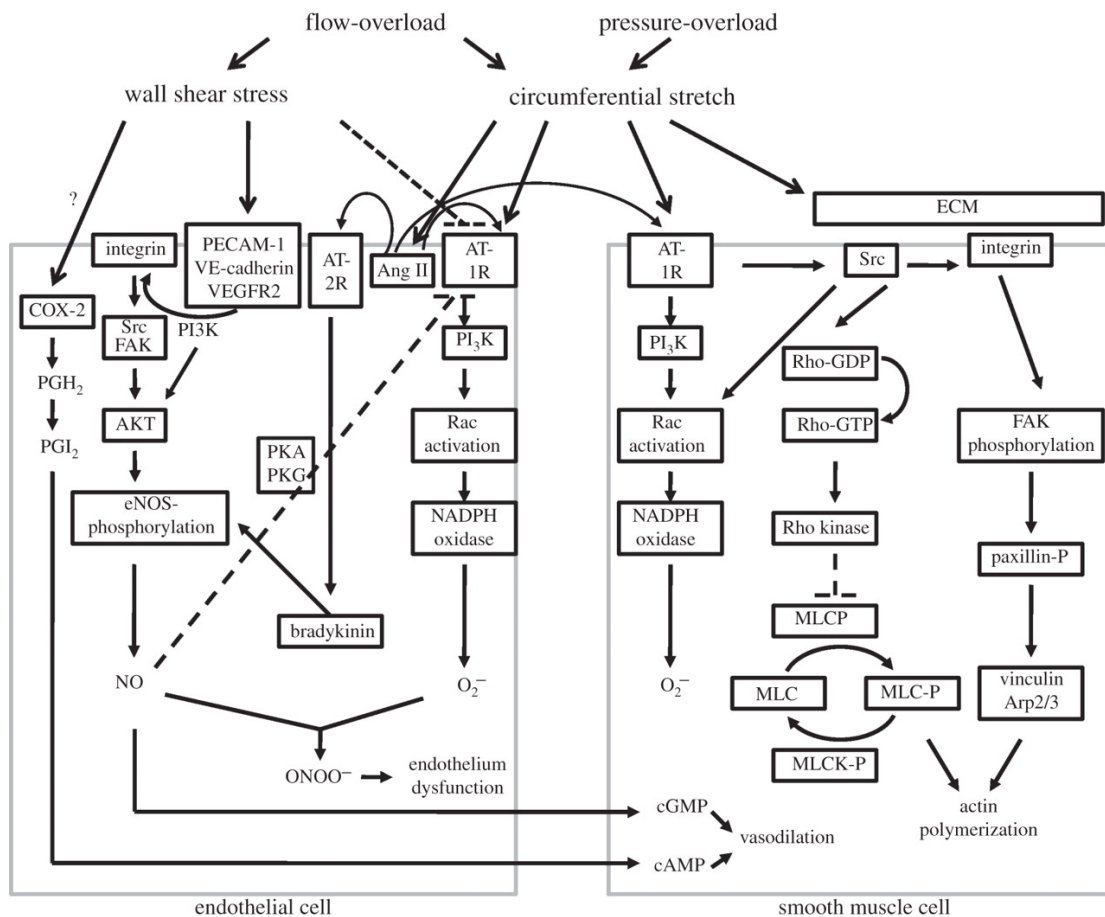
Figure 1 Biochemical pathways activated in response to flow, stretch, and pressure [32]

This figure demonstrates the importance of wall shear stress and stretch on activation of an array of biochemical pathways in both endothelial cells (EC) and vascular smooth muscle cells (VSMC). Solid arrows represent activation whereas dash marks indicate negative regulations or inhibitions.

1.2.4 The transport of macromolecules across the endothelial barrier

The transport of dissolved gases, ions, other solutes and fluid from the blood plasma to the interstitium of the subendothelial space of the arterial wall is controlled in part by the continuous endothelial monolayer. It is important to note that it is also dependent on the resistance of the whole wall to transmural flow and, under some circumstances, to transport in the concentration boundary layer in the fluid next to the wall; neither is considered further in this thesis. The main function of the endothelium is to act as a size selective, semi-permeable barrier with the ability to provide the essential nutrients across the arterial wall whilst regulating fluid homeostasis [34] and maintaining the oncotic pressure of plasma by holding back proteins such as albumin.

Permeability (P) is the rate of solute diffusion (Js) across unit surface area (S) of membrane per unit concentration difference across the endothelium (ΔC[35]) :

$$P = J_s/S\Delta C \qquad\qquad (1)$$

Although it is a convention in microcirculatory physiology that the term "permeability" refers only to the ease of this diffusional transport, in the engineering literature permeability can also refer to the ease of water flux: hydraulic permeability is the rate of flow under a unit hydraulic gradient through a unit cross-sectional area of the tissue. Because it is of importance in the transport of macromolecules via paracellular routes, the engineering convention is used in this thesis.

The magnitude of water flux is dependent on the net balance of Starling forces across the barrier (equation 2), and the overall flux of solutes is the sum of convective and diffusive components (equation 3).

$$Jv= (LpS)[(Pc - Pa)-\sigma(\Pi p - \Pi i)] \tag{2}$$

$$Js=Jv(1-\sigma)Cs + PS (\Delta C) \tag{3}$$

where Jv is the volume flux of fluid; Lp is hydraulic conductivity; Pc and Pi are luminal and interstitial fluid hydrostatic pressures; Πp and Πi are colloid osmotic pressures of plasma and interstitium, σ is the reflection coefficient, and Cs is the mean concentration of the solute within the cleft formed at the junction between endothelial cells in a monolayer [36]. Colloid osmotic pressure is the osmotic pressure exerted by proteins, notably albumin.

Because of the convective component, movement across the endothelium can be considered in part an ultrafiltration process across a semipermeable barrier. The endothelial monolayer transports lipid-insoluble solutes with a range of molecular radii (M_r) from 0.1nm (sodium ion) to 23nm (immunoglobulin IgM, and LDL) and some larger molecules such as VLDL. The endothelium behaves like a molecular sieve for solutes up to about the size of albumin but the transport of large macromolecules is less dependent on size and therefore requires an alternative pathway.

Two main pathways are thought to be responsible for the flux of fluid and lipophobic solutes across the endothelium: paracellular, for fluid, small solutes and the smaller macromolecules; and transcellular pathways or transiently widened paracellular routes ("hot spots") for larger macromolecules[29]. The two pathways (transcellular and paracellular) are thought to regulate endothelial barrier function independently of each other but growing evidence in recent years favours an interdependence [34].

1.2.4.1 Paracellular Permeability

The paracellular route, as noted, allows solutes with molecular radii up to about the size of albumin (Stokes-Einstein radius 3.5 nm) to traverse the endothelium via convective and diffusive transport through the extracellular spaces between contacting cells. The route is controlled by the properties of the interendothelial junctions (IEJs) and integrin receptors[34]. The majority of IEJs present in the endothelial barrier are known as adherens junctions (AJs). They are composed of vascular endothelial (VE) cadherin bound to a combination of catenins (p120, α,β,γ)[37]. Junctional permeability is regulated by the interactions of catenins with the actin/myosin cytoskeleton. Interendothelial gaps or transiently widened paracellular routes facilitating macromolecular transport are formed by actin/myosin driven contractions[37].

Tight junctions make up approximately 20% of IEJs and are more developed in arterial tissue than other vasculature. However, little is known about their role in regulating permeability. What is known is that the gaps are much smaller than adherens junctions and that they do not form continuous seals around the cells, with the exception

of the blood brain barrier (BBB) [36, 38]. They are essential in maintaining adhesiveness and barrier integrity and may transduce information with AJs via occludin and ZO-1 interactions.

Gap junctions (GJs) are made up of two hydrophilic, transmembrane connexons (Cx) that form a 2nm pore between adjoining cells. Gap junction formation provides a low-resistance pathway for current flow between cells that facilitates change in transmembrane potential and information exchange via second messengers. Phosphorylation plays a key role in regulating the channel gating and the rate of GJ assembly/turnover[34, 36].

Overall the adherens junctions (AJ) serve as the mechanical anchors with important functions in mechanotransduction while the tight junctions| (TJ) seal the intercellular space to limit paracellular permeability[39]. Both junctions are linked to the actin cytoskeleton which plays a vital role in controlling paracellular permeability. Maintenance and coordinated opening and closure of the interendothelial junctions is tightly regulated to prevent intercellular gaps forming under inflammatory conditions[39]. Spatiotemporal activity control of small GTPases Rac1 and RhoA and the balance of phosphorylation state are two of the main mechanisms that control intercellular junctions. Rac1 and Rho A activity is enhanced by junctional components, actin-binding proteins, cAMP signaling and other extracellular cues in a resting state. This is coupled with the prevention of phosphorylation of AJ components. When inflammation occurs AJ phosphorylation is induced and inflammatory mediators inhibit cell signaling, causing strong activation of RhoA which causes dissolution of TJs and endothelial barrier breakdown[39]. The inflammation can lead to prolonged vascular

hyperpermeability which is a common feature of many diseases[40]. Under these conditions it is believed that gap junction proteins or connexins contribute to basal endothelial permeability or dysfunction[40]. It is believed that there are potential mechanistic ties between the connexins and the junctional regulation. They also interact with the mural cells, tissue-specific perivascular cells and the interaction between the endothelium and components of the immune system, all of which have an impact on junction control[40]. There is an increasing level of evidence suggesting that crosstalk between the connexins and other junction proteins has an impact on maintenance of barrier integrity and function[40].

1.2.4.2 Transcellular permeability

The term transcytosis was first coined by N. Simonescu [41] when studying the transport of LDL by EM. The phrase describes the vectorial transfer of macromolecules within plasmalemmal vesicles from the luminal side of endothelial cells to the interstitium of underlying tissue. This vesicular transport mechanism is a putative second pathway for transport of macromolecules across the endothelial barrier. It has been studied by Palade, Florey, Simonsecu and Malik, amongst others [34]. It has been defined as a caveola-dependent (the large majority of uncoated vesicles in endothelial cells contain caveolin) and at times a receptor mediated [34] mode of transport. However, vesicles may be involved in transcellular transport in different ways, as discussed below.

Palade described a prominent population of "cave-like" vesicular structures on the luminal and abluminal surfaces of endothelial cells and hypothesized that they were the morphological equivalent of the large pore predicted by the physiologist Pappenheimer [42], which would account for the permeability of blood vessels to large macromolecules [43, 44]. Caveolae are 50- to 100 nm diameter cellular invaginations that were first described 60 years ago with the advent of electron microscopy [44, 45]. Caveolae remained somewhat unknown organelles with no set function due to the difficulties in characterising their biochemical composition and molecular nature [46, 47]. It was originally thought that their primary function was endocytosis alone, based on their morphological resemblance to clathrin-coated vesicles and dynamic movement between membrane and intracellular compartments. In-depth molecular analysis over the past few decades has led to caveolae being identified as complex organelles with cell-specific roles in signal transduction, tumorigenesis, lipid homeostasis and transport of macromolecules [46-48].

Studies have shown that the number of caveolae present in the endothelium corresponds to the permeability of macromolecules at different segments of the cardiovascular system - approximately 200 vesicles/μm^3 in arterioles, 900 vesicles/μm^3 in capillaries, and over 1,200 vesicles/μm^3 in venular segments [46]. There are fewer present in the blood brain barrier.

The assembly of caveolae on the surface of the endothelium is initiated by the recruitment of caveolin-1; the structural protein is incorporated into sphingolipid and cholesterol rich microdomains. This leads to the self-assembly of caveolin-1 into oligomers and mediates the invaginations of the plasma membrane [34].

Macromolecule binding to cavaloae is followed by the hydrolysis of dynamin and release of the vesicle [48]. This is an essential initial step that is closely regulated by the activation of receptors and dynamin oligomerization at the neck of the caveolae [34, 43]. The caveolae with macromolecules sealed inside them are then transported through the cell by an unknown mechanism to fuse to the albuminal side of the endothelium before discharging their contents into the extracellular space [47, 48]. Low-density lipoprotein and high-density lipoproteins are transported by vesicle-mediated transcytosis according to Predescu et al [48]. The protective coat surrounding the caveolae could allow them to resist temperature change, metabolic inhibitors, and most importantly differences in hydrostatic pressures [41, 48].

Endothelial cells express the highest levels of caveolin-1, and caveolae compose 20% of the cell volume [34, 46, 47]. Caveolin-1 (Cav-1) is a structural protein of caveolae and its expression levels along with the number of caveolae present on the luminal/subendothelial sides of an endothelial cell are regulated by free cholesterol. Both Caveolin-1/-2 are abundantly expressed by endothelial cells but the transcytosis of albumin is primarily regulated by Cav-1 [34, 46]. Cav-1 is so crucial for transcytosis that Cav-2 is unable to compensate for its loss. The removal of Cav-1 in knockout mice led to an increase in paracellular permeability to albumin, consistent with the interconnectedness of the two pathways noted above [34, 46]. The expression of caveolin-1 may also be strongly linked to atherosclerosis due to the changes in expression levels and roles in specific vascular cell types [49].

Caveolin-1 acts as a scaffold protein for caveolae based on its ability to enable the dynamic recruitment and interaction of signalling molecules into multiprotein

complexes [34]. Although vesicular transport used to be regarded as a low affinity passive route, there is increasing evidence for the role of receptors[50-52]. As already noted, albumin is transported by both paracellular and transcellular pathways, and there may be an interconnected pathway between both forms of transport [34]. There is additionally evidence of active transcelluar transport, as well as passive, fluid-phase transcytosis. The active form of transport requires the binding of albumin to a saturable 60kDa receptor known as albondin or gp60, or gp180. [53, 54]. One experimental study [53] demonstrated that tyrosine-kinase dependent activation of gp60 led to a threefold increase in transcellular transport, and albumin uptake [55].

Recent work has elucidated the involvement of specific receptors in LDL uptake and transcytosis in endothelial cells. The reason to investigate this phenomenon role is that humans and animals which lack a functional LDL receptor (LDLR) still demonstrate transport of LDL across the endothelium[56]. Hence other receptors may be involved. Using a genome wide RNAi screen, Sessa and co-workers demonstrated that the activin-like kinase 1 (ALK1) mediates LDL uptake into endothelial cells[56]. The ALK1 binds LDL with a lower affinity than the normal LDL receptor and mediates the LDL into endothelial cells via an unusual endocytic pathway that diverts the ligand from lysosomal degradation, promoting LDL transcytosis[56]. Other recent studies also suggest a role for receptor-mediated transcytosis in the transport of LDL[57]. The studies demonstrate a dependence on scavenger receptor B1 (SR-B1) as well as ALK1 and, contrary to the previous finding, the LDL receptor[57]. They have also determined that high-density lipoproteins transcytose endothelial cells through SR-B1, ATP-Binding cassette transporter A1 (SBCA1) and ABCG1. More work is required to determine the effect of transcytosis on endothelial permeability[57]. The identification of these pathways is an important step in highlighting the overlooked importance of active

transport in transendothelial transport, which is investigated for albumin as part of this thesis.

1.2.4.3 The relative importance of paracellular and transcellular routes

The relative importance of paracellular and transcellular routes for transport of macromolecules has been a matter of controversy for decades, as have the hemodynamic stresses that maintain normal endothelial function, and transendothelial transport's dependence on hemodynamic stresses[58]. During my PhD I was involved in supervising an MRes/PhD study that addressed this issue and was an author on the resulting paper. The study is presented here rather than in the main body of thesis because it was included in the thesis of the first author, Mean Ghim, who led the study[58]

.

The study involved developing and using novel *in vitro* methods, based on the methods of Dubroyskyi and colleagues [59], to visualize pathways for the transport of macromolecules of three different sizes across the endothelium [58]. The study thus had objectives related to this thesis of understanding transport across endothelial cells. Note that one of the tracers used in the study was similar in size to the Rhodamine-labelled albumin tracer used in the 3D bioreactor studies in this thesis.

The original *in vitro* method developed by Dubrovskyi and colleagues involved the coating of well plates with biotin-conjugated gelatin prior to seeding of endothelial cells. A tracer consisting of fluorescein isothiocyanate-labeled avidin (FITC-avidin; 66–69 kDa) is added to the cell culture medium above the endothelial cells cultured on

the biotinylated gelatin[58, 59]. The FITC-labelled avidin tracer crosses the endothelial monolayer and binds to the biotin molecules conjugated to the underlying substrate. The permeability of the monolayer can be calculated from the amount of tracer that binds to the biotinylated substrate as demonstrated by **Figure2.** More uniquely, the pathway by which the tracer crosses the endothelium can be determined by comparing the distribution of bound FITC-avidin with the structure of the overlying cells[58].
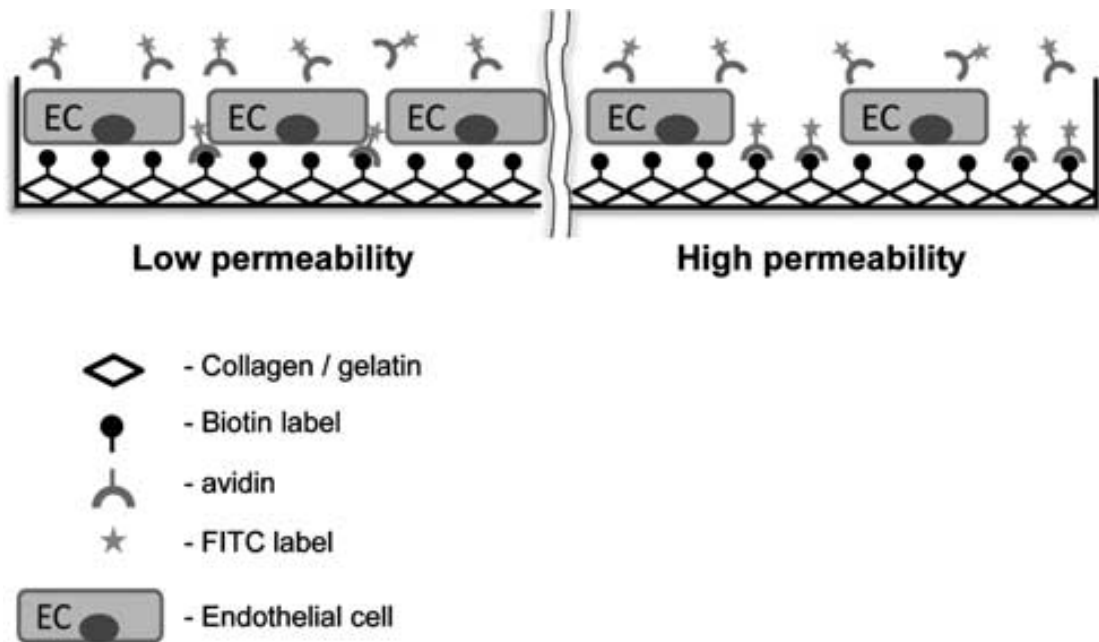
Figure 2 Endothelial Permeability Assay[58]

The Endothelial cells are cultured on top of a biotinylated substrate. The tracer, FITC-labelled avidin, is added to the media above the cells[58]. The transport of the tracer via paracellular and transcellular routes is assayed following the binding of the tracer to the biotinylated substrate. Regions of high or low cell permeability can be determined by the amount of tracer bound to the biotinylated substrate. High paracellular transport is show in the right-hand panel.

The novel concept for a cell permeability assay based on high affinity ligand-acceptor interaction was modified in our study with the use of FITC-labeled deglycosylated avidin (NeutraAvidin)[58] due to its more physiological isoelectric point. In addition to this, a fivefold larger tracer within the relative molecular mass range of HDL was synthesized by labelling the NeutraAvidin with *R*-phycoerythrin (RPE), a phycobiliprotein, while another tracer corresponding approximately to the size of LDL was obtained by using a streptavidin-labelled quantum dot 800 (Qdot 800) nanoparticle (diameter c. 20nm)[58].

The results of this work demonstrated that the FITC-avidin tracer was transported across the endothelial monolayers and bound to the biotinylated substrate in lines and spots of tracer as shown in **Figure 3A[58].** The comparison between nuclear staining patterns and phase-contrast images depicted lines at junctions between two neighboring cells which seemed to be indicative of bicellular junctions. The spots of FITC-avidin tracer appeared at the intersection of lines where there were three or more neighboring cells. These novel regions of transport discovered using this method were termed "tricellular junctions"[58, 60]. In **Figure 3B** thicker and less continuous lines of tracer were observed at cell borders for the FITC-NeutraAvidin tracer when compared to the FITC-avidin tracer. The spots at "tricellular junctions" were also less pronounced in experiments using the FITC-NeutrAvidin tracer[58]. However, the general pattern remained broadly the same as for FITC-avidin. In experiments where the NeutrAvadin was labelled with the larger *R*-phycoerythrin (RPE), only spots at the tricellular junctions appeared (**Figure3C**)[58] indicating the importance of these regions for transport of larger macromolecules.

In **Figure 4** it is possible to visualize the Qdot 800-streptavidin bound to the biotinylated substrate under the endothelial cells. In contrast to the previous experiments with smaller macromolecule tracers, the Qdot 800-streptavidin did not demonstrate any lines or spots of increased concentration at bicellular and tricellular junctions; the transport was transcellular[58]. The comparison with phase transport images suggested that the nucleus acted as a barrier to transcellular transport due to the decrease in intensity at nuclear regions. Tarbell and colleagues had previously proposed the existence of three pores in the transport of macromolecules across an endothelial monolayer in the form of bicellular junctions, vesicles, and leaky junctions [cited in ref [58]]. The data obtained in by this novel method did not demonstrate any substantial role of dying or dividing cells with leaky junctions under static conditions. Note that the experiments described in this section were under static conditions[58].

To validate the use of this type of technique *in vivo,* a fluorescent-labelled IgG raised against the NC1 domain of collagen type IV (a component of the basement membrane and therefore the substrate underlying endothelial cells in the body) was used to observe the transport pathways in aortas of rabbits. Its specificity to the endothelial basement membrane was tested first[58]. In **Figure 5,** showing a section of aorta stained with the antibody, there is a thin discontinuous line visible under the endothelium. The lack of fluorescence from the aortic media suggests that the smooth muscle cell basement membrane was not recognized by the antibody. Image B of **Figure 5** shows an en face view of the aorta of a rabbit that had been administered rhodamine-labelled anti-NC1 antibody intravenously[58]. The counterstained nuclei of endothelial and smooth muscle cells have distinct differences in orientation. The fluorescence from the antibody is present in both spots and lines. The pattern of the

lines and spots was similar to that of the bicellular and tricellular patterns of tracer experiments from **Figure 5A and B[58].**
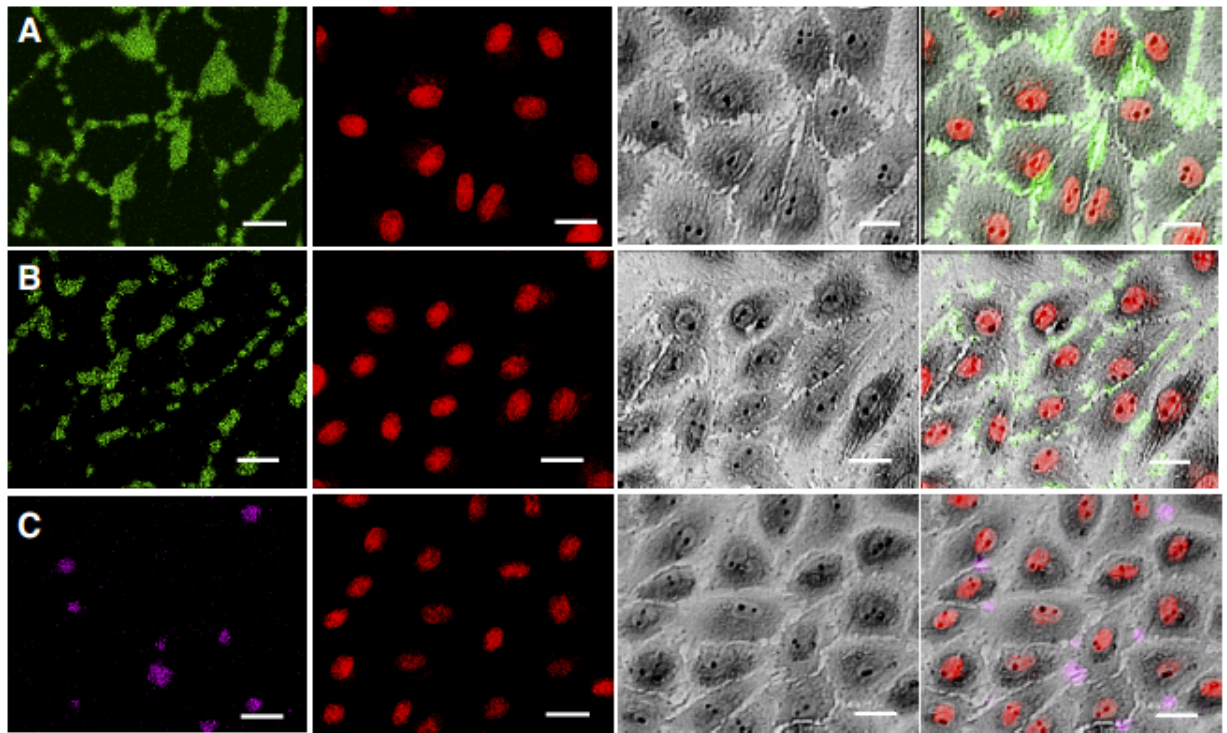
Figure 3 FITC-Avidin and FITC-NeutrAvidin tracer experiments[58]

This figure illustrates confocal images of the transport of different tracers across the endothelial monolayer together with DRAQ5-stained nuclei and greyscale phase contrast images[58]. The 69kDa FITC Avidin is represented in green in images A; 60kDa FITC-NeutrAvidin is represented in green in images B; and the 310kDa *R*-phycoerythrin-NeutraAvidin is represented by purple in images C. The scale bar is 20um. All images are overlayed in the right hand column to demonstrate tracer localization at different junctions.
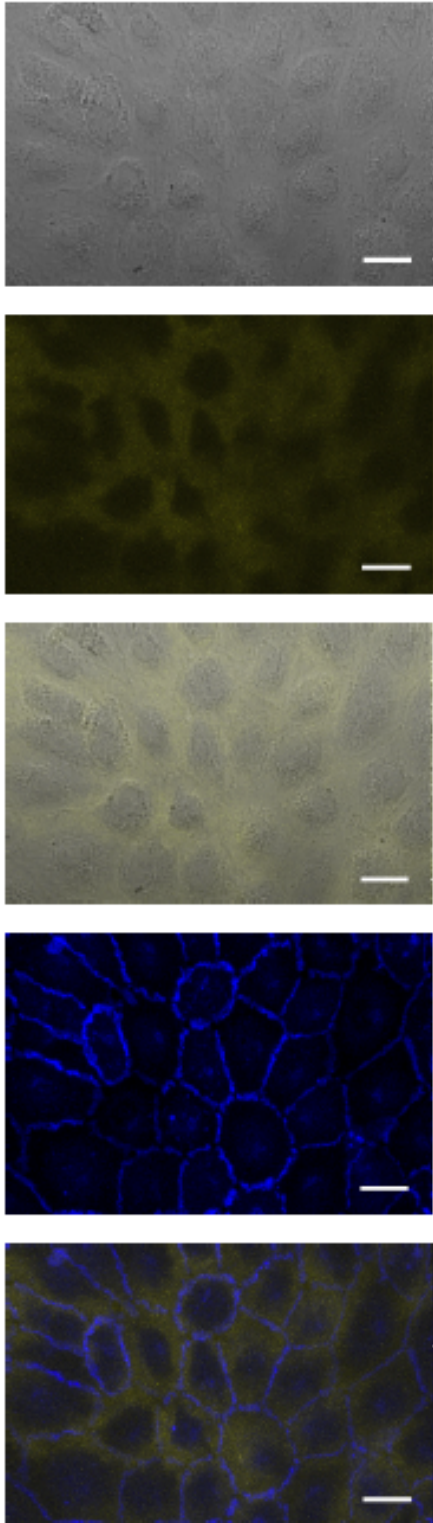
Figure 4 FITC-NeutrAvidin-Qdot 800-streptavidin tracer experiments[58]

From top to bottom this figure demonstrates confocal images of in vitro transport experiments starting with standard phase contrast (greyscale), Qdot 800-streptavidin (yellow), an overlay of the first two images, Anti-Vascular Endothelial (VE)-cadherin (blue), and an overlay of the VE-cadherin and Qdot images[58].
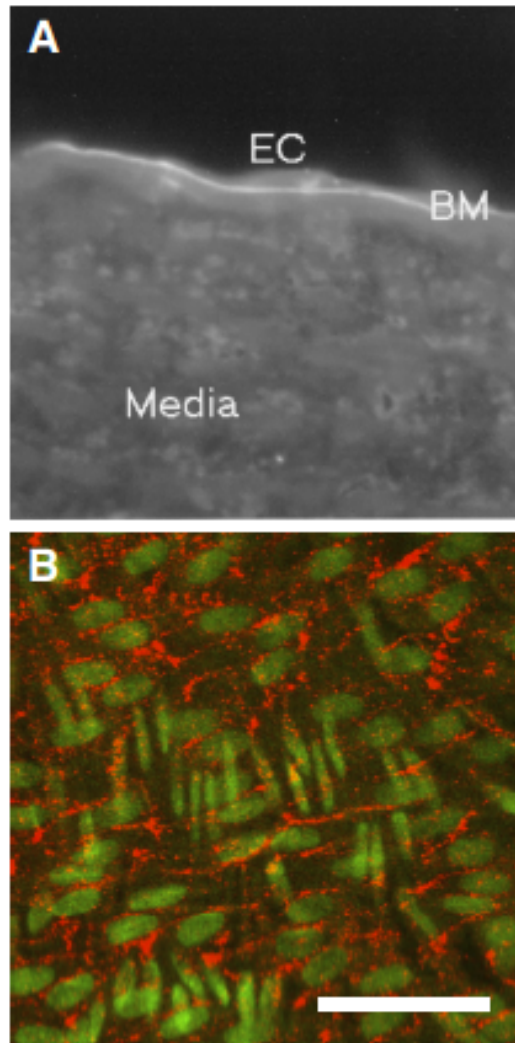
Figure 5 Alternate in vivo procedure used to identify transport through bicellular and tricelluar junctions[58]

Image A demonstrates antibody against NC1 domain of collagen type IV bound to endothelial cell (EC) basement membrane (BM) in a section of rabbit aorta. Image B demonstrates the maximum intensity projection of an en face confocal image stack of the descending thoracic aorta of a rabbit administered in vivo the same antibody labelled with rhodamine[58]. The nuclei of endothelial cells are labelled green and run from left to right with the smooth muscle cell nuclei running from top to bottom of the image. Antibody localization is labelled in red and corresponds to *in vitro* experiments with tracer underlying bicellular and tricellular junctions[58].

1.2.4.4 The effect of blood flow on endothelial permeability

For small molecules that cross the endothelium easily, such as oxygen, increased blood flow leads to increased transport of the solute into tissue simply because more of the solute is brought into the vessel. Transport of such solutes is termed "flow limited" and has been well studied in the microvasculature[35]. Transport of the macromolecules that are importance to atherosclerosis is not "flow limited" in this sense: although increased blood flow will still lead to increased quantities of the solute passing through the vessel per unit time, the decreased time that each element of blood spends in the vessel has the opposite effect of decreasing transport and these two effects tend to cancel[35].

Nevertheless, blood flow velocity can still alter the transport of solutes not traditionally regarded as "flow limited" because it can have an effect on the permeability of the vessel wall as well as on the delivery and residence time of the solute. This influence is likely to be mediated by the activation or release of signaling molecules or the alteration of structural molecules that play a role in the vesicular transport routes, or paracellular transport through junctions [61]. Under healthy physiological conditions the vasculature is in a resting state which allows for the sieving of macromolecules and solutes and restricts their extravasation to a significant extent. In disease-prone regions, however, the vessels may exhibit a weakened and leaky permeability barrier that can become hyperpermeable to large macromolecules, leading to disease initiation and propagation[61]. This is why studying the links between blood flow and vascular permeability is pivotal to understanding the underlying mechanisms that lead to disease.

In the study of the microscirculation, it had been assumed that vascular permeability was independent of blood flow until experiments carried out by Michel and colleagues determined that permeability increased in a rapid and reversible manner as flow was increased in perfused microvessels [62]. The original research suggested that flow-dependent permeability may be restricted to larger hydrophilic solutes. In a subsequent study they showed that the permeability to potassium molecules correlated with the velocity of perfused flow and was entirely independent of the changes in pressure[63]. Their most recent work has determined that microvessel permeability to other molecules such as sodium fluorescein was also dependent on the flow or shear stress in the vessels[62]. Flow-dependent increases in the permeability of capillaries to potassium and sodium fluorescein were both consistent with the opening of pores of 1nm radius[62, 63] and the studies demonstrated that the changes in vascular permeability occur within seconds of changes in the rate of perfusion, unlike the classical receptor-activated inflammatory changes in permeability[64].

Both publications provide convincing data to confirm the existence of flow-dependent increases in solute permeability[64] and are important contributions to understanding the mechanisms that regulate the exchange of macromolecules. However, they have not gone unchallenged. Studies by Weinbaum and colleagues demonstrated that the perfusion of the microcirculation in the direction of blood flow maintains stable low permeability characteristic of healthy vessels[65] but also found no increase in permeability with an increase in shear stress; increases in permeability only occurred with a change in flow direction[65].

In 2010 Williams demonstrated that an increase in shear stress causes changes in endothelial hydraulic conductivity (L_p) [66]. She also demonstrated that the disruption of the glycocalyx increased the sensitivity of the barrier to the fluid stimulus, confirming its role in the transduction of flow-induced stresses in relation to vascular permeability[66]. The relationship between the acceleration of blood flow and magnitude of both shear stress and hydraulic conductivity seemed to vary along the intact capillary lining which demonstrates the presence of sophisticated mechanisms at the luminal surface of the vessel wall for maintaining control of barrier function in response to changes in blood flow mechanics[66].

Although the studies by Michel et al were pioneering for the microcirculation, the putative relevance to atherosclerosis of effects of shear on permeability led to earlier investigations in arteries, although there have been surprisingly few such studies, presumably due to technical difficulties. For instance, some studies have only correlated existing variations in flow and permeability[67], such as the work carried out by Berceli et al. on the rates of low density lipoprotein (LDL) incorporation and degradation along the walls of the rabbit aorto-iliac bifurcation. This study investigated whether LDL metabolism changed in areas of disturbed flow in comparison to regions of undisturbed flow[67].The results demonstrated an elevated level of LDL uptake and metabolism in the lateral walls of the bifurcation, a region of flow recirculation, but no elevation in transitional or unidirectional hemodynamic zones. The implication that LDL metabolism and incorporation is induced by hemodynamic forces is indicative of why atherosclerotic lesion formation might occur in these regions in people.

Another *in vivo* study, carried out by Carew and Patel, looked at casual effects by altering flow[68]. They estimated the effect of transmural pressure, tensile stress and shear stress on endothelial permeability to Evans Blue dye labelled albumin in the left coronary artery[68]. They demonstrated that the staining density, indicative of the uptake of albumin bound to Evans Blue dye, increased in conjunction with an increase in transmural pressure, increase in tensile stress and strain, and increase in shear stress. It is unfortunate that this study used Evans Blue dye because nitric oxide is known to affect permeability and Evans Blue dye inhibits endothelium-dependent relaxation in rabbit aortic rings[69] .

Staughton et al (2001)[70] also examined effects of altering flow on permeability to albumin, this time focusing on areas around branch points in the descending thoracic aorta of anaesthetized rabbits. In mature animals, abolishing side branch flow altered the pattern of permeability around branch ostia.

For *in vitro* studies, where the permeabilities to albumin-sized tracers are notably higher than the results obtained from *in vivo* experiments, there have been numerous studies that employed EC grown on porous filters. For example, the Tarbell group [71] have shown that monolayer permeability to albumin is shear dependent and that the effects of shear are reversible. Subsequent studies [72, 73] from the same group have investigated the dependence of hydraulic conductivity and LDL transport on shear.

Another *in vitro* study, from this laboratory, used Transwell's and rhodamine-labelled albumin tracer experiments to understand the role of shear stress on endothelial

permeability [74]. More specifically, the study examined effects of acute and chronic shear stress on the permeability of macromolecules across the endothelial monolayer. As noted above, the reason for conducting this research was that the majority of studies[74, 75] that show shear stress increasing the transport of macromolecules across endothelial monolayers only applied shear stress acutely, while cells are exposed to chronic shear stress under *in vivo* conditions[74, 75]. The results of this particular study demonstrated that prolonged exposure of endothelial cells to shear stress had the opposite effect: acute application of shear stress to the endothelial cells cultured on Transwell's increased permeability to rhodamine-labelled albumin, but chronic application of shear stress reduced it. The study also determined that the exposure of endothelial cells to chronic shear stress reduced the permeability by a PI3K-NO-cGMP-dependent mechanism, which potentially explains the atheroprotective effects of shear and NO. Note that none of these *in vitro* studies were performed in a three-dimensional system which more closely replicates the *in vivo* environment, such as the one used for the experimental studies in this thesis.

I discussed above the static results from our experimental series involving FITC-Avidin and related tracers. Here I discuss the additional shear stress experiments conducted during that research. Briefly, cells cultured on biotinylated gelatin had tracer permeability experiments performed on them following exposure to shear stress. Shear stress was applied by swirling the wells on an orbital shaker. There was an increase in permeability to FITC-NeutrAvidin and RPE-NeutrAvidin at the centre of the wells, where time averaged shear stress is low and the flow is multidirectional, and decreased uptake at the edges of the wells, where the time averaged shear stress is higher and the flow is more uniaxial. In experiments with the Qdot 800-streptavidin tracer, there was

an almost uniform decrease in permeability across each well. These results were obtained using a fluorimetric plate reader and were verified by confocal imaging.

1.2.4.5 The effect of L-NAME and thrombin on endothelial permeability

This thesis examines effects of fluid mechanical forces on endothelial permeability by growing endothelial cells on the inner surface of porous capillary tubes in a bioreactor. As will become apparent in later sections, the chief drawback of the system is that the endothelial cells cannot be examined until after the experiment has been completed, and even then, only with difficulty. An alternative method is therefore required to determine whether the cells have formed a confluent monolayer.

One such method is to investigate whether compounds known to alter endothelial permeability do in fact do so in this system. If the cells have frequent or large gaps between them, the gaps are expected to dominate permeability. Weinbaum et al [76] have shown theoretically that even if only 1 cell in 400 is missing from the monolayer, the monolayer will not provide an effective transport barrier. Under such circumstances, a permeability-altering compound would be unlikely to have an influence. We used N^{ω}-nitro-l-arginine methyl ester (L-NAME) and thrombin as agents known to alter endothelial permeability. Previous studies of their effects are reviewed here.

L-arginine analogues are the most widely used inhibitors of nitric oxide synthase (NOS), and were used for example in the study that showed acute and chronic treatments with the reversible inhibitor L-NAME lead to a decrease in NO bioavailability which in turn causes changes in blood pressure and vascular reactivity[77]. The L-arginine analogues act as NOS inhibitors by competitive binding to the

enzymes[77]. L-NAME only inhibits NOS production following its hydrolysis to NG-nitro-L-arginine (L-NOARG)[78]. L-NAME administration mainly has the effect of lowering NO production but, due to feedback regulation, lower doses of L-NAME have over time produced an increase in NO production[77]. L-NAME increases the gene expression of both iNOS and eNOS by influencing the balance between transcription factor nuclear factor κB (NF-κB) and nitric oxide[77].

L-NAME has been shown to increases endothelial and intestinal epithelial permeability in ovine and feline models[79]. In the cat models there was an increase in endothelial permeability within the first hour following administration of L-NAME[79, 80]. In the sheep models the use of the NOS inhibitor increased permeability and reversed the hyperpermeability response to endotoxin infusion[79].

In cultured human aortic endothelial models, L-NAME enhanced a thrombin-induced increase in permeability by approximately 51%[81]. L-NAME reversed microvascular hyperpermeability in caveolin-1 knockout mice[82]. L-NAME has also been used to demonstrate that the inhibition of nitric oxide modulates VEGF-induced vascular permeability *in vivo[83]*.

It has recently been shown that vascular endothelial (VE)-Cadherin expression may play a role in how L-NAME alters endothelial permeability; the expression of VE-Cadherin is increased in endothelial cells in the presence of L-NAME[84].

Thrombin, a pro-coagulant serine protease, is another compound that can increase endothelial permeability in a reversible manner. It does so by disrupting and altering

the distribution of VE-cadherin and catenins in the intercellular junctions of the endothelial monolayer[85]. In response to thrombin administration, the GTPase, RhoA, and myosin light-chain kinase, MYLK, are activated which induces disassembly of endothelial adherens junctions. Disruption of the VE-cadherin-catenin complex alters the architecture of tight junction assembly[85]. This is associated with increased cell contraction and the formation of interendothelial gaps, that in turn leads to an increase in endothelial permeability[86]

The increased cell contraction induced by the edemagenic agonist means that thrombin is having an effect on the actin-myosin motor of endothelial cells, and indeed it has been shown to increase the isometric contraction force in monolayers 2.5 fold in 5 minutes, from a basal value of 70-132 dynes[86]. In order for this effect to take place, binding of the active enzyme to a receptor is required[85]. Thrombin binds to Protease-activated receptor-1 (PAR-1) on endothelial cells and induces proteolysis of the PAR-1 extracellular extension. This initiates downstream signaling events that lead to the increases in endothelial permeability described above[36, 86]. It is also possible that other isoforms of PARs play a role in amplifying thrombin-induced permeability. Although the downstream signaling events are not fully characterized, cleavage of the thrombin receptor is followed by an increase in intracellular calcium and PKC; these seem to be of importance in increasing endothelial permeability[85].

1.3 Existing models for studying endothelial permeability

The importance of endothelial permeability has led research groups to carry out experimental studies both *in vitro* and *in vivo*. Unfortunately, given the importance of local elevations of permeability in atherosclerosis, mechanisms linking mechanical stresses and permeability are particularly difficult to study. The most reliable information on transport in arteries comes from in vivo studies and has implicated defective tight junctions between neighboring endothelial cells as an important cause of elevated permeability [2, 3] but, as already noted, there are severe practical limits to the measurement and manipulation of mechanical stresses, and to cellular and mechanical interventions involving toxic or expensive reagents in living animals, in addition to the cost and difficulty of using animals. Some of these issues also apply to vessels perfused *in situ* or *ex vivo*. For this reason, many investigators use cultured endothelial monolayers; however, the requirements for a system that can be used rigorously to investigate mechanisms are daunting and have not been fully met.

Transport across endothelial monolayers on porous supports and exposed to chronic shear stress can be achieved by culturing cells on Transwell inserts in multi-well plates on an orbital shaker. As noted above, such studies have shown that acute shear increases the permeability of the endothelium [74, 87-89]. The ability to shear the cells chronically has also produced the potentially important result that chronic shear reduces endothelial permeability by a nitric oxide (NO)-mediated pathway. These results may help explain the atheroprotective effects of shear and NO [74].

Another system established by Tarbell and co-workers [89] involves endothelial cells grown on a porous support to which a hydrostatic pressure can be applied, and to which shear is also applied by spinning a disk above the cells. It allows for the measurement of transport under shear and pressure, but similar to other two-dimensional systems it does not analyze effects of stretch or pulsatile flow. Other groups have used flow chambers and microfluidics devices to investigate effects of shear stress on endothelial cell monolayers. However, these flow chambers do not permit the measurement of permeability: the flow gets increasingly sophisticated in them but because they do not have a porous substrate, permeability cannot be assessed. This might be a future application of the Dubroskyi/Ghim method; it could overcome the limitation because it permits permeability to be assessed by cells on an impermeable substrate. However, although the technique might enhance previous 2D studies by removing the need for Transwell® filters, it does not simulate the three dimensional environment that endothelial cells are exposed to in vivo, nor allow transendothelial pressure gradients, nor more prolonged studies.

1.3.1 The use of a novel hollow fibre bioreactor system

The technique of tissue culture has been available for over 100 years[90] and the most recent developments involve the use of 3-dimensional (3D) cell culture systems[91]. Interest in these methods has grown due to their ability to replicate an *in vivo* like cellular environment which allows for the study of cell functions under more physiological conditions. They have been of particular interest because of their potential role in tissue engineering.

The majority of tissue engineering approaches require the seeding of cells to a scaffold with varied chemical and mechanical properties and cultured in stirred tanks to deliver nutrients. These techniques offer limited improvements to the standard 2D cell culture techniques in recapitulating an *in vivo* environment[91]. However, hollow fiber bioreactors (HFBs) are a versatile 3D cell culture system available off-the-shelf. They were first described for use in cell culture by Knazek et al. [92]. The device was originally designed for the efficient production of cell-secreted molecules such as monoclonal antibodies [92].

They mimic tissue architecture: medium is circulated by a pump in a closed loop through numerous hollow fibres with porous walls, representing the vasculature, which are contained within a cartridge, equivalent to the tissue. Cells are conventionally grown in the volume outside the fibres; nutrients and oxygen are provided by diffusion through the porous walls of the fibres, while larger molecules such as antibodies are retained within the medium in the extra-fibrillar space, which can be collected. Since they mimic the native vasculature, one of the most important features of HFBs is their excellent mass transport properties which allows for the limitations of other systems to be overcome; nutrient transport occurs by diffusion over a large surface area.[93]

Although the majority of experiments involving HFBs have cells seeded on the outside of the porous fibers for cell expansion or antibody production, endothelial monolayers can be grown on the inside of the fibres, where they are subjected to flow [94]. The system mimics some aspects of the vascular environment and architecture [95]. The applied shear

stress can be calculated and, with modification, defined pressure can also be applied to the cells[91].

The hollow fiber bioreactor system that was used for this project is a modified version of the commercially available FiberCell System bioreactor. FiberCell System Cartridges for endothelial cell culture contain 20 fibres, each around 10cm long, with 700μm inner diameter, a wall thickness of 300μm, varied porosity (with individual pore sizes as low as 0.1 μm depending on cartridge type), and a surface area of 70cm^2, supporting approximately 10^8 cells. The fibres can be coated with extracellular matrix proteins to promote cell adhesion. Monolayers reach confluence[95] and transport of solutes across them can be assessed by including a tracer in the circulating medium and monitoring its accumulation in the cartridge.

In one study[96] bovine aortic endothelial cells were cultured under normal conditions within perfused hollow fibers for over a week. The results demonstrated that the cells formed confluent monolayers with flow but not under static conditions. The aortic cells also aligned themselves in the direction of the flow, with increased density of Weibel Palade bodies and lysosomes, which demonstrated the improvements offered by culture within hollow fibers under flow[96]. Similarly, Westmuckett and colleagues studied the effect of physiological shear stress on the expression and distribution of tissue factor pathway inhibitor (TFPI) in endothelial cells cultured within hollow fiber membranes[95]. When the endothelial cells were exposed to steady shear stress for 72 h the expression of TFPI was upregulated in direct correlation with the degree of shear[95]. They concluded that the use of endothelial cells cultured in hollow fibers allows endothelial

cells to be studied in an *in vivo*-like environment to determine that physiological shear stresses play a role in the regulation of TFPI expression[95].

The hollow fiber bioreactors have also been utilized in developing *in vitro* blood-brain barrier (BBB) co-culture models, with neuronal cells in the abluminal compartment. Stanness and colleagues established a BBB model within a hollow fiber bioreactor where neurites grew through the pores in the fibers from the abluminal space and interacted with the endothelial cells but did not disrupt barrier function[97]. In another permeability study, by Neuhaus *et al.,* immortalized microvascular endothelial cells were cultured in a hollow fiber BBB model[98]. This particular co-culture model increased the usability of the cell line from three days in a Transwell model to four months in the HFBs due to the application of high shear stress[98]. Glucose consumption rates were monitored daily (approximately 10 mg/day^{-1}) to confirm the integrity of the endothelial monolayer and cell viability[98]. This is discussed further later in this thesis. FITC-labelled 4 kDa dextran was used to determine paracellular transport across the endothelial monolayer[98]. Permeability coefficients were lower in the HFB BBB model than in parallel Transwell® studies. Scanning electron microscopy was used in this study to demonstrate that the cells formed a monolayer within the lumen of the hollow fibers. Overall, this study demonstrated that the culture of endothelial monolayers within HFBs led to a decrease in the rate of macromolecule transport due to the higher tightness of the endothelial monolayer. Another study investigated endothelial permeability to insulin in the HFB[99]. Cell growth and the endothelial monolayer integrity were again determined by measuring glucose consumption [100, 101]. The model maintained barrier features over a number of weeks [99]. Since the experiments were carried out on the same cells it meant that the differences in results could not be

accounted for by change in cell passage number [99]. This is another advantage of the HFBs, as it removes a possible source of variation from the data. The results demonstrated that the biochemical mechanisms involved in the transendothelial transport of insulin were comparable to *in vivo* and *ex vivo* studies, which supported the value of the model for endothelial permeability studies[99].

Other studies [102, 103] have also demonstrated that cells can be maintained for at least several weeks, meaning that numerous transport measurements can be made per bioreactor culture.

The initial experiments carried out for this thesis studied rhodamine-labelled albumin transport through a monolayer of primary aortic endothelial cells cultured under different shear stress conditions in a standard, unmodified bioreactor. Following these experiments, modifications were made to the bioreactor to incorporate steady and transmural flow into the system and hence to study their individual roles on endothelial permeability. One disadvantage with the FibreCell system is that the fibres are rigid, and as a result the cells cannot be cyclically stretched. Therefore, pilot studies were carried out to generate methods for producing distensible, porous, structures, which could be applied to the same bioreactor system in place of the commercial cartridges. The experimentation included copolymer synthesis, hydrogel formation, electrospinning and additive manufacturing (3D bioprinting and electrohydrodynamic printing).

1.4 Hypothesis and Objectives

1.4.1 Hypothesis:

In a culture system in which the endothelium is exposed to mechanical forces similar to those occurring *in vivo*:

1. Chronic shear stress reduces monolayer permeability to macromolecules by an NO-mediated pathway;

2. Permeability is sensitive to the presence, duration and temporal pattern of shear stress and transmural flow;

3. Permeability to albumin may depend on active processes

1.4.2 Objectives:

1. To develop novel methods permitting the chronic culture of endothelial cell monolayers under physiological stresses

2. To employ these methods to investigate endothelial cell permeability under different patterns of mechanical stress and after the introduction of pharmacological agents.

3. To research and develop novel 3D materials, machinery, techniques and methods for studying effects of cyclic strain endothelial permeability.

Chapter 2. Methods

2.1 Isolation of Porcine Aortic Endothelial Cells

Descending thoracic aortas were obtained from the slaughter of Landrace Cross pigs, aged 4-6 months. Two different tissue suppliers were used. The first (Cheale Meats, Essex, UK) provided aortas on the day of slaughter whilst the second (Fresh Tissue Supplies, East Sussex, UK) provided aortas one day following slaughter. The aortas were stored in Hanks Balanced Salt Solution (HBSS, Sigma-Aldrich) containing penicillin (200 U/ml), streptomycin (200 μg/ml), amphotericin (5 μg/ml), and gentamycin (100 μg/ml).

The isolation of porcine aortic endothelial cells (PAEC) was carried out using similar methods to those outlined previously [104]. Briefly, fat and connective tissue were trimmed from the vessels and the intercostal branches were ligated under asceptic conditions in a laminar flow hood. The proximal end of the aortic segment was cannulated and the aortas were flushed with phosphate buffered saline (PBS, Sigma-Aldrich). Each aorta was filled with 0.2mg/ml type II collagenase (Sigma-Aldrich) after the distal end was clamped. They were then incubated at 37°C for 10 minutes before being returned to the laminar flow hood. Here the aortas were gently massaged to loosen the endothelial cells and the collagenase solution was collected in a falcon tube. The samples of collagenase solution were centrifuged at 220 x g for 10 minutes. The PAEC's were resuspended in Dulbecco's Modified Eagle Medium (DMEM, Sigma-Aldrich) supplemented with 20% Fetal Bovine Serum (FBS, Sigma-Aldrich), penicillin (100 U/ml), streptomycin (100 μg/ml), amphotericin (2.5 μg/ml), gentamycin (50 μg/ml),

5mM L-glutamine, and 5 μg/ml endothelial cell growth factor (ECGF, Sigma-Aldrich). This solution is referred to in later sections as DMEM with supplements

These passage zero (P0) cells were plated onto T25 flasks for 1 h to allow cells to seed to the flask. Following this seeding period the medium was changed (which reduces smooth muscle cell contamination) and cells were cultured in a 5% CO_2 incubator at 37 °C overnight. The medium was changed in each T25 flask one day after seeding and then every 2 days until the cells became confluent. Once confluent (as determined by observations made with phase contrast light microscopy) the cells were passaged using a 3-minute exposure to Trypsin-EDTA (0.1:0.02%, Sigma-Aldrich) and centrifuged at 220 x g before being seeded to two larger T75 flasks. This procedure is referred to in later sections as trypsinization and centrifugation. The cells were cultured in the T75 flasks in a similar manner until confluent and were then used from Passages 1-3 for shear stress and other studies employing the Hollow Fibre Bioreactor, and for experiments with synthetic scaffolds or a microfluidics device.

Endothelial cell purity was assessed prior to the bioreactor from the internalization of Dil-labelled acetylated LDL (Molecular Probes), which was added to confluent monolayers at a final concentration of 10 μg/mL and incubated at 37 °C for 12 h. The wells were washed three times in PBS for 15 minutes. The cells were then fixed in 4% paraformaldehyde for 15 minutes and their nuclei were stained with DRAQ5 (BioStatus, 1:1000). The cells were washed again in PBS before being imaged using a laser scanning confocal microscope (Leica SP5) with a 10x 0.40NA objective. Dil-acetylated-LDL was excited at 514 nm and detected between 539-593 nm; equivalent

wavelengths for DRAQ5 were 633 and 675-725 nm. The fraction of cells taking up Dil-acetylated-LDL was determined with a manual counting program developed in MATLAB (The MathWorks, Inc).

2.2 Rhodamine-Labelled Albumin Tracer preparation

All hollow fiber bioreactor permeability experiments were carried out using rhodamine-labelled bovine serum albumin (Rh-BSA) as a macromolecular tracer. This tracer was prepared by conjugating sulphorhodamine B acid chloride to BSA, using a protocol modified from that of Narin (1964) and with the assistance of PhD student Yean Choi. Sulphorhodamine B acid chloride (1.5 g) was dissolved in acetone (100 ml) and then added in a drop-wise manner to bovine serum albumin (15 g) dissolved in 0.5 M bicarbonate buffer solution (750 ml, 440 mM $NaHCO_3$, 57 mM Na_2CO_3) at pH 9 while stirring in an ice bath. Stirring was continued for a further 60 minutes. Gel filtration was used to separate the unbound rhodamine from the rhodamine-labelled BSA. Briefly, the samples of Rh-BSA (180 ml) were filtered through a column (4 cm diameter, 70 cm length) of Sephadex® G-25 beads at a flow rate of 20 ml/min^{-1} with an elution buffer of 0.25 x Ringer's solution (50 mgl^{-1}KCl, 50 mgl^{-1} $CaCl_2$, 25 mgl^{-1} $NaHCO_3$ 2.25 gl^{-1} NaCl).

Threee absorption wavelengths (unbound albumin: 280nm, unbound rhodamine: 565nm, rhodamine bound to albumin: 575nm) were measured to identify the fraction containing rhodamine-albumin. The fraction was dialysed at 4 °C for 24 h against a 1/10 x Tyrode's Salt Solution (TSS, pH of 6.5, 0.20 gl^{-1} KCl, 0.20 gl^{-1} $CaCl_2$, 1.00 gl^{-1} $NaHCO_3$, 8.00 gl^{-1} NaCl, 0.20 gl^{-1}$MgCl_2$, 0.05 gl^{-1} NaH_2PO_4). The solution was snap frozen dropwise in liquid nitrogen and lyophilized for storage at -20 °C. To calculate the

protein and fluorophore concentration the absorbance at 575nm, total volume and total weight of solutes were recorded.

Before use in hollow fiber bioreactor experiments, the conjugate was reconstituted in sterile H_2O. The volume of water was calculated so that the tracer was suspended in 1 x TSS. The solution was purified of any remaining free dye one day before experiments by adding neutralized activated charcoal (0.35 g/g of protein) and placing it on a rotating platform for a 1-hour incubation at room temperature. The charcoal was removed by centrifugation (4 ^{o}C, 3000 x g, 2 x 15 minutes) followed by filtration twice through a 0.2-μm filter. The final concentration of purified tracer in the reservoir of each bioreactor with DMEM and supplements was 1 mg/ml. The absence of free dye in the purified tracer was confirmed by Dr. Yean Choi.
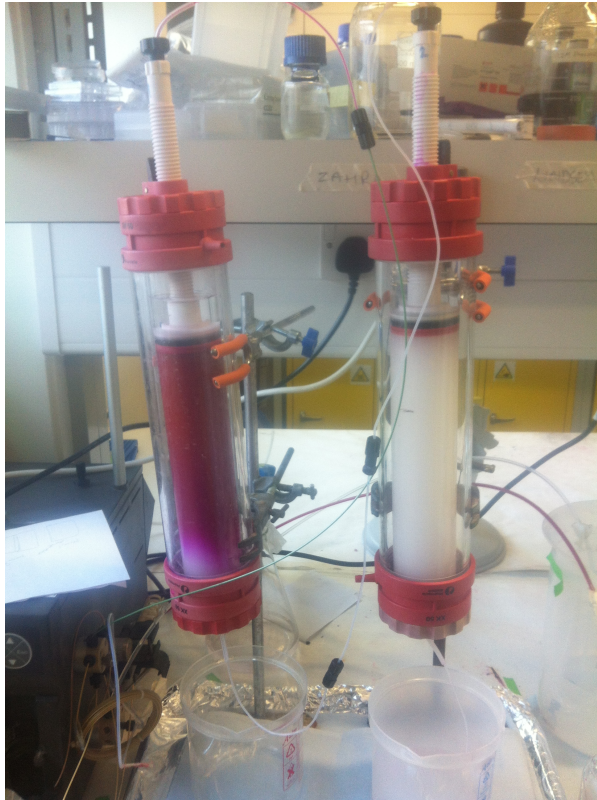
Figure 6 The preparation of Rhodamine Labelled Albumin

The images depict the filtration and freezing of the rhodamine labelled albumin prior to freeze drying.

2.3 The use of a hollow fibre bioreactor for permeability studies

2.3.1 Bioreactor Activation and Coating

The FiberCell hollow fiber bioreactors, connectors, and reservoir were all sterilized for approximately 2 h with UV light prior to cell seeding. Once placed within the laminar flow hood the entry ports were opened and a modified version of the FiberCell protocol was followed to ensure maximum sterility and coating efficiency. **Figure 7** illustrated the ports and stopcocks described in the next few paragraphs. In the first fibre activation step a 10ml syringe filled with 70% ethanol was attached to port A with 3-way stopcock #1. Stopcock #1 was positioned with the off position facing away from the cartridge to allow for flow into the cartridge. An empty syringe was attached

to port D with the off position of the 3-way stopcock #2 turned away from the cartridge to allow flow to enter the syringe at port D when pushed through port A.

The side port clamps (B and C) of the extracapillary space (ECS) remained closed as the ethanol was transferred through the bioreactor and into the empty syringe. The ethanol remained in contact with all 20 hollow fibers for approximately one minute prior to being flushed out with a new syringe filed with PBS (Sigma-Aldrich). This washing stage was repeated ten times to ensure that all ethanol was removed from the fibers. Once the fibers had been rinsed, a new syringe was filled with 5% gelatin and attached to port A with stopcock #1 positioned away from the bioreactor cartridge. New empty syringes were attached to ports B-D. The stopcock at port D was positioned away from the bioreactor cartridge. The gelatin coating solution in the syringe at port A was transferred through the bioreactor and into the syringe at port D. The coating solution was slowly flushed back and forth between ports A and D for approximately 10 minutes with emphasis on slow movement to prevent any trapped air bubbles.

In order to ensure that the coating solution covered all areas of the hollow fibers, 5ml of the coating solution was left in each of the syringes at port A and port D and coating solution was transferred to the ECS ports as follows to ensure the other side of the bioreactor hollow fibers were coated in the same manner, as outlined in the Fibercell protocol. Briefly, port C was opened and the stopcock #2 at port D was positioned towards the bioreactor cartridge. The gelatin solution in the syringe at port A was subsequently transferred to the syringe at ECS port C. Port C was then was closed and the off position of stopcock #2 was returned to face away from the bioreactor. The off position of the stopcock at port A was turned to face the cartridge and port B was opened. The 5% gelatin solution was then transferred from the syringe at port D to the syringe at

ECS port B. Port B was then closed and the off position at stopcock #2 was turned to face the bioreactor cartridge. The bioreactor was rotated 180º for ten minutes before being placed into the incubator for 1 h. The bioreactor was rotated 180º every 15 minutes in the incubator. The hollow fibers were then flushed with PBS and the reservoir filled with 200ml of DMEM and supplements was attached to the bioreactor circuit, before the system was in turn attached to the positive pressure displacement pump kept within the incubator. The DMEM with 20% FBS and supplements was pumped through the gas permeable tubing at a flow rate of 15ml/min for two hours prior to cell seeding.
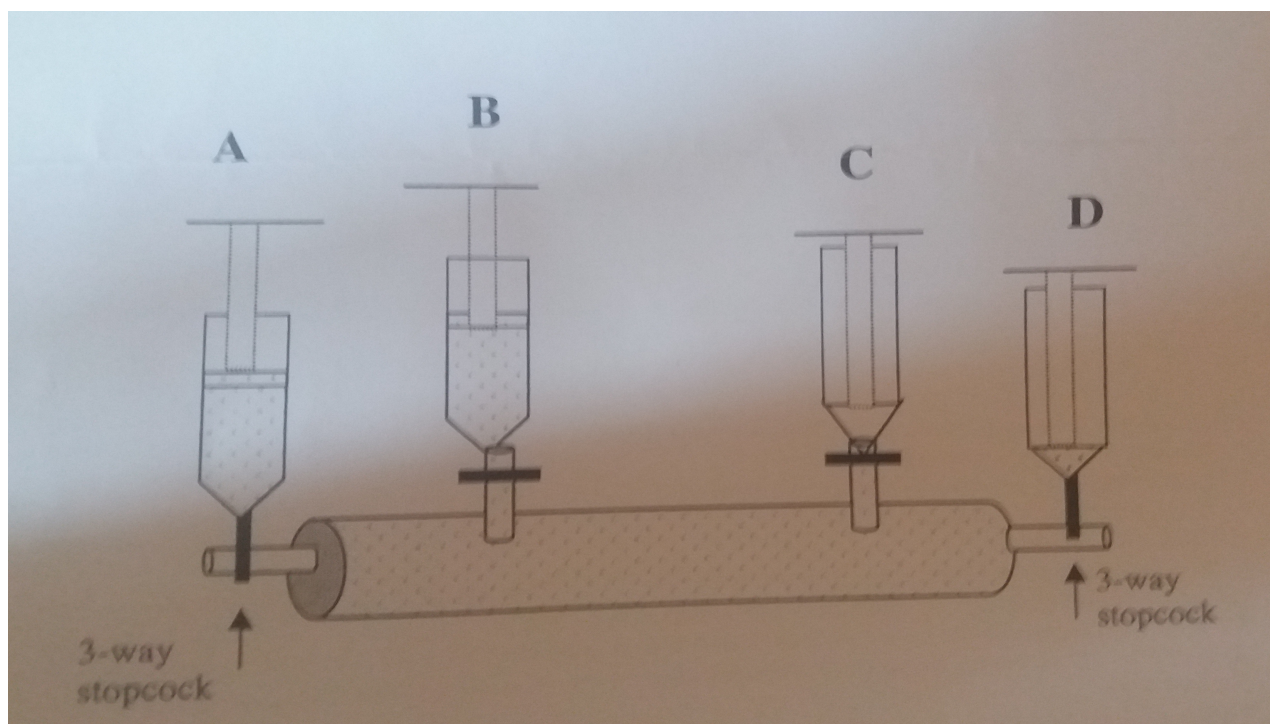
Figure 7 FiberCell Bioreactor Setup

This figure demonstrates the entry ports A-D for fiber activation, cell seeding and permeability experiments. Ports A and D are linked to the intracapillary space to allow for the coating of the internal hollow fiber membranes and the seeding of endothelial cells, along with the extraction of tracer samples. Ports B and C are linked to the extracapillary space and allow for the extraction of samples from that space for analysis in comparison to the intracapillary space. Stopcocks are also shown at each entry port to the bioreactor.

2.3.2 Seeding of Porcine Aortic Endothelial Cells in the Bioreactor

A modified version of the protocol outlined by FiberCell was used in order to ensure maximum seeding efficiency. The seeding process was started once the medium had been circulating within the gelatin-coated bioreactor for 2 h in the laminar flow hood. Two confluent T75 flasks of porcine aortic endothelial cells were required for the seeding of cells to each bioreactor. In the first stage, one confluent T75 flask (P1or P2) was trypsinized and pelleted down by centrifugation at 220 x *g* for 5 minutes as outlined previously. The pellet was resuspended in 5 ml of DMEM with supplements and the cells were counted (normally 5-8 x 10^6 cells per T75 flask).

When triturated properly the cell suspension was added to a 10 ml syringe that was attached to port A of the bioreactor cartridge (**Figure 7**) with the off position of stopcock #1 positioned away from the bioreactor cartridge. Ensuring that no bubbles were present, the off position on stopcock #2 at port D was turned towards the bioreactor and an empty 10ml syringe was attached port C of the extracapillary space which was opened. The cell suspension was transferred slowly through the hollow fibers and into the syringe at port C allowing cells to became trapped by the hollow fiber membrane. External ports A and C were closed and the bioreactor with pump and reservoir were returned to the CO_2 incubator for 1 h. The bioreactor was rotated 180° every 10 minutes over this period to ensure that cells seeded to all areas of the hollow fibres.

In the next step the second T75 flask at a similar passage was trypsinized and pelleted down by centrifugation at 220 x *g* for 5 minutes, as outlined, and used to seed the fibres a second time. This was a modification to the existing protocol that was adopted due to issues experienced in cell seeding with just one stage. Allowing some cells to seed for a few hours before seeding another batch that was at the same passage

was performed to speed up the rate at which a confluent monolayer formed. The bioreactor and reservoir were removed from the incubator and fresh medium in a 10 ml syringe was slowly flushed from port A to port D, avoiding air bubble contamination. The medium and any loose cells that were in the syringe at port D were counted to determine the seeding efficiency of cells to the coated hollow fiber membranes (approximately 40-60% depending on experiment). The second pelleted cell suspension was resuspended as before in 5ml of DMEM with supplements and added to a 10ml syringe and attached to port D of the bioreactor.

Ensuring that no bubbles were present, the off position on stopcock #1 at port A was turned towards the bioreactor and an empty 10ml syringe was attached to port B of the extracapillary space, which was opened. The cell suspension was transferred slowly through the hollow fibers from port D and into the syringe at port B allowing cells to become trapped by the hollow fiber membrane. Ports D and B were closed and syringes were removed, and the bioreactor and reservoir were returned to the CO_2 incubator at 37ºC for 1 h of seeding time. The bioreactor was rotated 180º every 5-10 minutes over this 1 h period to ensure that cells seeded to all areas of the right hand side of the hollow fibers. After one hour the bioreactor and reservoir were removed from the incubator and fresh medium was slowly flushed through the bioreactor. The medium and any loose cells that were in the syringe at port A were then counted to determine the seeding efficiency of cells to the coated hollow fiber membranes (approximately 40-50% depending on experiment).

Gas permeable tubing was removed from ports A and D of the bioreactor cartridge and attached to ports B and C of the extracapillary space and two 10ml syringes filled with fresh DMEM with 20% FBS and supplements were attached to either end of

the bioreactor cartridge. Once medium was present in the hollow fibers without any air bubbles the extracapillary side ports were opened and bioreactor was attached to the pump within the incubator with flow circulating through the extracapillary space at approximately 5ml/min^{-1}. The bioreactor remained under these conditions for 24-48 h, with medium in the syringes and bioreactor being replaced twice a day, to ensure that the cells had time to form a confluent monolayer. After 48 h the tubing was reattached to the bioreactor and the monolayer was exposed to flow of 5 ml/min^{-1} for 24 h before increasing the flow rate to 15 ml/min^{-1}. Samples of medium were taken from the bioreactor and glucose measurements were performed for 10-14 days following cell seeding and permeability experiments were started once the glucose levels had depleted to 40-50mg/dL from 100mg/dL with steady readings within the bioreactor; this was the main indicator of a confluent monolayer. The glucose concentration, and hence consumption, was determined using a GluCell meter with glucose detection strips. The validation series of experiments also included assessment of the permeability of cells to rhodamine labelled albumin in test bioreactors over time to determine at what point the cells had formed confluent monolayer or a strong barrier integrity, as imaging was not possible. Permeability to Rhodamine labelled albumin was performed for each bioreactor at the beginning of all the experimental series using that bioreactor, and acted as an indicator of whether barrier integrity had been compromised. The chronic shear stress (CSS) permeability controls were always carried out for all bioreactors as the readings under CSS acted as a baseline; even when other experimental procedures were introduced, it was possible to switch back to CSS at different time points, depending on the experimental series.

2.3.3 Measurement of endothelial monolayer permeability in the bioreactors

Each series of bioreactor experiments used the same protocol for the measurement of endothelial cell permeability to the rhodamine-labelled albumin tracer. A tracer experiment was performed on the day following the seeding of each bioreactor to get a control or baseline reading prior to the cells forming a confluent monolayer. Experiments were carried out to monitor the change in permeability over time under pulsatile flow conditions and this was compared to the glucose data. As instructed by FiberCell and their previous publications, the first set of tracer experiments were carried out when glucose was depleted by 40-50%, normally 10-12 days after cells had been seeded to the bioreactor. The measured permeability itself also served as an indicator of whether or not the cells had formed confluent monolayers on the fibres. Any permeability values that were close to the permeability measurement at day one after seeding prompted an increase in cell culture time and if no change was observed then the bioreactor was reseeded again.

A maximum of 9 permeability measurements was carried out per bioreactor. Experiments were normally ended 12-14 days after the first permeability experiment to allow for fixation, imaging, and flow cytometry. The serum content of the culture medium in the reservoir was reduced from 20% to 10% following 10 days of culture and reduced to 4% 24 h before each permeability experiment, in both the reservoir/intracapillary and extracapillary (cartridge) compartments. For the tracer measurement experiment itself, the solution in the reservoir and gas permeable tubing was replaced with DMEM, 4% BSA and supplements containing 1 mg/ml rhodamine-labelled albumin. The medium plus tracer was circulated in the reservoir for approximately 1 h in all experiments with the exception of static studies where the tracer

was not circulated but simply added to the intracapillary space using syringes, and studies of active transport where the time was 24 h. Samples (2.5 ml) were taken from intracapillary and extracapillary compartments of the bioreactor system after 1 h, and tracer fluorescence in each compartment was measured using a fluorimeter (model 6285, Jenway) with excitation and emission wavelengths of 570 and 600nm, respectively. The concentration of rhodamine albumin in each diluted sample was determined from a standard curve.

The permeability (P) of the monolayer may be defined as the rate of diffusion or transcytosis of solute (J_s) across the unit area of the membrane (S) per unit concentration difference across the membrane (ΔC) as follows:

$$P = J_S / (S \times \Delta C)$$

J_s was determined from the concentration of rhodamine albumin in the extracapillary space (C_{ECS}; in µg/ml), the volume of the extracapillary space (V_{ECS}; in ml), and the time after the addition of the tracer to the intracapillary space (t; in s) as follows:

$$Js = (C_{ECS} \times V_{ECS}) / t$$

Permeability was derived from J_s using the total area of the capillaries (S) and the initial concentration of rhodamine-labeled albumin in the intercapillary space (C_{ICS}) as follows:

$$P=J_S/(S \times C_{ICS})$$

(the low concentration of tracer in the extracapillary space was ignored when calculating the concentration gradient). The resistances of the membrane without cells, and membrane with the cell monolayer, obtained for the same bioreactor, were calculated as reciprocals of permeability. The former was subtracted from the latter to give the resistance of the cell monolayer alone, and then its reciprocal was taken in order to calculate the permeability of the monolayer.

2.4 Bioreactor Experimental Series I-V

2.4.1 Experimental Series I: The effect of static vs. acute vs. chronic shear stress on permeability

This first series of experiments carried out with the bioreactor aimed to determine the effect of different shear stress conditions on a confluent endothelial monolayer. The main advantage of the hollow fiber bioreactor system was the ability to change between static, acute and chronic shear stress conditions at any time point whilst concurrently assessing changes in permeability. Once cells had been cultured for approximately 10 days within the hollow fiber membranes and the glucose levels had decreased accordingly (40-50%), the first permeability measurements were performed as outlined in the previous section. As the cells were normally cultured for many days under flow (following the short, initial static period) as outlined in the section on seeding, the first results were categorised as chronic shear stress (CSS). The PAEC's within the bioreactor were then exposed to static conditions for 2-4 days followed by a short period of acute shear stress (ASS) and finally a repeat of the initial CSS condition. This cyclical change in exposing endothelial cells to different shear stress conditions was repeated 2-3 times per bioreactor. (It may be possible to increase the repetitions given that some literature reports a confluent monolayer can be maintained for up to 8 weeks.)

The differences between flow conditions (static, ASS and CSS) were obtained by modifying how the cells were exposed to medium from the reservoirs. CSS and ASS required DMEM medium and supplements to be pumped through the fibers of the bioreactor cartridge at a total flow rate of approximate 15 ml/min (equivalent to a WSS of 3.75 dynes/cm^2 according to the manufacturer's instructions). The flow rate set on

the pump was confirmed by use of a transit-time ultrasound flow probe device (Transonics) coupled to an analogue-to-digital converter and data analysis system (Notochord). Flow was maintained for 3-10 days at a time for CSS, depending on the interchanges between experimental conditions, and for 4 h after static conditions for ASS.

For static conditions, syringes were filled with DMEM and supplements and attached to either end of the bioreactor cartridge to ensure that cells had enough medium without any air bubbles. The gas permeable tubing was attached to ports B and C, which were opened, to allow for the pump-driven flow to pass through the extrafibrillar space of the cartridge. Thus cells on the fibers acquired nutrients and oxygen, and had waste products removed, by diffusion across the fibre. The cells were shielded from the direct influence of the flow, which was maintained at a flow rate of 5 ml/min^{-1}, by the wall of the fibre. PAEC's were exposed to these conditions for approximately 3-5 days prior to any experiments.

2.4.2 Experimental Series II: The effect of altering medium viscosity on permeability

Experiments were conducted in new bioreactors using medium that had been modified to obtain rheological properties analogous to those of blood. Following the technique outlined in[37], Xanthan Gum (XG, Sigma-Aldrich, 0.69g l^{-1}) was UV sterilized and added to the DMEM plus supplements to create a medium with viscosity of 4 x 10^{-3} Pa and shear rate of 200 s^{-1}. The solution was stirred for 24 h at room temperature before being added to the reservoir of the bioreactor. (NB the addition of XG to the medium was a slow process, requiring the addition of the powder to the DMEM one granule at a time.) Once the blood-analog medium was added to the reservoir the

experimental series was carried out as before i.e. in the Static-Acute-Chronic sequence during which tracer transport over 1 h was measured. (The tracer was prepared at 1 mg/ml in the blood-analog medium to ensure that no changes in viscosity occurred during the uptake measurements.)

2.4.3 Experimental Series III: pulsatile vs steady vs transmural flow

The third series of experiments carried out with the hollow fiber bioreactor system required the ability to switch between steady, pulsatile, and transmural flow conditions at different time points. Tracer measurements were performed as outlined previously, following the different types of axial and transmural flow. The normal axial experimental flow at a rate of 15ml/min, as used in the static vs ASS vs CSS study above, was generated by the pump periodically squeezing tubing that contained medium (similar to a peristaltic pump) in conjunction with a system of one-way valves. It gave pulsatile flow. In order to dampen the pulsatility of the flow and hence produce steady flow, four 50 ml syringes filled with air were incorporated into the flow circuit, between the pump and cartridge, using additional pieces of tubing and 3-way stopcocks.

The dampening of flow was confirmed with the use of the Transonics flow meter and Notocord software prior to any biological experiments. The setup was added to the bioreactor in a laminar flow hood and then transferred with the pump to an incubator. Care was required to prevent any possible source of contamination entering the bioreactor. For example, copious amounts of ethanol were used to ensure sterility. For the transmural flow experiments, one of the ports in the extracapillary space was opened

and a specially modified luer-lock syringe, with a sterile filter attached to ensure sterility, was added to the port to expose the system to atmospheric pressure. This modification created a pressure difference across the capillary wall and permitted transmural flow. After several hours, the transmural flow across the fibers and into the cartridge and syringe stabilized to approximately 0.1 ml/h. The experiments were carried out over approximately 3-5 days; the syringe was replaced every few hours in a laminar flow hood as the rising level of medium in it would otherwise alter the transmural pressure difference.

During the transmural flow tracer experiments, all fluid entering the ECS and attached syringe was collected and analyzed with the fluorimeter, to permit calculation of permeability. All pulsatile, steady and transmural flow experiments were carried out for approximately 3-5 days prior to 1 h tracer transport measurements. Experiments under each type of flow were repeated in several bioreactors.

2.4.4 Experimental Series IV: The effect of pharmacological agents on endothelial permeability

In the fourth series of experiments, cells were treated with biological agents and inhibitors to determine whether the responses found under different flow and shear stress conditions were due to the presence of cells, as well as to assess the roles of the agents themselves. An observation of changes in permeability in response to known inhibitors or stimulators of cellular permeability would provide confirmation that the resistance of the system was dominated by the cells rather than the fibre membranes or effects of flow on diffusion boundary layers, and hence that the cells were confluent and behaving in a physiological manner.

In a number of CSS (pulsatile) bioreactor experiments the production of nitric oxide was inhibited for 24 h with the addition of the L-arginine analog Nω-nitro-l-arginine methyl ester (L-NAME; Sigma-Aldrich; 500 μM) prior to a permeability measurement. Alternatively, thrombin (Sigma-Aldrich; 10 U/ml) was added for a period of 1 h before permeability was quantified.

2.4.5 Experimental Series V: Active Transport and Biological Studies

The fifth series of studies arose serendipitously as a result of data obtained during a switch between pulsatile and steady flow experiments. Briefly, tracer was allowed to circulate within the cartridge for 24 h in one experiment and then fluorescence emissions were obtained with the fluorimeter in a similar manner as for the conventional 1-hour transport experiments. When processing the data from these results it was found that the tracer circulating within the system and the tracer in the cartridge were not at equilibrium, contrary to expectations. Instead, the tracer concentration in the cartridge space was higher than that inside the fibres, suggesting that active transport from the fibre lumen to the cartridge space may have occurred.

This possibility was investigated further. The 24-hour experiments were repeated with and without cells present in bioreactors to determine if it was plausibly a result of active processes rather than some artefact; pulsatile and steady flow conditions were used in an attempt to modulate the behavior of the cells. Additionally, rhodamine-labelled dextran (70 kDa, Sigma-Aldrich) of similar mass to albumin was used as a tracer, at the same concentration (1mg/ml) as the albumin, for 1-hour and 24-hour

experiments under pulsatile and steady flow, as a negative control; it was considered unlikely that any receptors responsible for active transport would recognize dextran. Furthermore, Dynasore (Adipogen), an inhibitor of vesicular transport, was also added to the system under pulsatile flow conditions at concentrations of 40 µM for 1-hour and 80 µM for 24-hour experiments, to see if inhibition of dynamin ring formation had an effect on the observed excess of tracer in the extracapillary compartment at 24 h. It was also added to determine whether the inhibition of transcellular transport had an effect on the transport of tracer across the cell monolayer via the paracellular route, since there is reciprocal regulation of the transcellular and paracellular pathways (see above).

2.5 Imaging of confluent monolayers on Hollow Fibre membranes

Once the permeability experiments were completed for each bioreactor, the cells were fixed to the fibers with 4% paraformaldehyde using careful syringe movements from port A to port D. This protocol was later updated to the use of 15% formalin in the fiber and the cartridge space as the original fixation protocol did not work as well as expected. The fixation process for both methods was 1 h at room temperature with the bioreactor being rotated every half an hour. Once fixed the bioreactor and fibers were rinsed three times with PBS (Sigma-Aldrich) before the bioreactor was opened with a pipe cutter. Individual fibers were removed from the bioreactor and carefully sectioned with a razor blade. The cell monolayer is so delicate when on the fibers that it required the development of a custom built fiber jig for slicing the hollow fiber membranes. SEM verified the need for this jig - it was possible to visualize damage to the cell monolayer that occurred when sectioning by hand.

The first approach to imaging cells on the hollow fiber membrane employed nuclear staining with Draq-5 (Biosensors; 1/1000) followed by imaging with confocal microscopy. These experiments failed due to the high autofluoresence of the hollow fibres at any wavelength above 400nm. Since the cells and the fibre were in different optical planes, this problem should have been solvable by better optical sectioning. Multiple methods were incorporated to improve the rejection of out of focus light, including immersing the fibers in oils and other materials to homogenise the refractive index. Two-photon confocal microscopy was also attempted but the same issue of autofluorescence persisted. The two following techniques were then employed to gain useful images of a confluent monolayer on the hollow fibers.

The first of these techniques involved the staining of sectioned fibers for ten minutes with the UV (350nm) excitable nuclear stain Hoechst 3342 (1/1000) (ThermoFisher Scientific). With these shorter wavelengths, unusually, autofluorescence was less severe and the fibres were successfully imaged, using a Zeiss LSM-510 inverted confocal microscope.

The images demonstrated the presence of nuclei on the hollow fibers but did not give any further information about cell morphology. For this reason it was decided also to use scanning electron microscopy (SEM). All of the fixed samples were dehydrated in a series of increasing concentrations of ethanol (25-100% at 10 minutes each). The samples were stored in the 100% ethanol prior to being further dried using a critical point dryer (Samdri795, Tousimis) which replaced the ethanol with CO_2. The samples were then positioned onto individual conducting carbon pads on an aluminium stub. Each sample was coated with gold in a vacuum (1x 10^{-1} mBar, 20mA,) for 2 minutes. When imaged by the scanning electron microscope (JEOL JSM 5610 LV [0.5-35 kV]),

each specimen was introduced into the specimen exchange chamber ($1x10^{-1}$ mBar). The accelerating voltage of the electron beam was set to 20 kV and the emission current (Ie) set at a value of 10 µA. Images of each sample were acquired at increasing magnifications.

2.6 Flow Cytometry Analysis of Cells from Bioreactor

To gain more insight into changes in inter-endothelial cell junction formation within the bioreactor, flow cytometry analysis was conducted on cells taken from the bioreactors following static or chronic shear stress experiments to determine if there were any differences in PECAM-1 expression under the two conditions. (It was not possible to stain the fibres for PECAM-1 due to the autofluoresence problem described above.)

Cells were removed from the fibres of static and sheared bioreactors by 15 minutes of trypsinization in a similar solution to that used previously. The cells were flushed out of the bioreactor by being mixed between both entry ports. The cell suspension was then pelleted down using centrifugation (220 x g for 5 minutes). The pellet was resuspended in 4% paraformaldehyde solution for 20 minutes. The fixed cell suspension was then pelleted down again using centrifugation (220 x g for 5 minutes). The fixative was discarded and the pellet was resuspended in PBS for a rinse cycle. The cells were pelleted down again (220 x g for 5 minutes) and resuspended in a permeabilizing solution (0.1% TritonX-100, Sigma-Aldrich) and 10% goat serum (Jackson Immuno Research Labs) for 15 minutes and pelleted down (220 x g for 5mins).

The PBS rinse cycle was repeated with the inclusion of goat serum as a blocking agent. The PBS was removed and the cells were resuspended in a solution containing a rat anti-mouse-PECAM-1 antibody (1:300, BD BioSciences) for 1 h. The PBS rinse cycle and centrifugation step was repeated twice and cells were then resuspended in a solution of fluorescently conjugated secondary anti-rat antibody labeled with Alexa Fluor ® 594 (1:1000, ThermoScientific) for 20 minutes. The PBS rinse cycle and centrifugation step was repeated twice and cells were resuspended in PBS and passed though a cell strainer. A sample of fixed and rinsed cells without any labeling was used as a control for cell autofluoresence. All cells underwent FACS analysis (488-530 nm laser) using the Fortessa 1 at the flow cytometry facility in South Kensington.

2.7 Data Analysis

The statistical significance of differences was calculated using Student's *t*-test or ANOVA within each group of experiments and for all controls. The analyses were performed using GraphPad Prism Software (GraphPad Prism Software Inc, USA) and differences were deemed significant when the P-value was <0.05.

Within each experimental series there was a statistically-significant difference between the different conditions but no difference between bioreactors, so all bioreactors were treated as equal. When control bioreactor data from all experimental series were combined there were differences, so it was deemed necessary to compare between experimental and control data only within each group or experimental series.

Chapter 3 Results

3.1 Optimization of Porcine Aortic Endothelial Cell Isolation

One of the main requirements for the assessment of endothelial cell permeability was to have a stock of cells at a high density from isolation onwards, and a low percentage of contaminating cells. The need for a low proportion of contaminating cells arises because endothelial cells do not form tight junctions with other cell types, and that would lead to leaky monolayers. The need for high density cultures from P0 arises because cells at low density have a limited replication capacity and are more prone to senescence as they divide. Additionally, high density cultures become confluent in a shorter period of time, allowing additional time for the formation of tight junctions. This improves the efficiency and reproducibility of experiments. In initial studies, PAECs were isolated at a low density. The cells had difficulty becoming confluent within T25's and in some cases the cells did not remain seeded to the T25's. Solving this problem was a priority.

The original aortas used for isolations were obtained from Fresh Tissue Supplies. When isolating from 6 aortas, only 1-3 of the flasks would have cells the following day. In the flasks that did have cells, the cells were at a low density and required 7-10 days to become sufficiently confluent for passaging. These low densities following isolations are demonstrated in **Figure 8 [A-B]**. The problem was probably not due to human error as others within the lab were having difficulties in reproducibly conducting satisfactory isolations.

The first attempt to rectify the problem involved using a new stock of collagenase type II and increasing the incubation time with collagenase from 10 to 15 mins. Even with the new steps in place, however, there was very little change in the

low density P0 cultures (**Figure 8 [C-D]**) and it seemed as though the problem varied from vessel to vessel, which would not be the case if the collagenase were the problem.

As the aortas from FTS were kept overnight by the supplier following slaughter, poor (and variable) tissue quality might have been the reason for only obtaining a few cell clusters in each isolation. This led us to obtain aortas from a new tissue supplier, Cheale meats. The tissue from Cheale meats arrived in the lab on the day of slaughter. One day after the isolation of cells from these aortas using the same protocol (with increased exposure to collagenase type II), 6 out of 6 isolations gave high-density cultures (**Figure 9**). These positive results have been reproduced over the duration of the PhD. The P0 cells had no visible contamination with smooth muscle cells as assessed by phase contrast microscopy. The P0 cells were confluent and ready to be passaged within 3 days following isolation. Half-way through the PhD project, Cheale meats stopped supplying the aortas to the department but by then the quality of Aortas from Fresh Tissue Supplies had improved and isolations were successfully performed from that supplier.
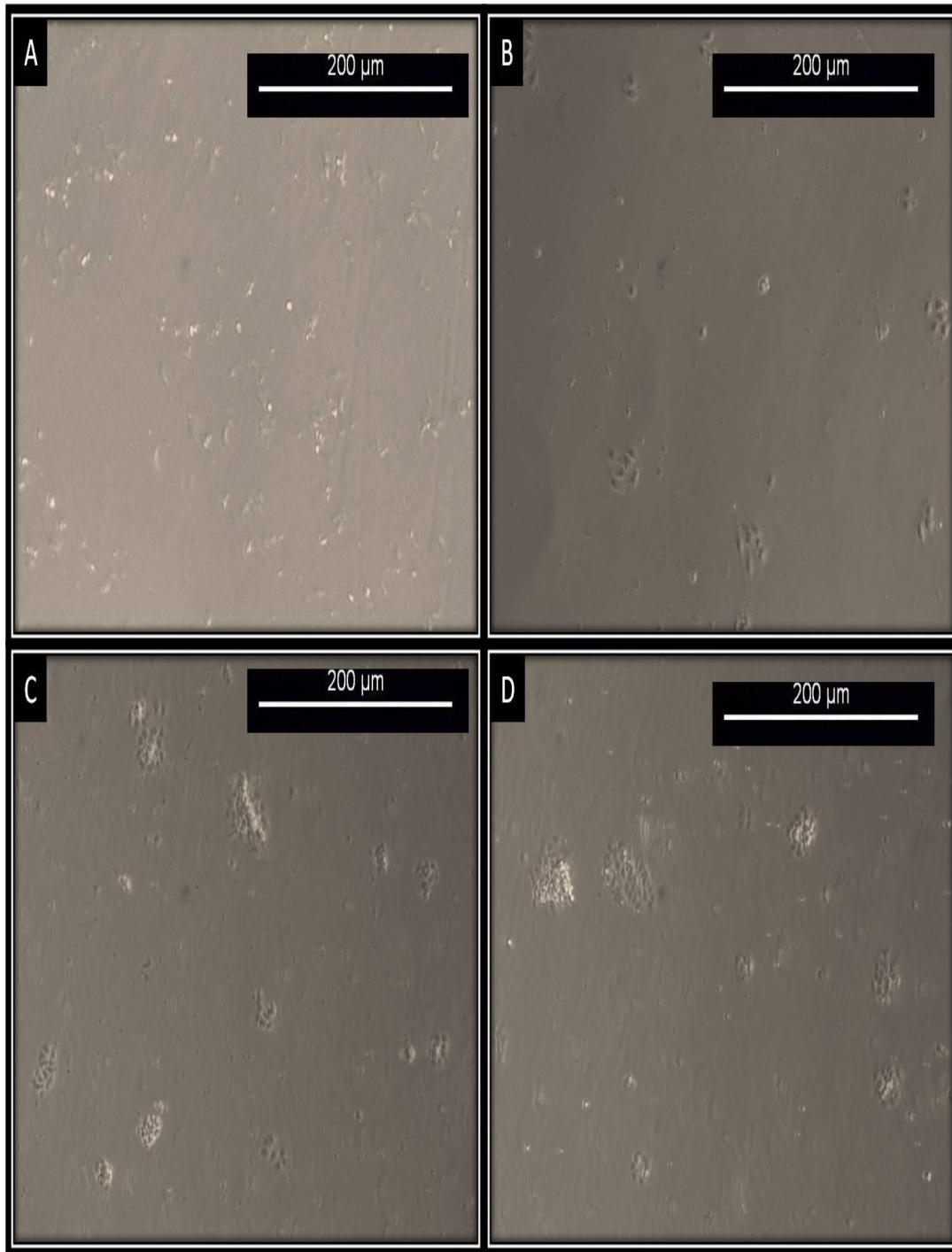
Figure 8 Images of low-density endothelial cell isolations

 [A-B] Phase contrast images of PAEC one day after isolation with a 10-minute exposure to collagenase type II. [C-D] Phase contrast images of PAEC one day after isolation with a 15-minute exposure to collagenase type II. The cells exhibit the standard cobblestone morphology of ECs. There were few cell clusters present in the T25 flasks. The space between cell clusters was too great for cells to become confluent within a few days.
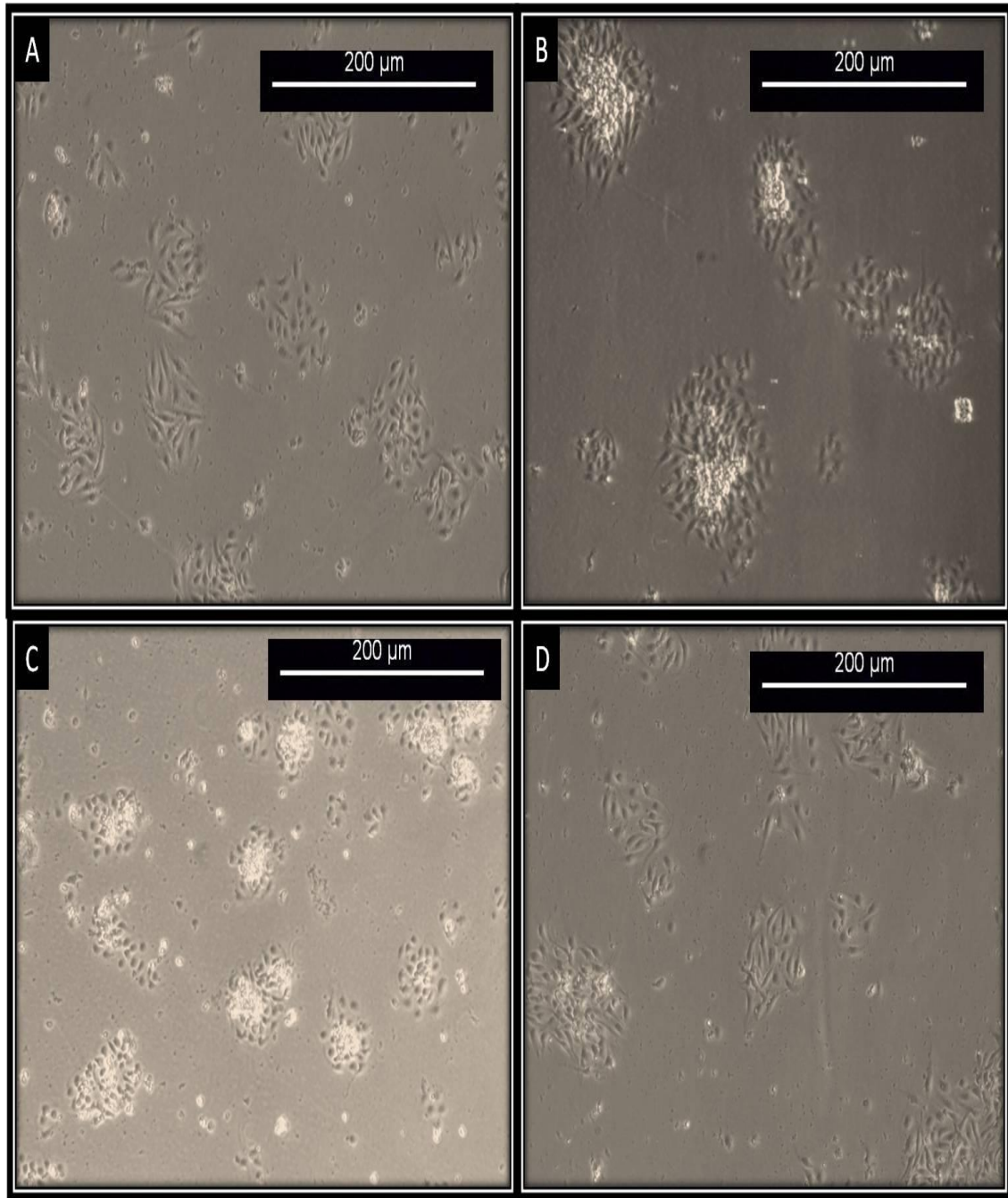
Figure 9 Images of high-density endothelial cell isolations

[A-D] Phase contrast images of PAEC one day after isolation with a 15-minute exposure to collagenase type II. The cells exhibit the distinct cobblestone morphology of ECs. Note the increase in cell clusters in close proximity. These cells were confluent within 2 days of culture.

3.2 Validating the purity of porcine aortic endothelial cells following isolations for bioreactor experiments

Although it was possible to determine from simple microscopical observations whether the cultures contained substantial contamination by cells that lacked a cobblestone morphology, it was essential for all experiments that involved permeability that the isolations gave better than 99% endothelial purity, in order to obtain physiologically relevant results.

Endothelial cell purity was assessed from the internalisation of Dil-labelled acetylated LDL. The fraction of cells taking up Dil-acetylated-LDL (**Figure 10**) was 99.72% (SEM 0.07%; n=5 isolations).
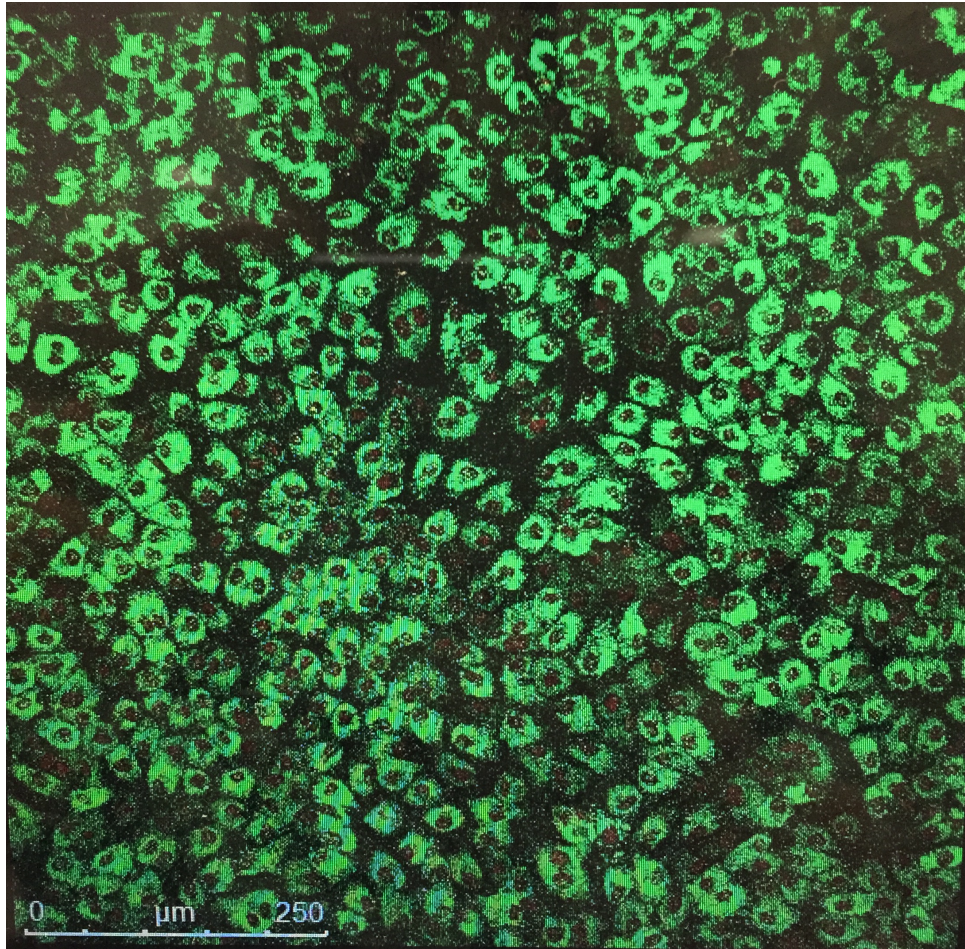
Figure 10 Confirmation of endothelial cell purity with Dil-acetylated-LDL

An image taken from a sample of endothelial cells incubated with Dil-acetylated-LDL demonstrated that the cells had better than 99% purity, which was confirmed with the use of Matlab software for cell counting.

3.3 Imaging of endothelial monolayers on hollow fibre membranes

One of the primary drawbacks of the bioreactor system is the difficulty of imaging cells on the hollow fibre membranes. Attempts were made with multiple nuclei and membrane staining techniques but the only one that succeeded was the Hoescht UV fluorescent stain for cell nuclei.

The Hoescht staining of the hollow fibers provided evidence for confluence because there were no obvious gaps (**Figure 11**), but a rigorous conclusion required Scanning Electron Microscopy (SEM), which shows the cells as well as the nuclei. As demonstrated by **Figures 12-13** there was a visible difference between hollow fibers with cells present on the membrane and those without cells. Furthermore, the cell-cell junctions show the position of the endothelial cells, and it was apparent that the monolayers were confluent.
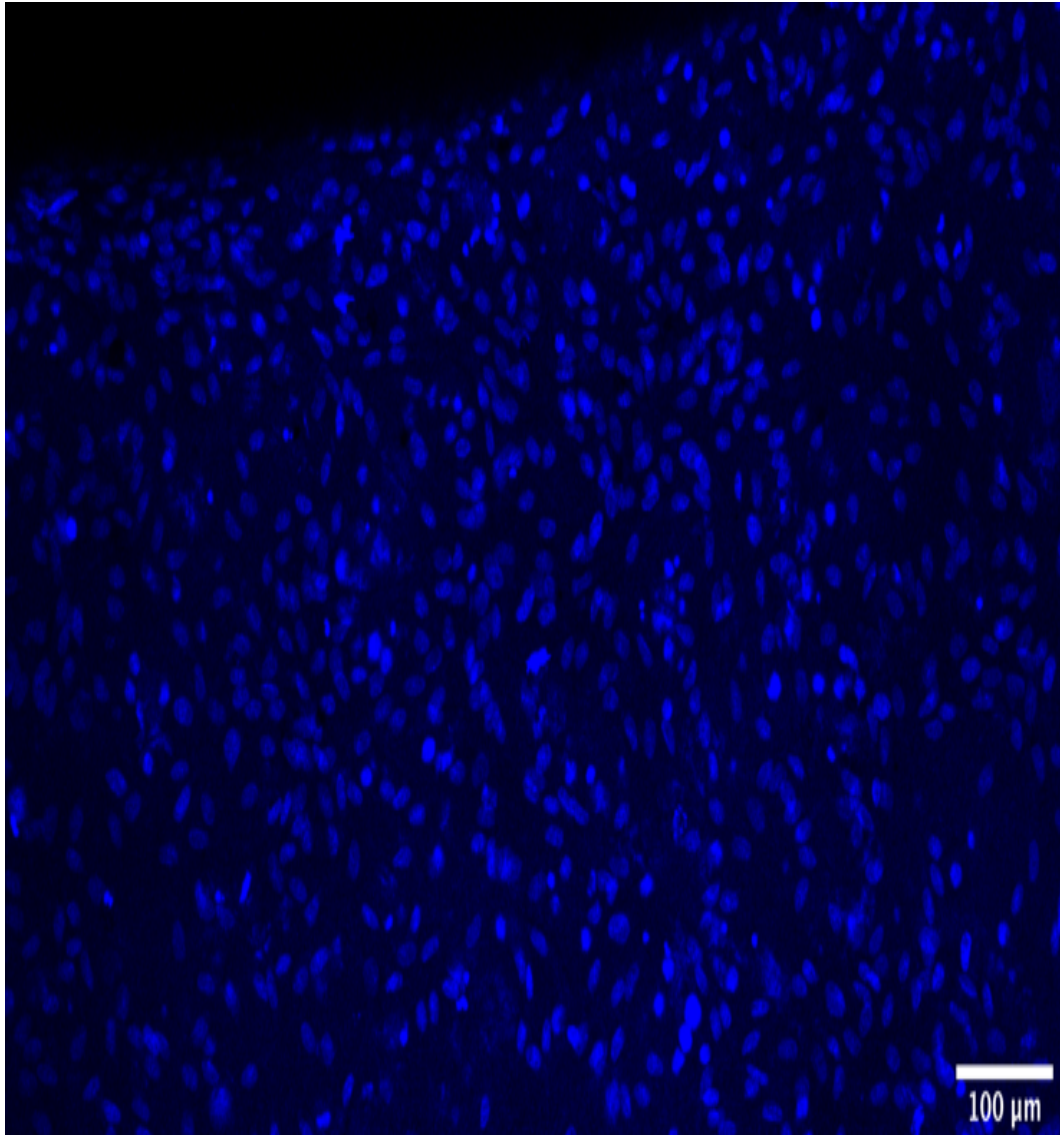
Figure 11 Hoescht staining of endothelial cell nuclei on hollow fibres

Cell nuclei on the hollow fibre membrane were successfully stained with the Hoescht nuclear stain. This method demonstrated an endothelial monolayer with no visible background autofluorescence. It provided evidence for confluence because there were no obvious gaps. This sample was from a bioreactor that experienced chronic shear stress for approximately 20 days prior to fixation.
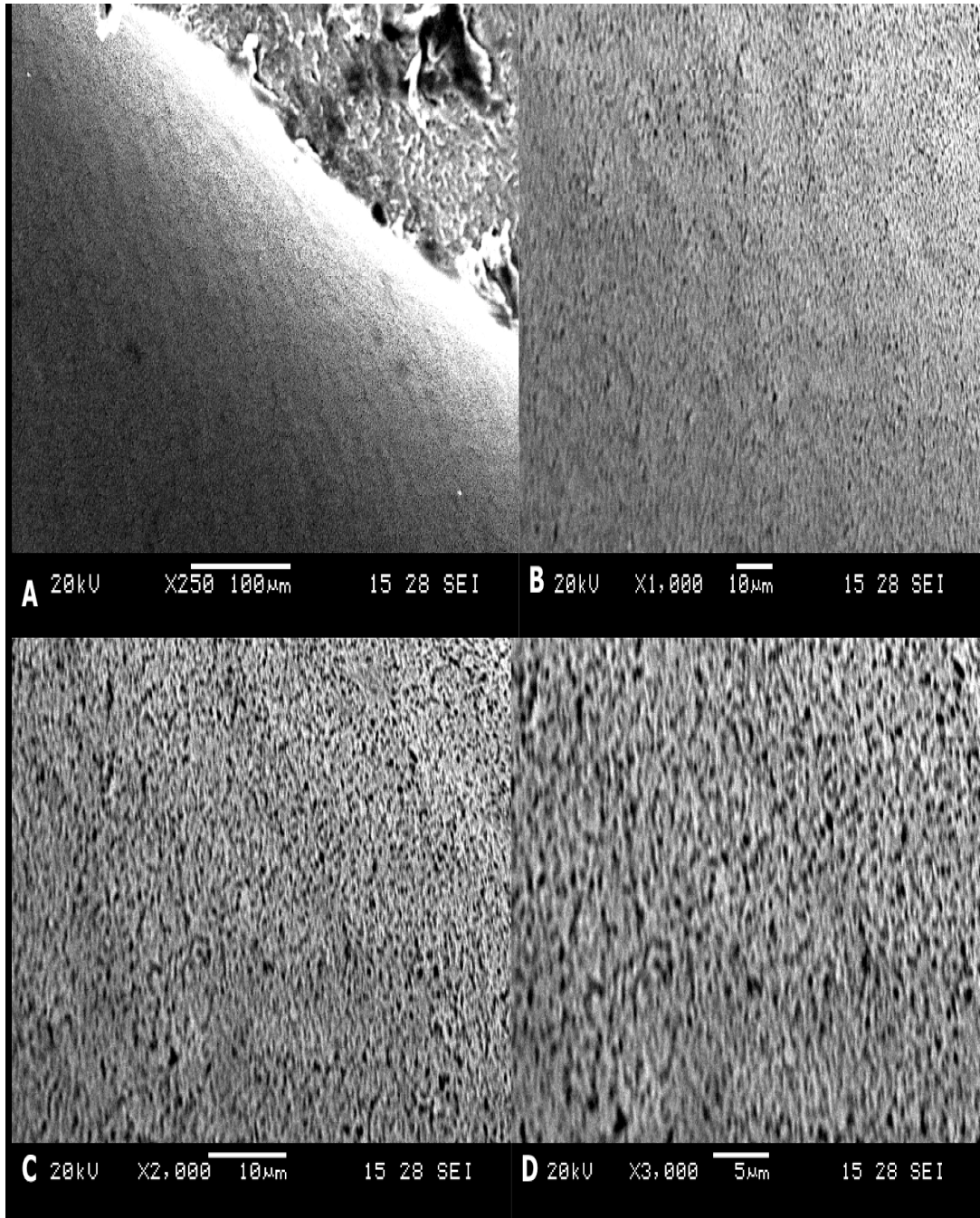
Figure 12 Scanning electron micrographs of hollow fibre membrane

In these control (i.e. cell free) SEM images it is possible to visualize the porosity of the membrane. The images increase in magnification from A-D. At the highest magnification it can be seen that the pore size is below 1µm.
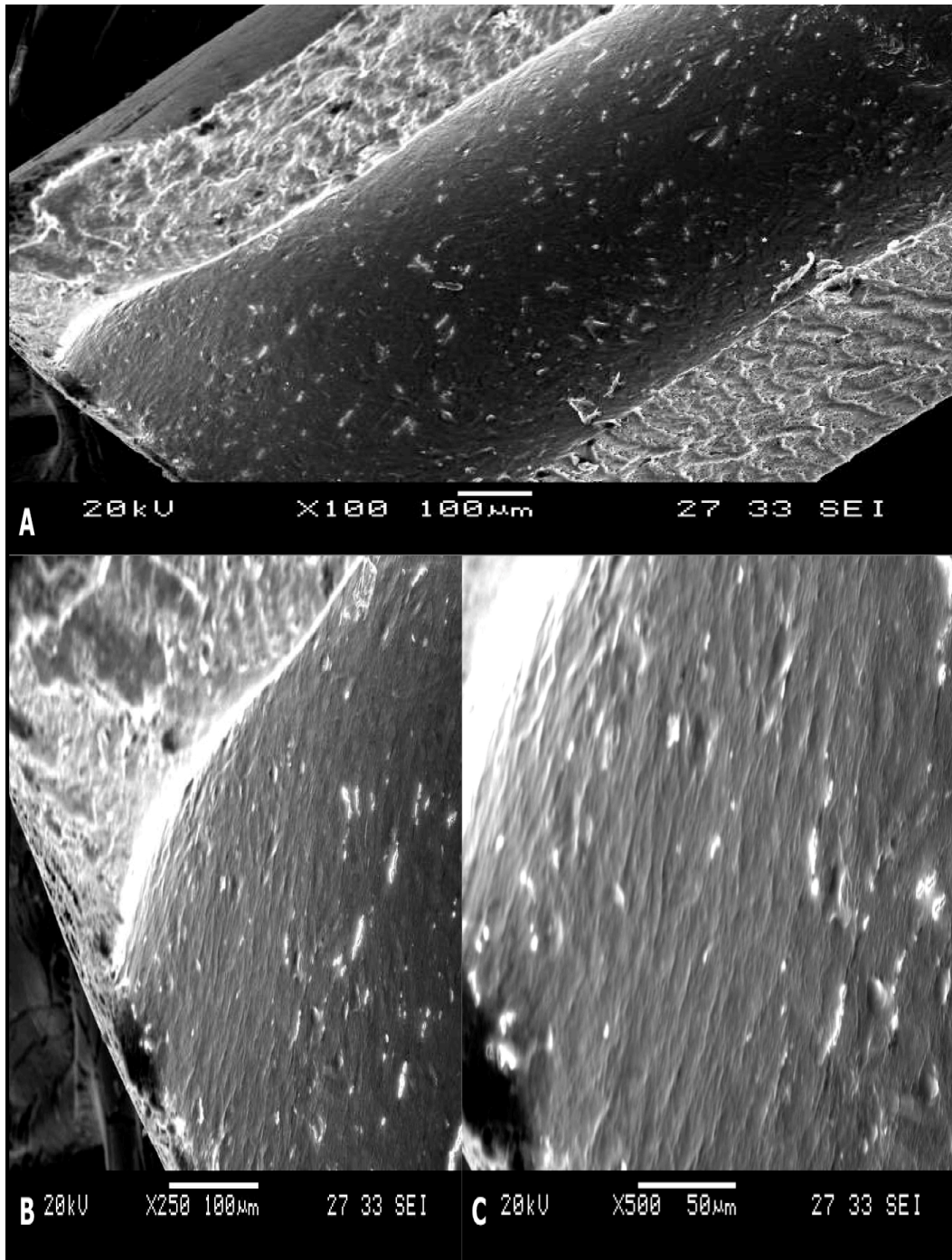
Figure 13 Scanning electron micrographs of confluent monolayer on hollow fibres

Images [A-C] taken at increasing magnifications show that cells remained confluent on the hollow fiber membranes after prolonged experiments.

3.4 Testing the monolayer by monitoring glucose and permeability changes over time

Due to the difficulties associated with imaging of the cells within the bioreactor during each experimental series, alternative validation methods were used to assess confluence. It was possible to determine the percentage of cells that seeded to each bioreactor, but further studies were required to gain a better understanding of what was happening within the bioreactors over time. The first validation method was the monitoring of glucose consumption, a method for confirming the presence of a confluent monolayer of cells used by previous investigators. Following the instructions for the FiberCell Bioreactor System the glucose concentration of the cell medium was monitored and medium was changed when it was approximately 50% depleted.

The consumption of glucose over time demonstrated that the cells were metabolizing. Glucose measurements were taken every two days and once the concentration of glucose dropped to 50% the experimental series were initiated. **Figure 14** demonstrates the average concentration of glucose over time for all bioreactors (n=27). A linear segment from 2 days to 6 days indicates that a steady state (as opposed to a growth phase) was occurring during this period and is consistent with the cells having formed a confluent monolayer 2-3days after seeding. (Fibercell also stated that cells would normally be confluent by two days following cell seeding based on previous studies and research publications.) After 6 days, there was a reduction in the rate of decrease meaning that the rate of glucose consumption has slowed down; this is attributed to metabolism having switched to alternative fuel and indicates the need for glucose to be replenished in the medium. Monolayers were not used for tracer experiments as soon

as they had formed (i.e. at 2-3 days) but after waiting for over a week, to give time for

the formation of a stable monolayer with tight junctions.
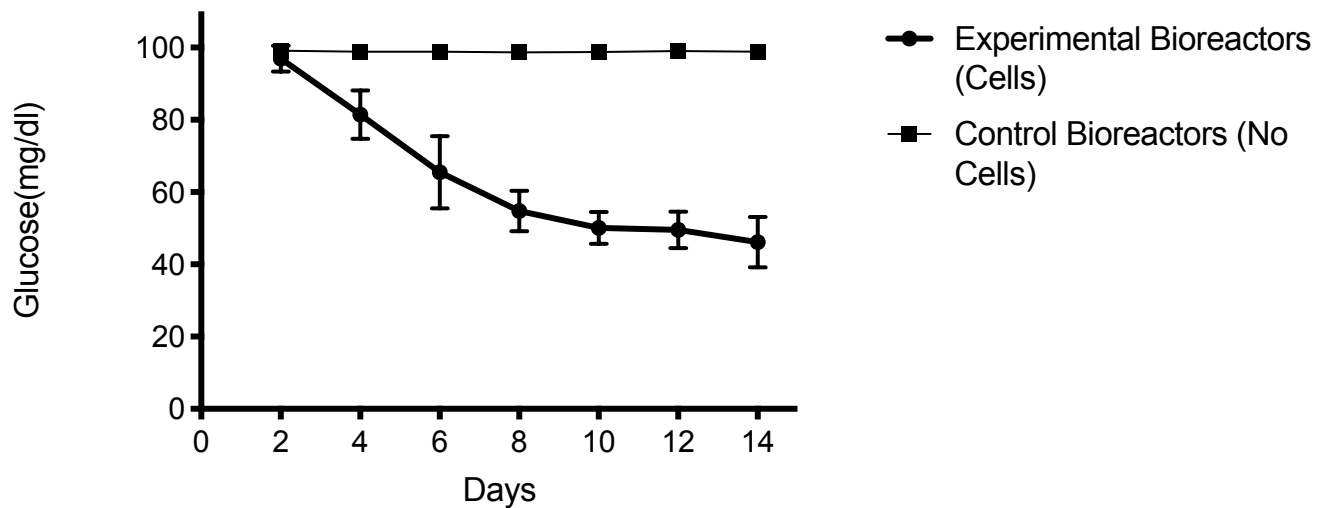
Figure 14 Glucose consumption over time in the hollow fibre bioreactor

Glucose concentration in the medium was measured every second day and experimental series were only started when glucose reach a depletion level of approximately 50%. Note not all bioreactors reached 50% glucose depletion within 12 days: it ranged from 10-16 days in different bioreactors. This graph represents the mean± SEM of all experimental bioreactor experiments (n=27).

A second technique incorporated into this testing or validation stage was studying the differences in tracer permeability with cells in the bioreactors over time. At day one following the seeding of all bioreactors a tracer measurement was made to understand the baseline permeability value with cells present within the bioreactor. It was used as

a way to determine what the permeability of the endothelial cells to tracer was like prior to the cells forming a confluent monolayer with tight junctions. Once the glucose consumption had reached 50% depletion the medium was changed, and permeability tracer experiments were initiated. The tracer experiments were continued over time, permeability being assessed every 2-3 days. A lower permeability value would indicate a more confluent monolayer or tighter barrier formation.

Figures 15 and **16** show data from a series of test-phase glucose and permeability measurements made in four bioreactors that were exposed to the standard pulsatile chronic shear stress conditions. Although there was some variation in the permeability measurements in the four test bioreactors, for each individual bioreactor the permeability of the monolayer stabilized at a lower value than the original permeability value taken following cell seeding, thus indicating the formation of a confluent monolayer or tight junction formation between cells.

These experiments served as an indication for all future experiments of what permeability was to be expected for a confluent monolayer under pulsatile chronic shear stress conditions. Permeability values changed over time under different experimental conditions such as static or acute shear stress and often in a different order for different bioreactors. However, pulsatile chronic shear stress tracer measurements were always incorporated into the susequent experimental series as the cell controls, in addition to cell free controls, to permit comparison with the data presented in the testing and validation stages and hence to ensure the presence of a confluent monolayer.
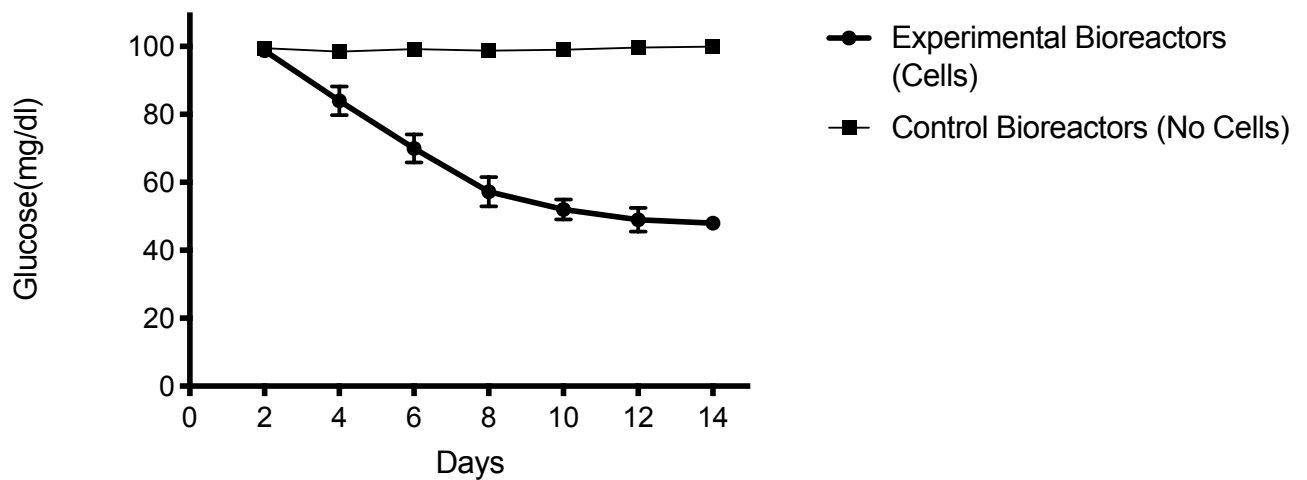
Figure 15 Glucose consumption over time under chronic shear stress validation experiments in hollow fibre bioreactor system

Glucose (mg/dl) concentrations in the medium were measured every second day in bioreactors (n=4) that were exposed to chronic pulsatile shear. Note not all bioreactors reached 50% glucose depletion within 12 days. Two of the four bioreactors reached this 50% reduction by day 10. Data are shown as mean±SEM.
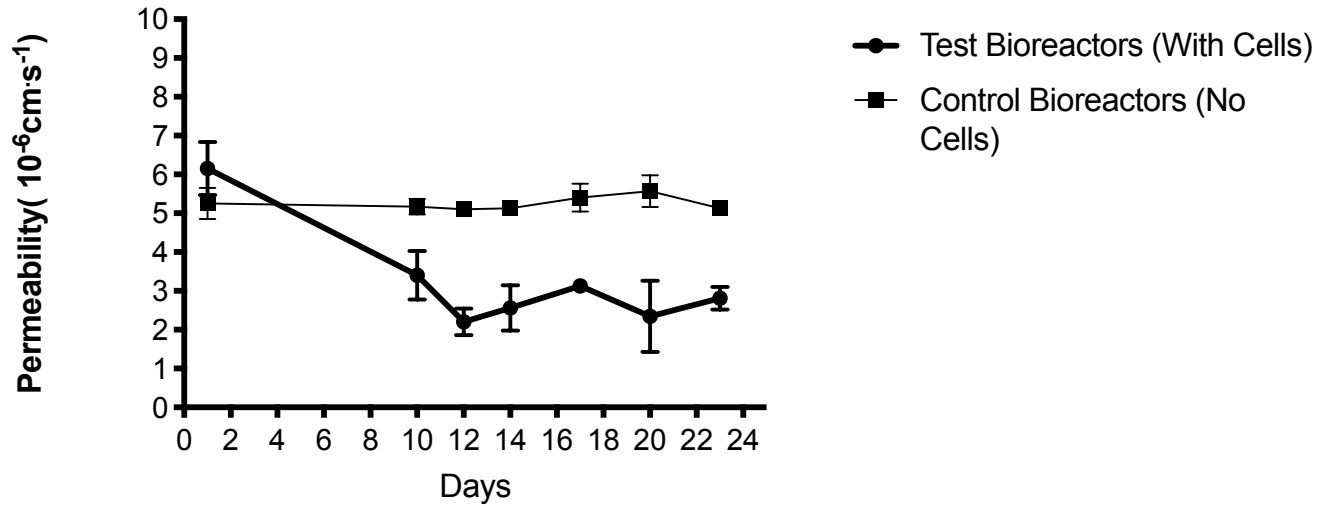
Figure 16 Cell permeability to Rhodamine-labelled albumin over time under chronic shear stress validation experiments in hollow fibre bioreactor system

Permeability to rhodamine-labelled albumin determined in four bioreactors exposed to chronic pulsatile flow. The first measurement was made following cell seeding and all subsequent readings were taken after glucose reached 50% reduction as indicated in Figure 16. Not all permeability readings for each bioreactor were taken on the same days due to differences in when each bioreactor reached 50% glucose depletion. Permeability to rhodamine-labelled albumin was also measured for control bioreactors. Data are mean±SEM.

3.5 The effects of acute and chronic shear stress

3.5.1 Effects of shear stress on permeability in hollow fibre bioreactors

The average permeability value for the hollow fibre membrane alone was 5.05×10^{-06} cm/s^{-1}. This membrane permeability (P_m) value was used to determine the resistance of the hollow fiber membrane alone, and this value was subtracted from the resistance obtained in experiments with cells present to give the resistance of the cells alone. The permeability of the cell monolayer was then obtained from the reciprocal.

The first series of experiments (**Table 1**) involved the confluent monolayers being acutely (4 h) or chronically (3-7 days) exposed to pulsatile flow that gave a mean wall shear stress of 3.75 dynes/cm^2, or to static conditions. The permeability (Mean ± SEM) of cells to the tracer was increased by acute pulsatile shear ($8.78 \pm 0.62 \times 10^{-06}$ cm/s; n = 14; $p < 0.0001$) (**Figure 17)** and decreased by chronic pulsatile shear ($2.57 \pm 0.24 \times 10^{-06}$ cm/s; n = 9; $p < 0.0001$) (**Figure 18**) compared to static conditions ($5.09 \pm 0.25 \times 10^{-06}$ cm/s^{-1}; n = 13).

Table 1 Permeability experiments for static conditions and acute and chronic shear stress

Bioreactor	Conditions	Permeability Values x10^{-06}
E	Static	6.38
E	ASS	10.6
E	CSS	1.6
E	Static	7.27
E	ASS	6.18
E	CSS	1.8
E	Static	3.5
E	ASS	8.13
E	Static	3.2
E	ASS	5.52
F	Static	4.31
F	ASS	8.2
F	CSS	2.76
F	Static	4.6
F	ASS	11.9
F	CSS	2
F	Static	5.39
F	ASS	8.53
F	CSS	2.22
F	Static	4.82
F	ASS	6.98
F	CSS	3.67
F	Static	4.14
F	ASS	5.89
G	Static	5.44
G	ASS	8.75
G	CSS	3.11
G	Static	4.94
G	ASS	13.11
G	CSS	2.22
G	Static	5.61
G	ASS	8.98
G	Static	5.22
G	ASS	7.9
G	Static	2.62
G	ASS	6.44
G	CSS	11.89

Table 1 Permeability experiments for static conditions and acute and chronic shear stress
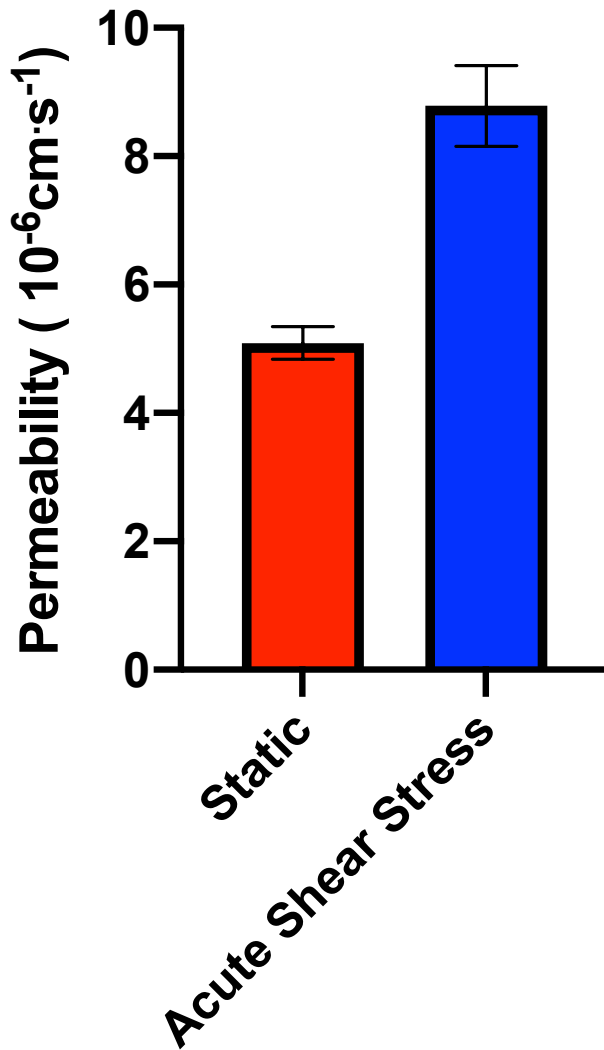
Figure 17 The effect of acute pulsatile shear stress on endothelial permeability in the bioreactor

The exposure of the endothelial monolayer to 4 h of pulsatile flow (acute shear stress) led to an increase in permeability of cells to the tracer (8.78 ± 0.62 x10^{-06} cm/s; n = 14; $p < 0.0001$) when compared to the permeability of the cells under static conditions (5.09 ± 0.25 x 10^{-06} cm/s; n = 13). Mean $\pm$ SEM and t-test values.
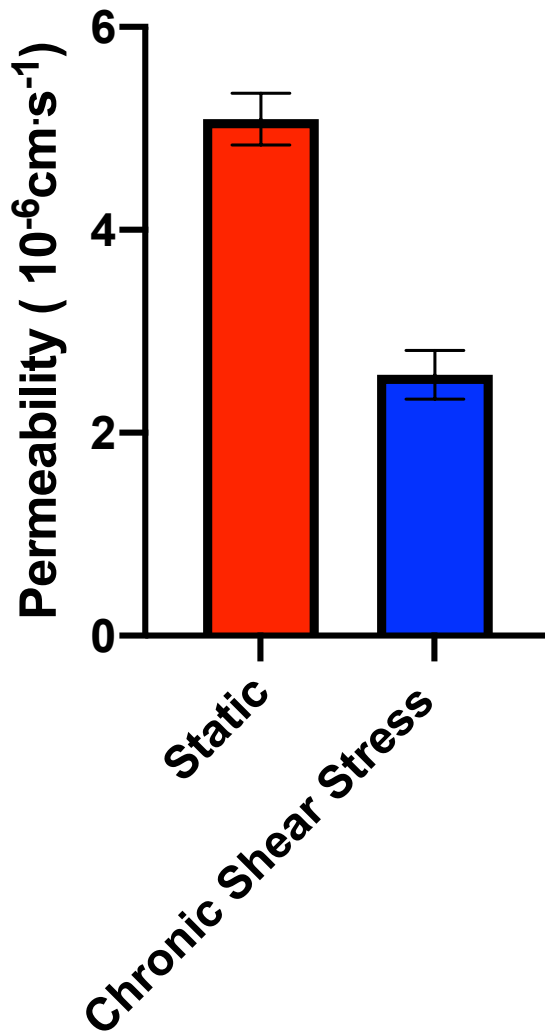
Figure 18 The effect of chronic pulsatile shear stress on endothelial permeability in the bioreactor

The exposure of the endothelial monolayer to 3-5 days of pulsatile flow (chronic shear stress) led to a decrease in cell permeability ($2.57 \pm 0.24 \times 10^{-06}$ cm/s; n = 9; p < 0.0001) when compared to static conditions ($5.09 \pm 0.25 \times 10^{-06}$ cm/s; n = 13). Mean $\pm$ SEM and t-test values.

3.5.2 Flow cytometry analysis of cells exposed to static conditions or shear stress

Although the use of UV fluorescent stains and Scanning Electron Microscopy provided confirmation of endothelial cell presence and confluence, further work was required to obtain insight into what was happening at junctions or with receptors. FACS analysis was used for this purpose in the first experimental series as a validation step but also to determine if there were any differences in the protein expression under the different experimental conditions.

The median Raw Fluorescence Unit (RFU) data from the flow cytometry analysis (**Figure 19**) demonstrated a proportionally small but statistically significant decrease in PECAM-1 expression under chronic pulsatile flow when compared to static conditions (mean ± SEM values of 624.4 ± 29.76 for chronic pulsatile flow vs. 720.8 ± 25.89 for static conditions, n=11, p=0.0239). The antibody-free cell control gave a mean ± SEM value of 185 ± 48.5; n=11.
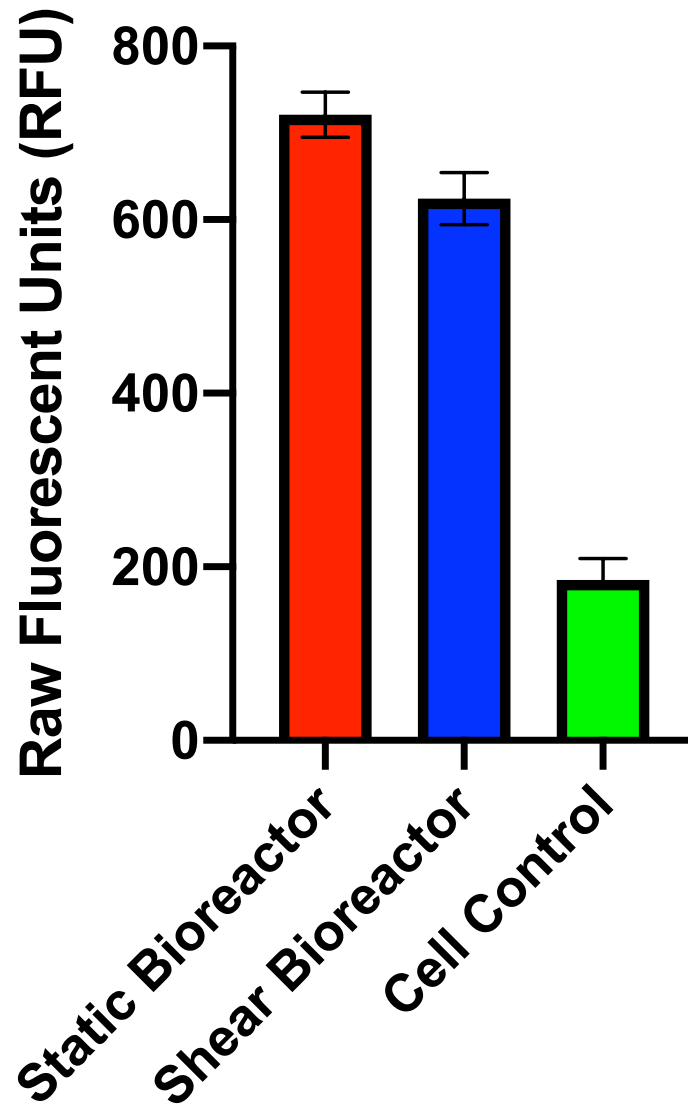
Figure 19 FACS Analysis of PECAM-1 in cells exposed to static conditions or chronic shear stress in hollow fibre bioreactors

Chronic pulsatile shear stress caused a small but statistically significant decrease in PECAM-1 expression when compared to cells from a static bioreactor (n = 11, p = 0.0239). The antibody-free cell control was carried out to indicate background autofluorescence during the FACS analysis. Data are Mean ± SEM.

3.6 The effect of medium viscosity on endothelial permeability bioreactors

This series of experiments (**Table 2**) was carried out to distinguish between effects of shear rate and shear stress on permeability. Xanthan Gum (XG, Sigma Aldrich, 0.69 g/l) was used to increase the viscosity of the circulating medium. The presence of XG would cause some increase in osmotic pressure but this would not have directly affected transport across the endothelium because there was a constant volume of extra-capillary space and hence no transendothelial flux of water. It may have had an influence on permeability through the removal of water from the endothelial cells. However, static experiments provided controls for such potential side effects. Experiments were carried out as before, following the pattern of static, acute, and then chronic shear stress.

The permeability (Mean ± SEM) of cells to the tracer under increased viscosity was increased by acute pulsatile shear (5.77 ± 0.60 x 10^{-06} cm/s; n = 7) (**Figure 20)** and decreased by chronic pulsatile shear (1.17 ± 0.19 x 10^{-06} cm/s; n = 11) (**Figure 21)** compared to static conditions (4.43 ± 0.41 x10^{-06} cm/s; n = 7). The increase under acute shear stress conditions was not statistically significant in comparison with the static result ($p = 0.0916$) whereas the reduction under chronic shear stress was ($p < 0.0001$). The results suggest that increasing viscosity (and hence shear stress, but not shear rate) decreases (and perhaps abolishes) the permeability-increasing effect of ASS and perhaps increases the permeability-reducing effect of CSS.

In comparison with the results from the first experimental series it is important to note that the increased viscosity had an effect on the monolayer under the applied shear stresses, which is demonstrated in **Figure 22**. In the acute shear stress

experiments the presence of xanthan gum generated permeability results that were significantly lower than the first experimental series (p = 0.0067). The chronic shear stress value with high viscosity was also lower than that from the first series of experiments (p = 0.0002), suggesting a need for media with increased viscosity for more physiologically relevant permeability results in other 2D and 3D *in vitro* studies. There was no effect of increased viscosity under static conditions (p = 0.1718), consistent with an absence of an influence of the osmotic pressure of the gum on transport.

Table 2 Permeability experiments for static conditions, acute shear stress and chronic shear stress under increased viscosity

Bioreactor	Conditions	Permeability Values x 10^{-06}
X	CSS	2.3
X	CSS	1.9
X	CSS	0.83
X	Static	3.642
X	ASS	4.66
X	CSS	2.1
X	Static	2.86
X	ASS	3.96
X	CSS	1.07
Y	Static	4.8
Y	ASS	6.57
Y	CSS	0.986
Y	Static	3.51
Y	ASS	8.81
Y	CSS	1.04
Y	Static	5.86
Y	ASS	6
Y	CSS	0.4
Z	Static	5.05
Z	ASS	5.52
Z	CSS	0.87
Z	Static	5.32
Z	ASS	4.88
Z	CSS	0.7
Z	CSS	0.673
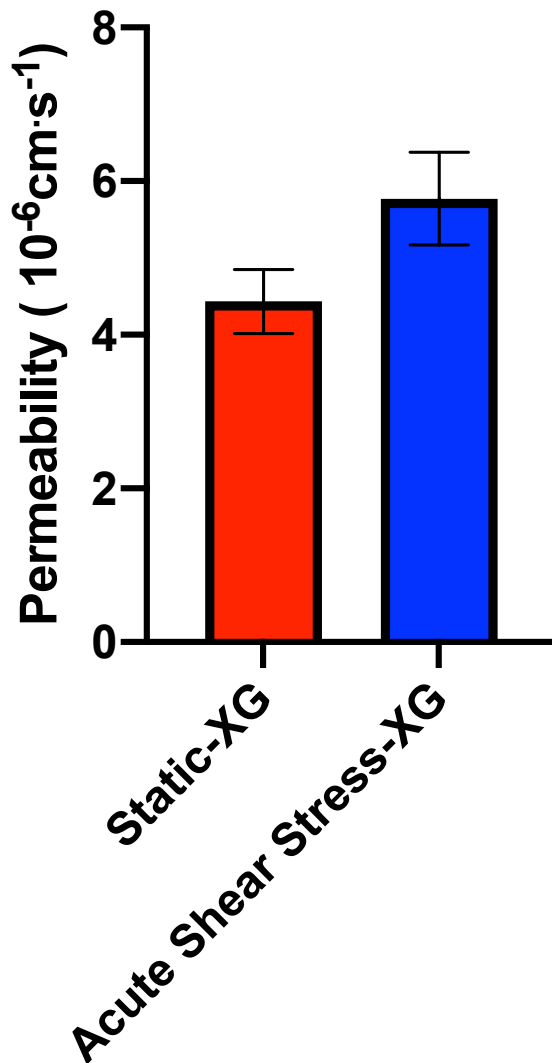
Figure 20 The effect of acute pulsatile shear stress on endothelial permeability under increased viscosity in the hollow fibre bioreactor

The exposure of the endothelial monolayer to 4 h of flow (acute shear stress) led to a non-significant increase in the permeability of monolayers to the tracer ($5.77 \pm 0.60 \times 10^{-06}$ cm/s; $p = 0.0933$) when compared to the permeability of monolayers under static conditions ($4.43 \pm 0.41 \times 10^{-06}$ cm/s; $n = 7$). Data are shown as mean $\pm$ SEM.
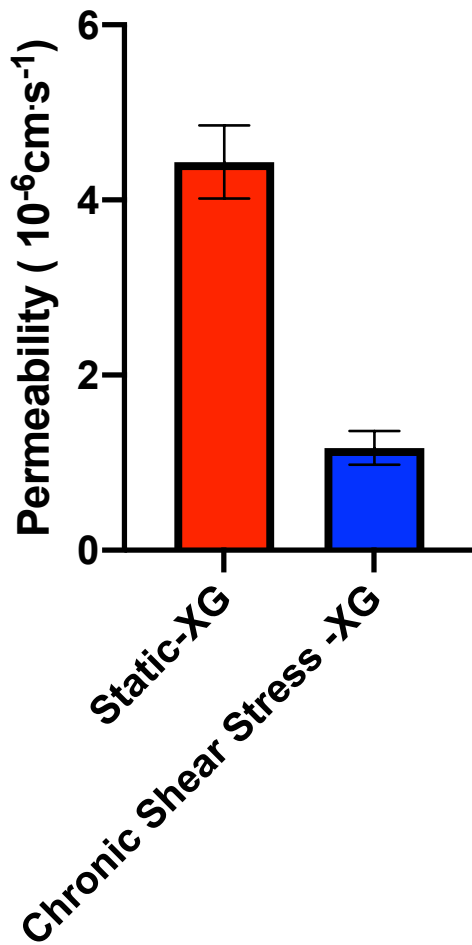
Figure 21 The effect of chronic pulsatile shear stress on endothelial permeability under increased viscosity in the hollow fibre bioreactor

The exposure of the endothelial monolayer to 3-5 days of pulsatile flow (chronic shear stress) led to a decrease in cell permeability ($1.17 \pm 0.19 \times 10^{-06}$ cm/s; n = 11; p < 0.0001) when compared to static conditions ($4.43 \pm 0.41 \times 10^{-06}$ cm/s; n=7). Data are shown as mean $\pm$ SEM.
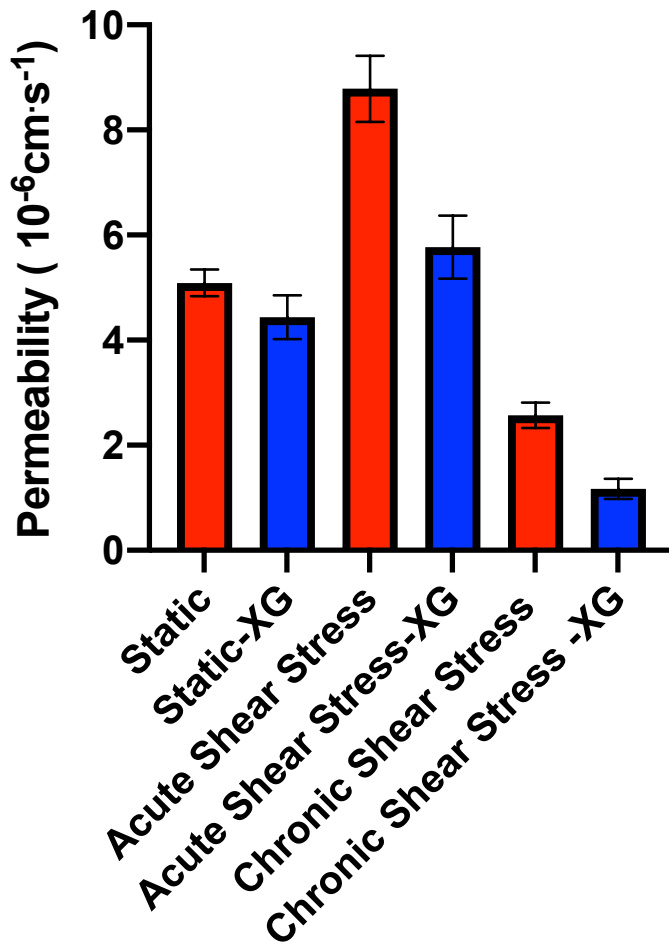
Figure 22 Effects of acute and chronic shear stress on permeability with and without increased viscosity of the medium in the hollow fibre bioreactor

Comparison between the permeabilities obtained with viscosity increased by xanthan gum (XG) and the permeabilities obtained in the first shear stress experimental series. Permeability values were higher under acute shear stress conditions without XG (n=14) than with it (n=7; p = 0.0067). The same trend was observed under chronic shear stress: permeability values were higher without XG (n = 9) than with it (n=11; p = 0.0002). Under static conditions, there was no statistically significant difference with the XG (n = 7) than without it (n = 13; p = 0.1718).

3.7 The effect of pharmacological agents on permeability under chronic pulsatile shear

Permeability was assessed before and after the introduction of pharmacological agents. Like the effects of shear, effects on permeability provided further validation that there was a confluent endothelial monolayer with intact barrier properties within the bioreactor system.

One set of pharmacological experiments (**Table 3**) involved exposing cells in the bioreactors to thrombin (10 U/ml) [105, 106]. Thrombin was allowed to circulate for 1 h under chronic pulsatile shear stress conditions and the tracer experiments were performed after that hour; results were compared to chronic shear stress conditions. The results shown in **Figure 23** demonstrate that thrombin significantly increased permeability to $8.26 \pm 0.75 \times 10^{-06}$ cm/s (n = 9) compared to chronic shear stress without thrombin ($3.27 \pm 0.425 \times 10^{-06}$ cm/s; n = 10; p < 0.0001).

A second set of experiments (**Table 4**) examined effects of L-NAME, a nitric oxide synthase inhibitor, under chronic pulsatile shear stress. L-NAME (500μM) was added to the bioreactor system for 24 h under chronic shear stress conditions before permeability was measured. The permeability ($5.62 \pm 0.62 \times 10^{-06}$ cm/s; n = 9) was significantly higher than the permeability for the controls ($2.89 \pm 0.18 \times 10^{-06}$ cm/s; n = 9; p < 0.0001) (**Figure 24).**

Table 3 Permeability experiments under chronic shear stress conditions with and without thrombin

Bioreactor	Conditions	Permeability Value x 10^{-06}		Bioreactor	Conditions	Permeability Value x 10^{-06}
B	Thrombin	12.2		B	CSS	6.43
B	Thrombin	7.45		B	CSS	3.16
B	Thrombin	8.17		B	CSS	3.32
I	Thrombin	11.45		B	CSS	3.92
I	Thrombin	7.33		I	CSS	2.44
I	Thrombin	9.14		I	CSS	2.18
W	Thrombin	6.9		I	CSS	1.79
W	Thrombin	6		I	CSS	2.08
W	Thrombin	5.7		W	CSS	3.6
Average		8.26		W	CSS	3.8
SD		2.277992537		Average		3.272
				SD		1.345608495
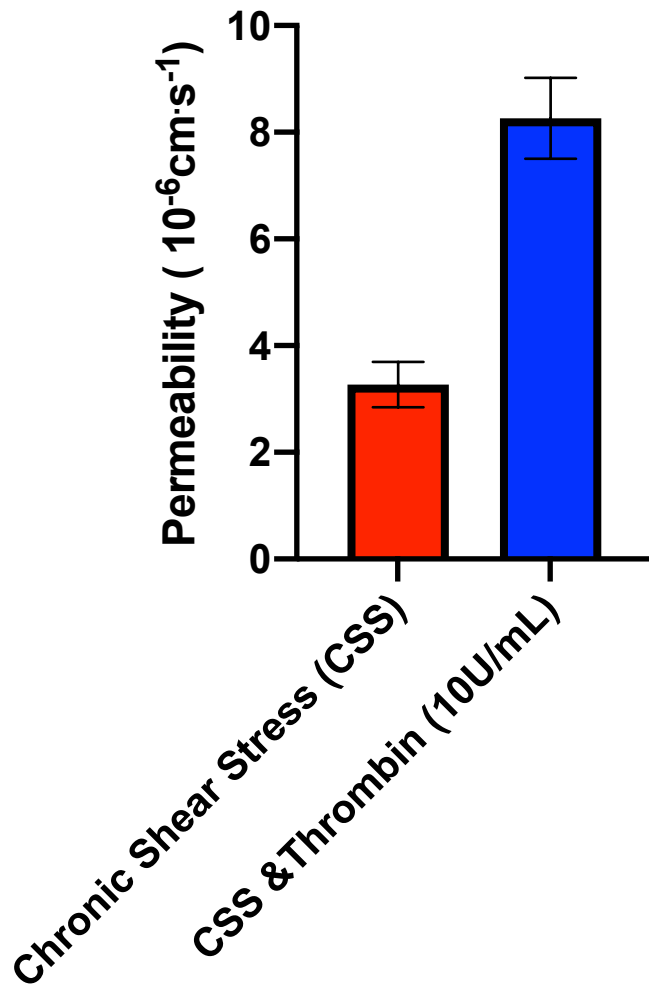
Figure 23 The effect of thrombin on endothelial permeability under chronic pulsatile shear

Permeability after thrombin (10 U/mL) was allowed to circulate for 1 h under chronic pulsatile shear stress conditions and under chronic shear stress conditions without thrombin. Thrombin significantly increased permeability to 8.26 ± 0.75 x10^{-06} cm/s (n = 9, p < 0.0001) compared to the chronic shear stress alone (3.27 ± 0.425 x10^{-06} cm/s; n = 10). Data are shown as mean±SEM.

Table 4 Permeability experiments under chronic shear stress conditions with and without L-NAME

Bioreactor	Conditions	Permeability Value x 10^{-06}		Bioreactor	Conditions	Permeability Value x 10^{-06}
C	L-NAME	4.4		C	CSS	2.7
C	L-NAME	5.1		C	CSS	2.5
C	L-NAME	4.8		H	CSS	4.08
H	L-NAME	8.68		H	CSS	2.9
H	L-NAME	6.03		H	CSS	2.48
H	L-NAME	6.3		H	CSS	2.715
H	L-NAME	8.04		U	CSS	3.4
U	L-NAME	4.046		U	CSS	2.8
U	L-NAME	3.268		U	CSS	2.4
Average		5.629333333		Average		2.886111111
SD		1.812811904		SD		0.537504522

Table 4 Permeability experiments under chronic shear stress conditions with and without L-NAME
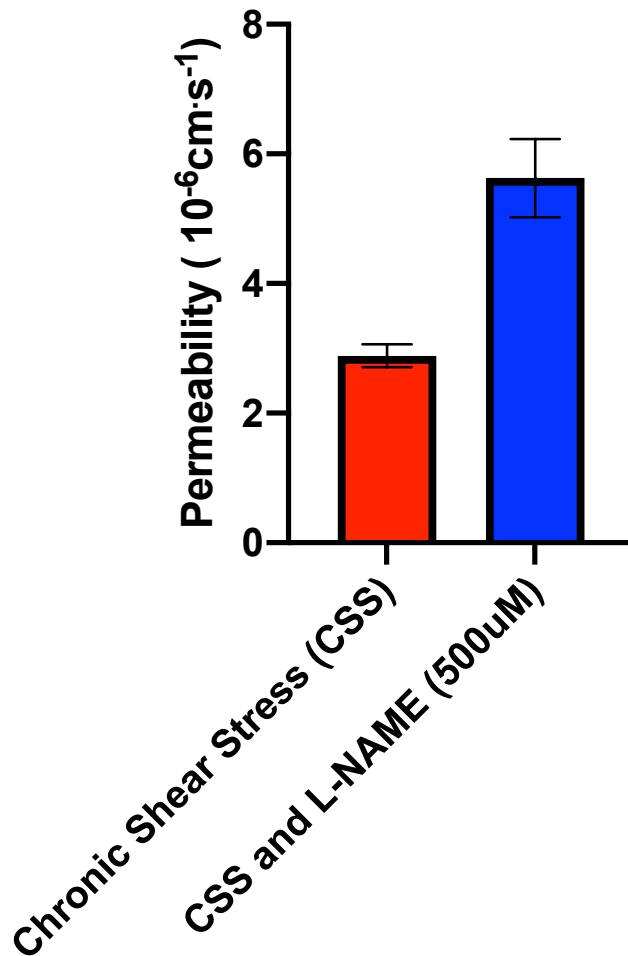
Figure 24 The effect of nitric oxide inhibition on endothelial permeability under chronic pulsatile shear

L-NAME (500 μM) was added to the bioreactor system for 24 h under chronic shear stress conditions before permeability was measured. There was a statistically significant increase in permeability ($p < 0.0001$) with L-NAME (5.62 ± 0.62 x 10^{-06} cm/s; n = 9) compared to chronic shear stress conditions without L-NAME (2.89 ± 0.18 x 10^{-06} cm/s; n = 9). Data are shown as mean±SEM.

3.8 The effect of flow waveform on endothelial permeability

3.8.1. Modification of the bioreactor to produce different flow types

This series of experiments determined permeability under the normal pulsatile flow, produced by the positive pressure displacement pump and valves described above, and under steady flow; chronic exposure was used for both flow waveforms. The hollow fibre bioreactors had to be modified to obtain steady flow. This waveform was obtained by the addition of four 50mL air-filled syringes to the flow circuit. The air in the syringes compressed and expanded as the perfusion pressure cyclically increased and decreased, damping the fluctuations in flow in the classical "windkessel" manner to an amplitude where it could be deemed "steady."

The Transonics ultrasound device was used to characterize the flow before and after the modification to the flow setup. **Figures 25 and 26** show the measured flow with zero, two and four 50 mL syringes attached to the bioreactor. Flow without any damping chambers resembled physiological flow in the aorta: there was forward-going flow over approximately one third of the cycle, then a period of reverse flow having smaller amplitude, and finally a period of low amplitude forward-going flow. The amplitude of the waveform decreased from approximately 24 to 3.5 to 1.5 ml/s with zero, two and four syringes; due to the use of a positive displacement pump, the mean flow will have remained constant.
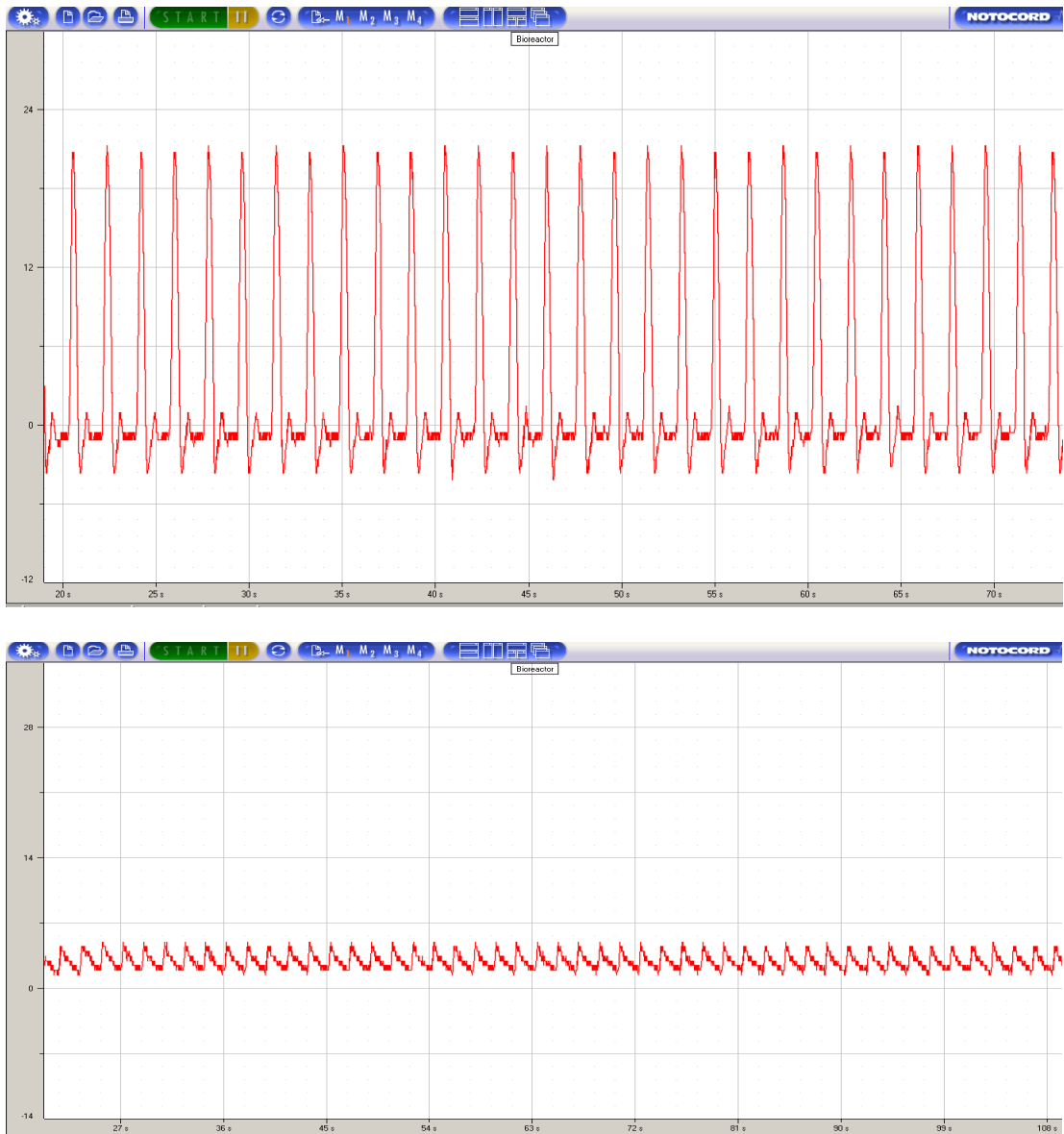
Figure 25 Control and damped flow waveforms

The images demonstrate the pulsatile (top) and steady (bottom, damped with four 50-ml air-filled syringes) flow waveforms, which was measured using the Transonics ultrasound device and Notochord software.

115
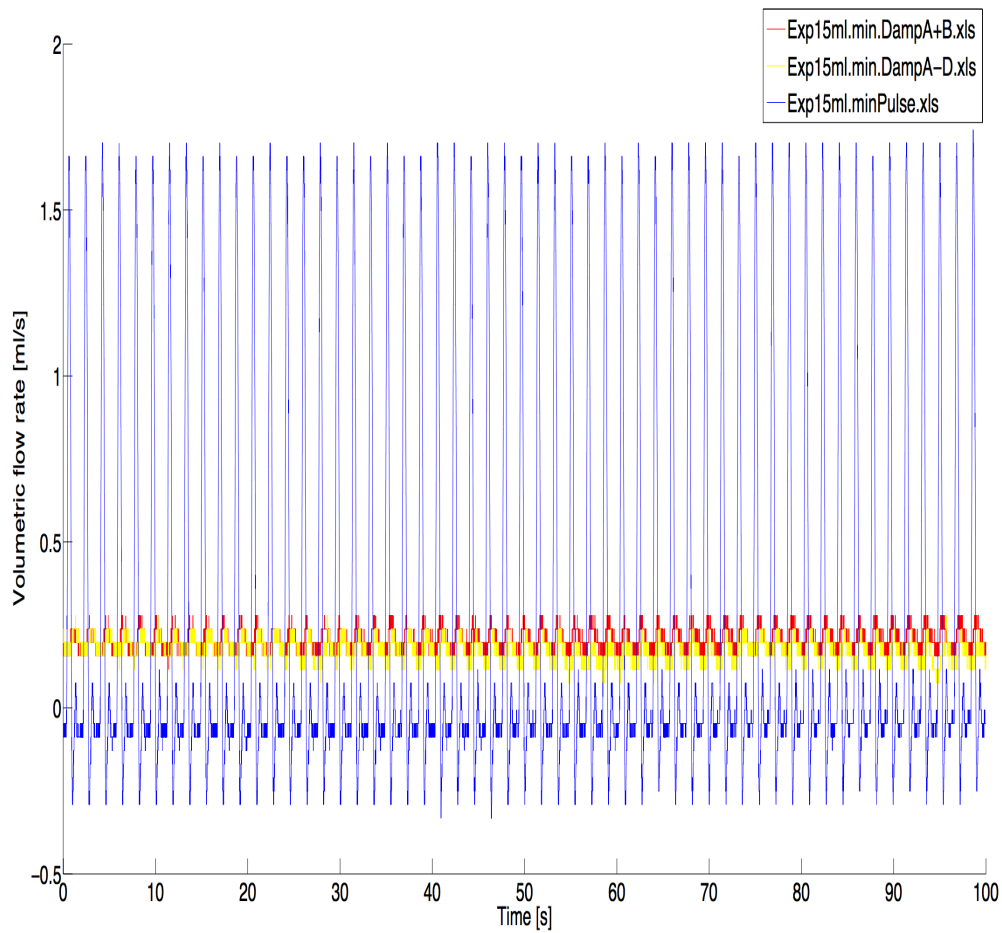
Figure 26 Control and damped flow waveforms

As in **Figure 25** except that flow waveform obtained with two air-filled syringes (red line) as well as zero syringes (blue line) and four syringes(yellow) syringes is shown, and the data are all plotted on the same graph to facilitate comparison of the mean flow rate.

3.8.2 The effect of steady flow on endothelial permeability

Endothelial cells within the hollow fibres of the bioreactor were exposed to pulsatile or steady flow over 3-10 days. Then 1-hour tracer experiments were performed as outlined in previous experimental series (**Table 5**). There was a statistically significant increase in endothelial cell permeability when cells were exposed to steady flow compared to the permeability values under pulsatile flow (**Figure 27**). Permeability (mean $\pm$ SEM) increased to 6.94 ± 0.87 x10^{-06} cm/s (n = 15) under steady flow conditions, compared to pulsatile flow values of 3.15 ± 0.218 x10^{-06} cm/s (n = 24). The difference was statistically significant (p < 0.0001).

Table 5 Permeability experiments under chronic steady and pulsatile flow

Bioreactor	Conditions	Permeability Value x 10^{-06}		Bioreactor	Conditions	Permeability Value x 10^{-06}
J	Pulsatile	2.86		j	Steady	9.5
J	Pulsatile	3.05		K	Steady	11.34
L	Pulsatile	1.6		K	Steady	15.3
L	Pulsatile	3.73		M	Steady	9.8
K	Pulsatile	3.14		N	Steady	5.89
K	Pulsatile	2.31		O	Steady	8.31
M	Pulsatile	3.76		P	Steady	3.92
M	Pulsatile	4.71		Qii	Steady	7.54
M	Pulsatile	2.59		Qii	Steady	4.82
N	Pulsatile	5.35		Qii	Steady	3.24
N	Pulsatile	3.27		Qii	Steady	4.79
N	Pulsatile	2.71		Qii	Steady	3.52
N	Pulsatile	3.44		T	Steady	5.2
O	Pulsatile	3.92		V	Steady	5.24
O	Pulsatile	4.24		V	Steady	5.63
P	Pulsatile	3.03		Average		6.936
P	Pulsatile	3.98		SD		3.365575306
Qii	Pulsatile	1.68				
Qii	Pulsatile	2.37				
T	Pulsatile	4.7				
T	Pulsatile	2.1				
T	Pulsatile	3.84				
V	Pulsatile	2.133				
V	Pulsatile	1.09				
Average		3.150125				
SD		1.069390087				
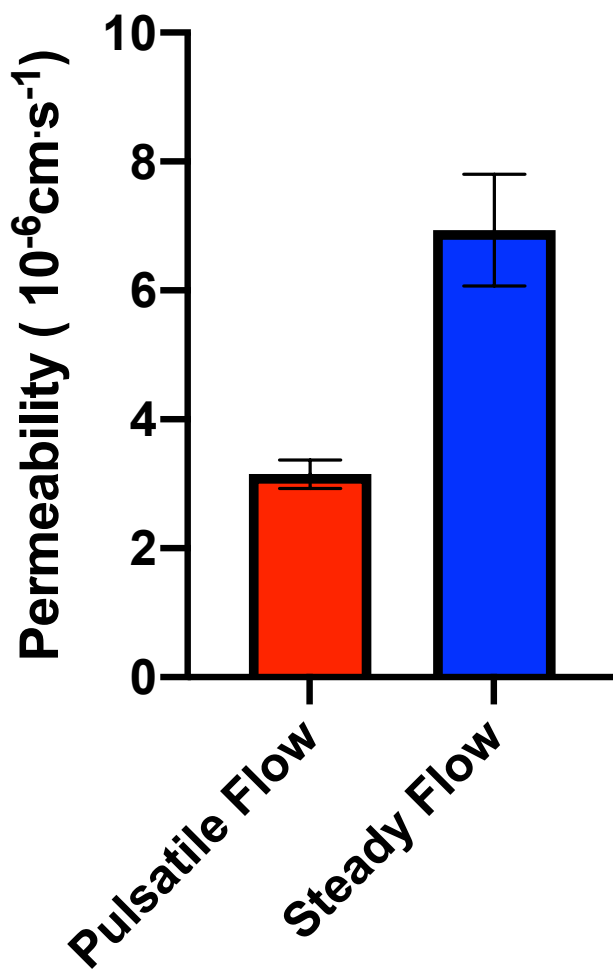
Figure 27 The effect of flow waveform on endothelial permeability in the hollow fibre bioreactor

The introduction of chronic steady flow led to a statistically significant increase ($p < 0.0001$) in endothelial permeability under steady flow conditions ($6.94 \pm 0.87 \times 10^{-06}$ cm/s; n = 15), compared to the normal pulsatile flow conditions ($3.15 \pm 0.218 \times 10^{-06}$ cm/s ;n = 24). Data are shown as mean $\pm$ SEM.

3.9 The effect of transmural flow on endothelial cell permeability

A second modification to the bioreactor system allowed the incorporation of transmural flow, in addition to axial flow. This was achieved by opening one extracapillary port after attaching a syringe with the plunger removed and a 0.22 um filter attached through an airtight joint – see **Figure 28**. This allowed air in the syringe to be replaced by fluid from the cartridge (the air leaving via the filter, which prevented contamination) and hence removed the constraint of a constant extracapillary space.

The modification coupled with the pressure difference occurring across the capillary walls resulted in approximately 0.1 ml/h of flow into the cartridge space and syringe; this flow could occur whilst maintaining the axial flow rate for one day, to accommodate the sealing effect. The meniscus in the syringe was monitored by eye and syringe and medium replacements were carried out as needed during the chronic pulsatile axial flow and transmural flow experiments by temporarily closing the tap. Frequent sterilization of the bioreactors and syringes with 70% ethanol was essential to this modification as opening the flow circuit led to more frequent contamination than with the standard experimental procedure.

Endothelial cells cultured within the bioreactor were exposed to chronic pulsatile flow, as above, but additionally were exposed to 0.1 ml/h transmural flow for 2-5 days (**Table 6**). Rhodamine-labelled albumin transport over 1 hour was then measured, as outlined previously, except that for these experiments the tracer in the extracellular space was not all in the cartridge itself: the extracapillary space included

the fluid that had been collected in the syringes, all of which was collected and used in the fluorimetric measurements.

The introduction of transendothelial flow increased endothelial transport of rhodamine-labelled albumin (to $8.56 \pm 1.65 \times 10^{-06}$ cm/s; n=15) when compared to pulsatile flow without transmural flow ($2.62 \pm 0.38 \times 10^{-06}$ cm/s; n = 8; p = 0.0175). A flow of 0.1 ml/h across the capillary surface area of 70 cm^2 is equivalent to a convective mass transfer coefficient of 0.37×10^{-6} cm/s, which is approximately 10% of the difference between these two results, so it could not directly account for the increase in albumin transport even if the reflection coefficient (σ) for albumin were approximately zero. In practice, such coefficients are around 0.73 in cultured endothelial monolayers subject to an applied pressure difference, even in the absence of axial flow [107]. Hence we conclude that the increase in albumin transport is instead due to an increase in permeability of the monolayer induced by the transmural flow. Permeability results are shown in **Figure 29**.

Figure 28 The modification of the bioreactor to permit transmural flow

An image of a bioreactor demonstrating the addition of the syringe and filter to the extracapillary space to permit flow across the monolayer and fibre wall. The bioreactor is situated at the bottom of the image and is given a pink colour by the medium inside it. The syringe to the right – initially empty – collects fluid from the extracapillary space. A 0.22-µm filter is attached through an airtight seal to its open end to maintain sterility.

Table 6 Permeability experiments on effects of flow waveform

Bioreactor	Conditions	Permeability Value x 10^{-06}	Bioreactor	Conditions	Permeability Value x 10^{-06}
Q	Pulsatile	2	Q	Transmural	4.88
Q	Pulsatile	2.5	Q	Transmural	9.27
Q	Pulsatile	2.2	Q	Transmural	13.5
R	Pulsatile	1.7	R	Transmural	24
R	Pulsatile	1.9	R	Transmural	13.3
T	Pulsatile	4.7	R	Transmural	7.786
T	Pulsatile	2.1	R	Transmural	3.331
T	Pulsatile	3.84	R	Transmural	12.197
Average		2.6175	R	Transmural	16.61
SD		1.070724054	T	Transmural	2.17
			T	Transmural	2.363
			T	Transmural	2.39
			T	Transmural	4.39
			T	Transmural	9.4
			T	Transmural	2.819
			Average		8.5604
			SD		6.401118617
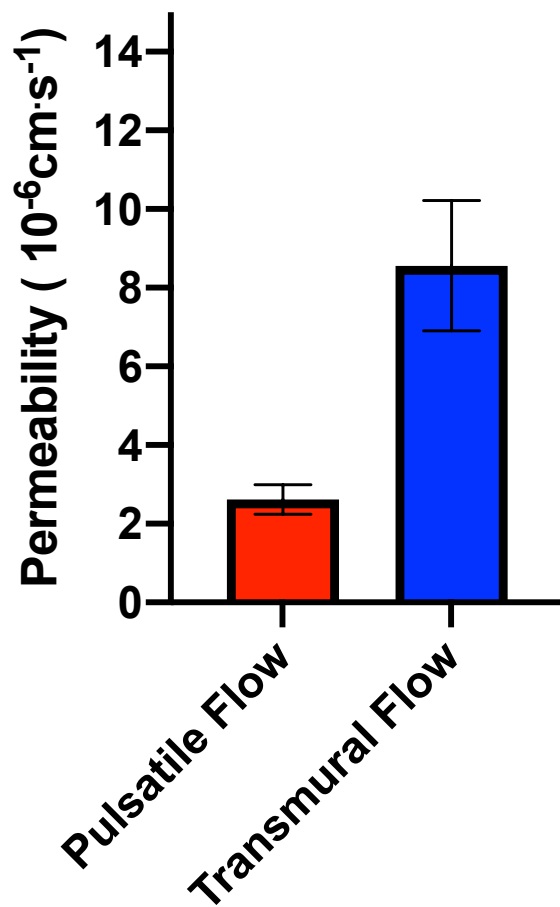
Figure 29 The effect of transmural flow on endothelial permeability

The introduction of transmural flow caused a statistically significant increase (p = 0.0175) in permeability of the endothelium to rhodamine-labelled albumin (8.56 ± 1.65 x 10^{-06} cm/s; n = 15) when compared to pulsatile axial flow alone (2.62 ± 0.38 x 10^{-06} cm/s; n = 8). Ata are shown as mean±SEM.

3.10 The role of active transport in transendothelial transport of albumin

Tracer experiments were performed with rhodamine-labelled albumin circulating for 24 h instead of 1 h, to determine whether tracer concentrations in the intra- and extra-capillary spaces reached equilibrium after this time. In the first few experiments, there was an unexpected excess of tracer in the cartridge space after 24 h of between 20 and 60%, so further investigation was considered necessary. Data are presented below; note that unlike the experiments described above, a consistent effect was not obtained.

After eighteen experiments (**Table 7**), the average excess of tracer concentration in the extracapillary space under pulsatile flow conditions after 24 h was 17.41 ± 5.22%. The 24 h tracer experiments were also carried out in bioreactors that were exposed to steady rather than pulsatile flow conditions. After eleven experiments (**Table** 7), the average excess tracer concentration in the extracapillary space was 9.43 ± 1.79%. When compared to the expected equilibrium of tracer, i.e. zero excess in the extracapillary space, the results were statistically significant for pulsatile ($p = 0.0039$) and steady ($p = 0.0004$) flow conditions. There was no statistically significant difference ($p = 0.2558$) between the two sets of experiments

Control experiments were carried out in a bioreactor with no cells to confirm that these recordings were not due to the bioreactor system itself. The percentage excess in bioreactors with no cells after 24 h of rhodamine albumin tracer exposure was 3.20 ± 1.14% (n=6). Although the mean value was much smaller than in the experiments with cells, the SEM was also smaller; hence when these control data were compared with the expected excess of zero, there was a statistically significant difference ($p =$

0.038). Further confusing the statistical interpretation of the data, when the pulsatile and steady data with cells were compared to the cell-free control, there was a p-value of 0.136 for pulsatile conditions and 0.029 for the steady flow conditions. Overall, the results suggest active transport at least under steady flow; the small but (moderately) significant excess tracer in the extracapillary space of the cell-free control cannot currently be explained. Results are shown in **Figure 30**.

Table 7 Permeability experiments for investigating active transport under chronic steady and pulsatile flow

Bioreactor	Conditions	% Increase
J	Pulsatile	60
J	Pulsatile	70
L	Pulsatile	14
L	Pulsatile	22.7
L	Pulsatile	23.9
L	Pulsatile	35.4
M	Pulsatile	-7
M	Pulsatile	28.4
M	Pulsatile	9.4
N	Pulsatile	-11.4
N	Pulsatile	14.7
N	Pulsatile	-12.6
N	Pulsatile	18.6
O	Pulsatile	22
O	Pulsatile	13.6
P	Pulsatile	13
P	Pulsatile	-9.2
Qii	Pulsatile	8
Average		17.41666667
SD		22.17155703

Bioreactor	Conditions	% Increase
K	Steady	20.7
M	Steady	0.028
M	Steady	13.3
M	Steady	9.31
O	Steady	6.4
O	Steady	10.7
P	Steady	9.9
Qii	Steady	7.2
Qii	Steady	9.8
Qii	Steady	1.2
Qii	Steady	15.3
Average		9.439818182
SD		5.905209934

Bioreactor	Conditions	% increase
Q	Control	1
Q	Control	7.6
Q	Control	2.2
R	Control	6
R	Control	1
T	Control	1.4
Average		3.2
SD		3
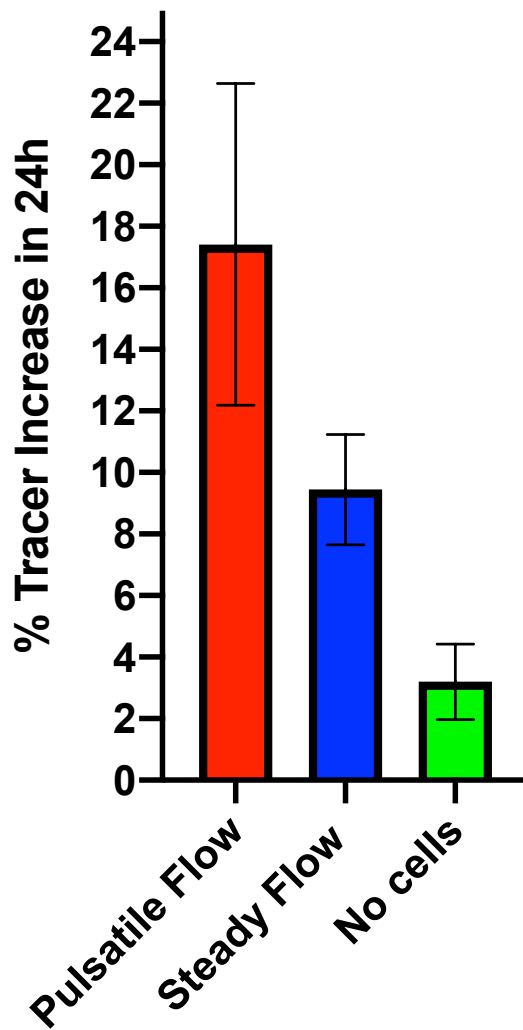
Figure 30 Excess tracer concentration in the extracapillary space 24 h after the introduction of rhodamine-albumin

After 24 h of tracer transport, there was a 17.41 ± 5.22% (n = 18) excess tracer concentration in the extracapillary space under chronic pulsatile flow and a 9.43 ± 1.79% (n = 11) excess tracer concentration in the extracapillary space under chronic steady flow. If the bioreactor was not seeded with cells, the excess was 3.20 ± 1.14% (n = 6). Statistical significance is discussed in the text.

Due to the apparent presence of active transport, further experiments were conducted to examine transport of rhodamine-labelled dextran. Dextran is less likely to be actively transported across endothelium, whereas there are reports of albumin and denatured albumin being actively transported across the endothelial barrier.

Rhodamine-labelled dextran was used in 1 h and 24 h tracer experiments under chronic steady and pulsatile flow conditions. The 1-hour experiments (**Table 8**) are considered first. As shown in **Figure 31,** the endothelial permeability to rhodamine-labelled dextran under pulsatile conditions was 4.56 ± 0.43 x10^{-06} cm/s (n = 6), which was not statistically different (p = 0.5784) compared to steady flow conditions with the same tracer, which gave permeability values of 5.23 ± 0.91 x10^{-06} cm/s (n=6). **Figure 32** compares the 1-hour rhodamine labelled dextran pulsatile and steady flow experiments to the previous rhodamine labeled albumin pulsatile and steady flow experiments.

Table 8 Permeability experiments examining 1-hour transport of rhodamine-labelled dextran under chronic pulsatile and steady flow conditions

Bioreactor	Conditions	Permeability Value x 10^{-06}		Bioreactor		Permeability Value x 10^{-06}
N	Pulsatile(Dex)	5.06		N	Steady(Dex)	3.233
P	Pulsatile(Dex)	2.77		N	Steady(Dex)	2
P	Pulsatile(Dex)	3.53		Qii	Steady(Dex)	5.98
P	Pulsatile(Dex)	2.94		Qii	Steady(Dex)	5.35
V	Pulsatile(Dex)	6.39		V	Steady(Dex)	7
V	Pulsatile(Dex)	6.68		V	Steady(Dex)	7.8
Average		4.561666667		Average		5.227166667
SD		1.731050741		SD		2.224210459
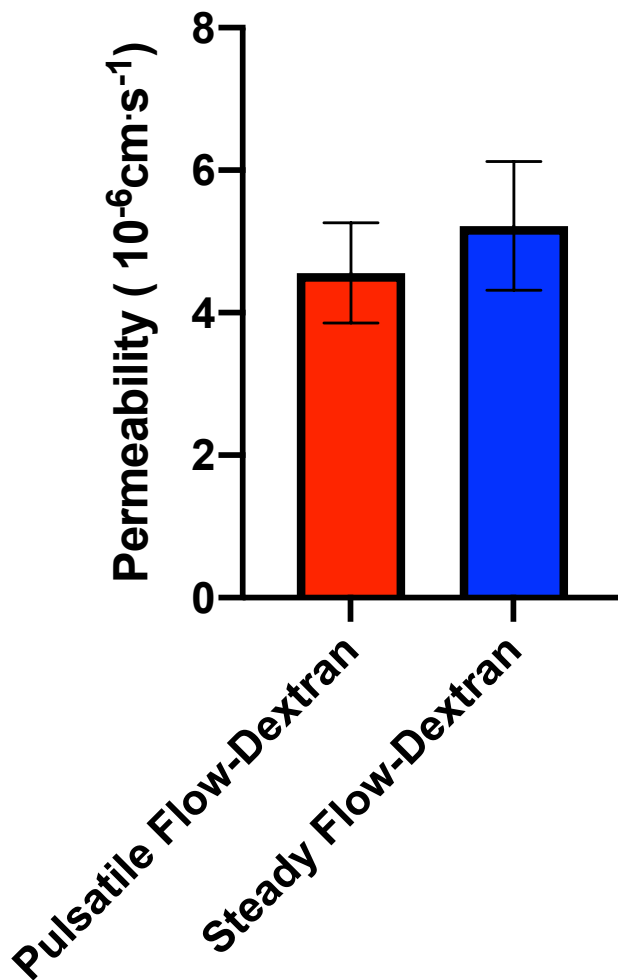
Figure 31 Effect of pulsatile vs steady flow on the 1-hour transport of rhodamine labelled dextran in the hollow fibre bioreactor

The permeability to rhodamine-labelled dextran under chronic pulsatile flow ($4.56 \pm 0.43 \times 10^{-06}$ cm/s, n = 6) was not significantly different from the permeability under chronic steady flow ($5.23 \pm 0.91 \times 10^{-06}$ cm/s, n=6; p = 0.5784). Data are shown as mean±SEM.
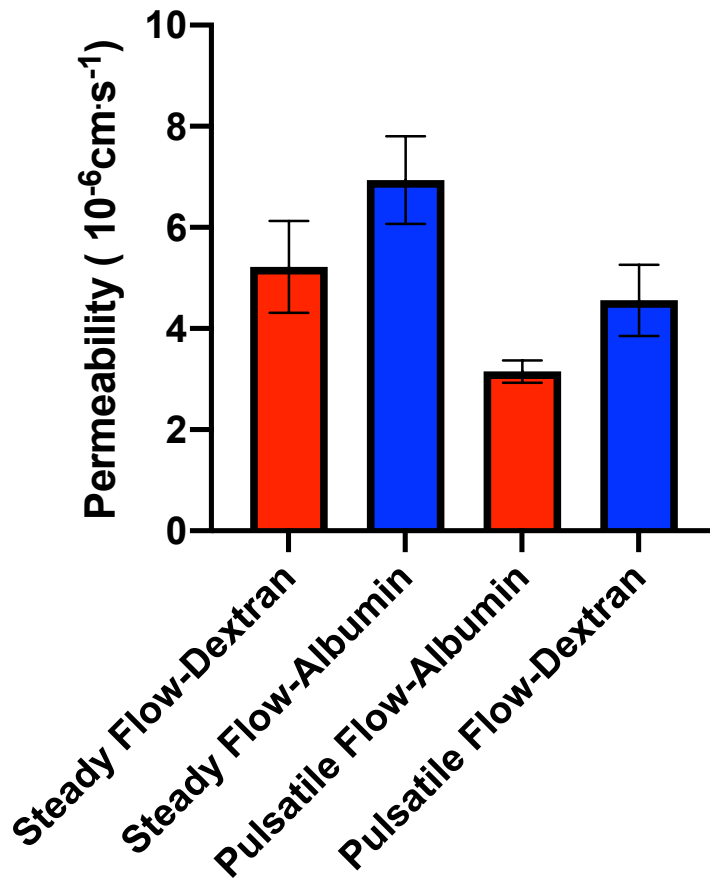
Figure 32 Comparison of pulsatile vs steady flow for the 1-hour transport of rhodamine-labelled dextran and rhodamine-labelled albumin

A side-by-side comparison of the data for steady and pulsatile flow experiments for rhodamine-labelled albumin and rhodamine-labelled dextran.

Thus the significant difference in 1-hour transport between steady and pulsatile flow conditions seen with albumin was not seen with dextran. Clearly a difference in transport mechanisms (e.g. active vs passive) is one possible explanation. To investigate that further, 1-hour rhodamine labelled albumin transport was measured in the presence of the dynamin inhibitor Dynasore (**Table 9**). The introduction of 40 µmol/L Dynasore 1 h before the transport experiment led to a statistically significant increase in endothelial permeability (6.41 ± 0.60 x10^{-06} cm/s; n=7) to albumin when compared to the normal pulsatile flow tracer experiments with 0.1% DMSO as a vehicle control (2.73 ± 0.274; n = 6; p=0.0003) (**Figure 33**).

Table 9 Permeability experiments examining the effect of Dynamin on rhodamine-labelled albumin transport under pulsatile flow conditions

Bioreactor	Conditions	Permeability Value x 10^{-06}		Bioreactor	Conditions	Permeability Value x 10^{-06}
S	CSS(0.1%DMSO)	3.219		S	Dynasore	5.819
S	CSS(0.1%DMSO)	3.7		S	Dynasore	3.87
Qi	CSS(0.1%DMSO)	2.1		S	Dynasore	7.306
Qi	CSS(0.1%DMSO)	1.9		Qi	Dynasore	5
Ui	CSS(0.1%DMSO)	2.7		Qi	Dynasore	6.9
Ui	CSS(0.1%DMSO)	2.8		Ui	Dynasore	7.5
Average		2.7365		Ui	Dynasore	8.5
SD		0.673998145		Average		6.413571429
				SD		1.601458071
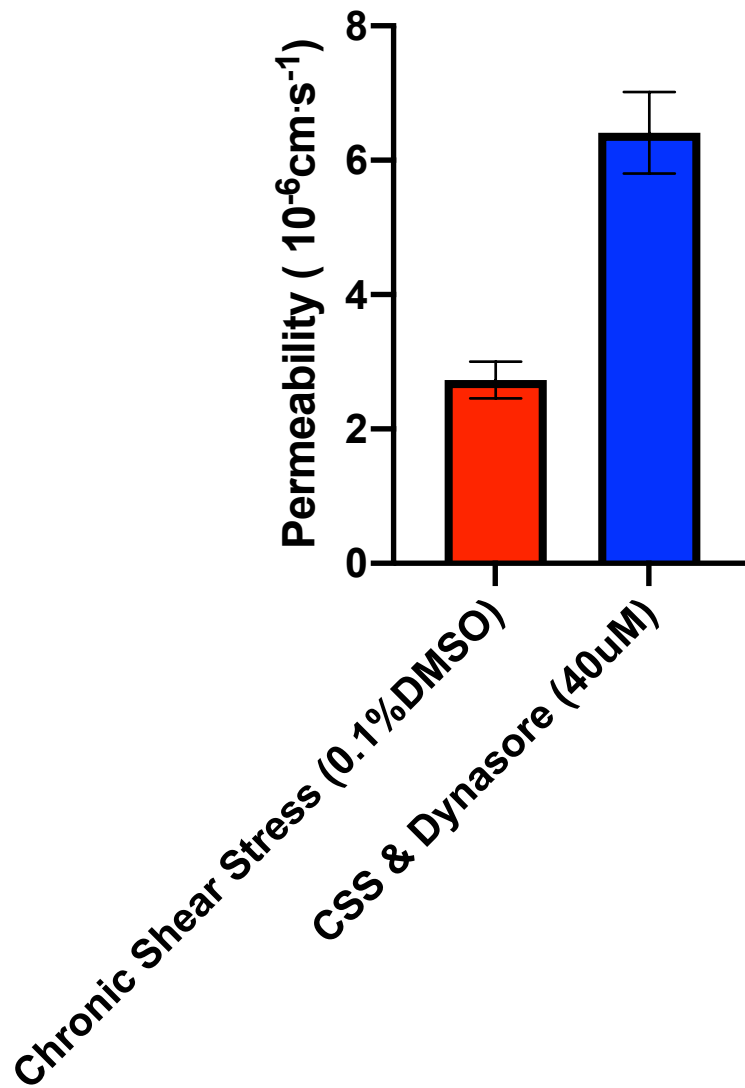
Figure 33 The effect of dynamin inhibition on endothelial permeability to rhodamine-albumin under pulsatile flow

The introduction of 40 μmol/L Dynasore led to a statistically significant increase in endothelial permeability (6.41± 0.60 x10^{-06} cm/s; n=7; p=0.0003) when compared to the pulsatile flow tracer experiments with a 0.1% DMSO vehicle control (2.73 ± 0.274; n = 6).

For the 24-hour experiments (**Table 10**), the rhodamine-labelled dextran results were different from the earlier rhodamine-labelled albumin data, as demonstrated side by side in **Figure 34**. Under pulsatile flow conditions, there was only a 4.85 ± 0.80 % (n = 6) excess dextran concentration in the cartridge. Under steady flow, the excess dextran concentration was 5.98 ± 1.22 % (n = 6). The difference between pulsatile and steady flow was not statistically significant (p = 0.4581). When the 24 h results for dextran were compared to the expected equilibrium of tracer – i.e. zero excess in the extracapillary space – the results were statistically significant under pulsatile (p = 0.002) and steady (p = 0.0055) flow conditions. For the dextran cell-free control, the p value was statistically significant for both pulsatile flow (p= 0.0182) and steady flow conditions (p=0.0176). T-tests to compare the excess rhodamine-labelled dextran concentration against the excess rhodamine-labelled albumin concentration in the extracapillary space at 24 h demonstrated no statistically significant difference under either pulsatile (p = 0.1859) or steady (p = 0.207) flow conditions.

Table 10 Permeability experiments for 24-hour uptake of rhodamine-labelled dextran showing the excess concentration in the extracapillary space under pulsatile and steady flow conditions

Bioreactor	Conditions	% Increase	Bioreactor	Conditions	% Increase
N	Pulsatile(Dex)	5.6	N	Steady(Dex)	7.2
P	Pulsatile(Dex)	3.1	N	Steady(Dex)	8.7
P	Pulsatile(Dex)	3.7	Qii	Steady(Dex)	5.8
P	Pulsatile(Dex)	2.6	Qii	Steady(Dex)	9.9
V	Pulsatile(Dex)	6.9	V	Steady(Dex)	2.5
V	Pulsatile(Dex)	7.2	V	Steady(Dex)	1.8
Average		4.85	Average		5.983333333
SD		1.986705816	SD		2.99634036

Bioreactor	Conditions	% increase
P	Control(Dex)	3.5
P	Control(Dex)	2.3
N	Control(Dex)	2.1
N	Control(Dex)	3.2
N	Control(Dex)	1.8
V	Control(Dex)	1.5
Average		2.4
SD		0.789
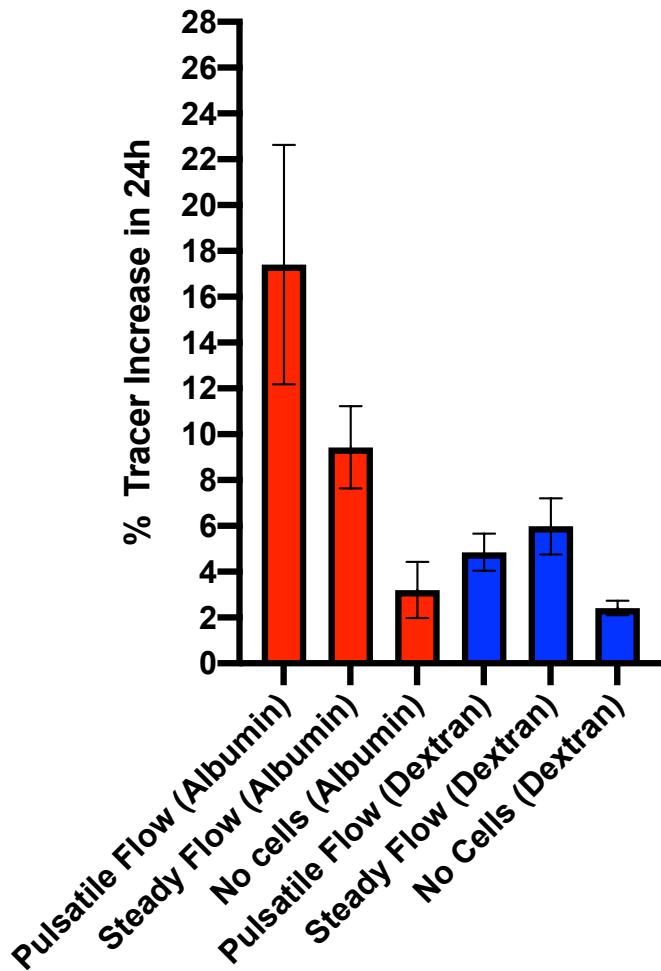
Figure 34 The percentage excess tracer concentration in the extracapillary space after 24-hour transport of rhodamine-albumin and rhodamine-dextran

The excess of rhodamine-labelled dextran in the extra-capillary space under pulsatile flow conditions (4.85 ± 0.80 %; n = 6) was not significantly different from the equivalent data obtained under steady flow excess dextran concentration (5.98 ± 1.22 %; n = 6; p = 0.472). Compared to the expected equilibrium of tracer – i.e. zero excess in the extracapillary space – the results were statistically significant under pulsatile (p = 0.002) and steady (p = 0.0055) flow. Previous 24-hour results for rhodamine-albumin are shown again for comparison.

The introduction of Dynasore (**Table 11 and Figure 35**) to the medium in two separate doses, 40 μmol/L one hour before the 1-hour tracer experiment followed by an additional dose four hours before the 24-hour tracer reading, which was performed after the 1-hour reading, led to a non-significant reduction in the excess rhodamine-albumin concentration in the extracapillary space after 24 h under pulsatile flow, from $15 \pm 3.86\%$ (n=6) to $6.78 \pm 1.59\%$ (n=7; p=0.0512).

Table 11 Permeability experiments examining the effect of Dynasore on excess rhodamine-labelled accumulation in the extra-capillary space after 24 h under pulsatile flow

Bioreactor	Conditions	% Increase
S	Dynasore(Albumin)	8.9
S	Dynasore(Albumin)	9.5
S	Dynasore(Albumin)	10.6
Qi	Dynasore(Albumin)	4.8
Qi	Dynasore(Albumin)	1.6
Ui	Dynasore(Albumin)	11
Ui	Dynasore(Albumin)	1.1
Average		6.785714286
SD		4.229037941

Bioreactor	Conditions	% Increase
W	CSS (0.1%DMSO)	11
W	CSS (0.1%DMSO)	6
W	CSS (0.1%DMSO))	14
Y	CSS (0.1%DMSO))	12
Y	CSS (0.1%DMSO))	15
Z	CSS (0.1%DMSO))	32
Average		15
SD		8.89

Bioreactor	Conditions	% increase
Wi	Control(Albumin)	5.2
Wi	Control(Albumin)	4
Wi	Control(Albumin)	3.3
Yi	Control(Albumin)	1.6
Yi	Control(Albumin)	7.2
Zi	Control(Albumin)	3.4
Average		3.84
SD		1.88
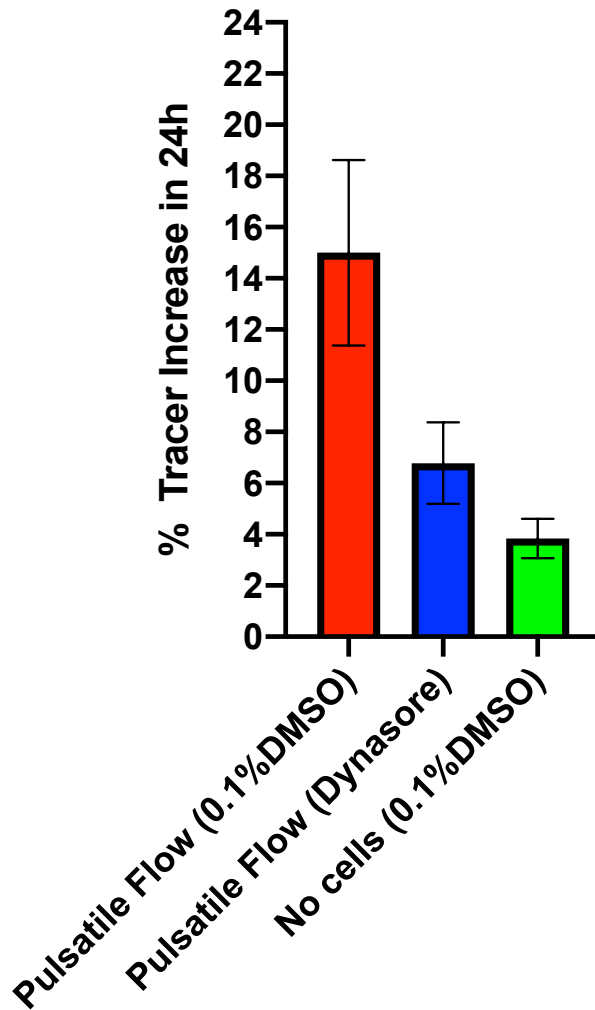
Figure 35 The percentage excess concentration of rhodamine-albumin in the extracapillary space after 24 h under pulsatile flow, with and without Dynasore

The excess concentration of rhodamine-albumin in the extracapillary space after 24 h under pulsatile flow was more than halved in the presence of Dynasore. With Dynasore present the percentage increase was $15 \pm 3.86\%$ (n=6) compared to percentage increase with 0.1% DMSO of $6.78 \pm 1.59\%$ (n=7). The difference was not statistically significant (p=0.0512). Data are shown as mean±SEM.

Chapter 4 Discussion

4.1 Utility of the Bioreactor System

Transport of macromolecules across vascular endothelium is essential for the normal function of tissue – for example, in the maintenance of the oncotic pressure of tissue and in the delivery of hormones and other signalling molecules to cells. Additionally, such transport appears to be important in pathological processes, particularly in atherosclerosis where transendothelial transport into the arterial wall of cholesterol-carrying lipoproteins such as LDL is thought to trigger the disease. Controlling the resistance of the arterial wall to lipoprotein entry might provide a method for slowing the development of atherosclerosis that is as powerful as, and synergistic with, current strategies based on lowering the concentration of lipoproteins in plasma. Developing ways to control the resistance requires detailed information about transport that is not yet available, mainly because of a lack of suitable experimental techniques.

One of the main issues associated with studying endothelial permeability is the difference between *in vitro* and *in vivo* research. The results from *in vivo* research demonstrate lower permeability than results from *in vitro* systems. Researchers studying the endothelium *in vitro* have attempted to resolve this problem for over 20 years[108]. Broadly, it is likely that *in vitro* studies have not replicated the permeabilities obtained *in vivo* because the cells are removed from their natural environment in terms of other cell types (including blood cells), the chemical milieu, the mechanical stresses to which the cells are exposed, the duration of the experiments and the extracellular matrix to which the cells adhere.

The permeability measurements presented in this thesis did involve chronic culture, physiological-type flow and a more physiological geometry. At present no

systems other than the FiberCell bioreactor and related devices have replicated this combination. Nevertheless, the permeability values obtained for albumin remained similar to those obtained other *in vitro* studies[109-112], which vary between 0.9–9 x 10^{-6} cm/s; under *in vivo* conditions it is 100–1000x lower (typically 1 x 10^{-8} cm/s for whole arteries[113]).

This thesis does describe simple modifications to the hollow fiber system which allowed the effects on permeability of steady flow and of transmural flow to be investigated. (The commercially available device produces only pulsatile flow and does not permit transmural flow.) The majority of *in vitro* studies have not been able to obtain measures of hydraulic conductivity but the modifications enable that in our system. Values of 4 x 10^{-7} cm/s were obtained, which is essentially identical to what is found in perfused capillaries and in aortas that are pressurized *in situ*[114]. Existing *in vitro* studies with the exception of the Tarbell group have only shown hydraulic conductivity values in the range of 1-5 x 10^{-6} cm/s[107, 115]. Even in the case of the Tarbell group[88, 111, 116, 117], who obtained a hydraulic conductivity value of 1 x 10^{-7} cm s^{-1}, the system that is used does not allow cells to experience the uniform, uniaxial, vascular-type flows that were produced in the capillaries of the hollow fibre system.

An inherent advantage of the hollow fibre bioreactor for permeability experiments is that throughput is high: multiple experiments can be conducted in the same bioreactor. Also, the bioreactor can theoretically be used to examine effects of co-culture, by adding a second cell type to the extracapillary space, although that possibility was not employed in the present study. Co-culture might lower permeabilites; this has been demonstrated for co-culture of endothelial cells with

dendritic cells[75]. A further advantage is that the close loop system allows the addition of bioactive substances to the medium at reasonable cost. One compound that would be worth trying is sphingosine-1-phosphate (S1P); S1P has been shown to reduce *in vitro* mass transfer coefficients to levels closer to *in vivo* values[75]. Ultimately, it may prove possible to construct hollow fibres by 3D bioprinting all of the materials in the extracellular matrix of an artery and adding all cell types to the matrix which occur *in vivo*[118, 119]. The topic of creating a more realistic fibre material is addressed in the Future Work section.

The main limitation of the system is the impossibility of imaging living cells within the system during the experiments, and indeed even the difficulty of *en face* imaging fixed cells on the walls of fibres that had been removed from the cartridge and sliced open. The problems with fluorescent imaging were detailed by the manufacturer and we were able to circumvent the issue with scanning electron microscopy and making comparisons to glucose consumption over time. The preliminary experiments proved vital in determining the utility of glucose and tracer measurements. The rhodamine labelled albumin tracer measurements in conjunction with glucose analysis provided suitable data on what was happening within the system without the need for visualization or other techniques that would have had an effect on the endothelial barrier and caused potential issues with data analysis.

Additional limitations were the inability to impose multidirectional (as opposed to oscillatory) flows and the rigidity of the fibre material, which prevented the

examination of effects of cyclic strain. The latter is, again, discussed in the Future Work section.

4.2 The role of shear stress, viscosity, and pharmacological agents on endothelial permeability in the hollow fibre bioreactor

.

The mechanical environment experienced by the surface of the endothelial cell is crucial in maintaining the appropriate state for transendothelial fluid and macromolecule transport in all blood vessels. Shear stress exerted by blood flowing over the endothelial cell surface is an important factor in controlling and maintaining this physiological barrier. The response of an endothelial monolayer to shear stress can depend on the cell source. For example bovine aortic endothelial cells respond like the retinal endothelial cells *in vitro* but when similar experiments are performed in human umbilical endothelial cells there are different responses [88]. Porcine aortic endothelial cells (PAEC's) were the cell of choice because our group has already documented shear-dependent changes in permeability and other properties with this cell type [74], and because we are interested in the systemic arteries that are susceptible to atherosclerosis.

Furthermore, the cells were readily available and the optimization of methods for their isolation as part of this PhD project led to good purity and yield.

In the first experimental series, the hollow fiber bioreactor system was used to study the effects of shear stress on endothelial permeability. With the hollow fibre bioreactor, the cells are cultured on the inner surface of cylindrical tubes – the geometry that is found *in vivo* – and the shear stress under a steady flow waveform can be calculated simply from Poiseuille's law since the Reynolds numbers are low and entrance lengths are consequently short. The pulsatile flow waveform had approximately the shape that occurs for large arteries in vivo.

As noted above, the ability to use the same cells over a period of weeks was a primary advantage of this particular system. Over time it was possible to use the permeability data as a marker of how the cells were performing as a monolayer. For instance, permeability to rhodamine-albumin was typically on the order of 10^{-6} cm/s under chronic conditions; any result deemed too high was noted and the experiment would be repeated again or a number of days later. If the result remained abnormal, the bioreactor was fixed and kept for imaging of potentially damaged monolayers by scanning electron microscopy. With careful handling of the bioreactor and gentle extraction of tracer-containing medium, these problems were rare. Hence permeability could be investigated on the same monolayer under different flow conditions.

Pulsatile chronic shear stress lowered endothelial permeability to rhodamine-labelled albumin when compared to static conditions, whereas acute shear stress led to

an increase in permeability. These trends are consistent with data previously obtained by Warboys et al using the non-uniform swirling flow obtained by placing the Transwell system on an orbital shaker [74].

Acute application of shear stress is deemed more physiologically significant in the microcirculation, in which flow rate responds over short timescales to changes in demand by specific organs such as skeletal muscle [88]. When exposed to acute changes in shear stress, endothelial cells act as a biomechanical force-sensing interface which respond by activating pathways that can influence permeability [120]. Multiple molecular elements such as vascular endothelial growth factor (VEGF), ion channels, G-protein-coupled receptors (GPCRs), integrins, and platelet endothelial cell adhesion molecule-1 (PECAM-1) sense the application of shear stress. The introduction of acute shear stress would activate these elements and an interplay of signals would then cause an initial increase in cell permeability that would presumably later reduce and then plateau, as found here when cells are exposed to chronic shear stress conditions. Since permeability was lowered under chronic shear stress, there is presumably a period when permeability is decreasing from the initially increased level to the plateau level.

Integrins play an important role in endothelial cell acute shear stress responses; they are activated within one minute and their effects can persist for as long as 6 h [120]. Once activated, they modulate cell signaling, which could have an effect on the stability of junctions between cells or facilitate the remodelling of the endothelial monolayer. In the case of ion channels, a study by Olsen and colleagues [121] found that the short term introduction of shear stress led to activation of membrane permeability to potassium. Similar studies [122] on calcium channels found an increase in calcium ion permeability

in response to shear stress. Both of these changes in response to acute shear stress could explain the changes in endothelial cell function that lead to an increase in monolayer permeability to albumin [120].

The chronic pulsatile flow experiments are more relevant to flow in arteries. They may have relevance to variation of endothelial cell characteristics between regions having diverse blood flow environments. Hence, if applicable to lipoproteins, they may be relevant to the non-uniform distribution of atherosclerotic lesions within such vessels e.g. at the inner vs outer walls of bifurcations[88]. It was for this reason that the subsequent series of experiments focused more on chronic than acute shear stress.

Because it has previously been difficult to apply chronic shear stress to endothelial monolayers and assess the effect on permeability, less is known about mechanisms underlying responses to chronic shear. Warboys et al[75] demonstrated that nitric oxide plays an important role in maintaining barrier function to albumin under chronic shear stress conditions. Long-term exposure to chronic shear stress upregulates endothelial nitric oxide synthase (eNOS) which leads to an increase in the levels of nitric oxide [74]. Nitric oxide is also linked to the shear-sensing interface under these chronic conditions. VEGF in particular is a potent permeability-increasing factor that exerts effects on vascular permeability through Src kinase activation in a process mediated by nitric oxide produced by eNOS. Nitric Oxide derived from eNOS controls the balance of Rho and Rac activation, which is important under shear conditions [123]. It is also possible that the effects on permeability of chronic shear involve large-scale structural changes. For example, it has been demonstrated in previous studies that the

cells take over 24 h to align and re-form their tight junctions in response to chronic changes in flow [88].

Overall, the acute and chronic shear stress experimental series demonstrated how the hollow fiber bioreactor could be used to determine endothelial monolayer responses to different hemodynamic conditions exerted by flow in a three-dimensional culture system. It led to the next series of experiments to determine if the system was useful in obtaining results under the set pulsatile flow conditions with pharmalogical agents present as well. Further validation of the bioreactor system was carried out by adding agonists or antagonists known to affect endothelial permeability. Chronic shear stress conditions were maintained.

The inhibition of eNOS in the bioreactor system with L-NAME was used to test whether results could be obtained that were consistent with the earlier data from Warboys et al[75]. Thrombin was also used in the bioreactor system to test for an intact monolayer; it is known to increased endothelial permeability by reversibly altering cell morphology, causing contraction and the formation of gaps between cells [85]. Under chronic shear stress conditions in the bioreactor, the endothelial cells transported more rhodamine-labelled albumin across the endothelial monolayer into the extracapillary space when the nitric oxide pathway was inhibited or the thrombin pathway was activated. Both experiments therefore helped to validate this method of measuring permeability.

PECAM-1 is a cellular adhesion and signalling receptor that is highly expressed at cell junctions. The receptor is known to make endothelium less permeable to albumin by reducing macromolecular transport across junctions between endothelial cells. Its homophilic interactions are more important for paracellular permeability than signalling [124]. In the present study, it was found that surface expression of PECAM-1 *decreased* with chronic exposure to pulsatile shear, compared to static controls, correlating with the decrease in permeability. This was contrary to expectations. In general, loss of PECAM-1 is associated with an *increase* in permeability [124]. At present we have no explanation of this discrepancy with the literature. It could be due to an overriding influence on PECAM-1 expression on the cell surface rather than in the cell junctions.

Experiments in which xanthan gum was added to the medium tested the effects of viscosity on permeability. Xanthan gum is a shear thinning fluid: like blood, its viscosity decreases as shear rate increases, and it has been used in perfusion systems because of that property [37]. The Womersley number, which defines velocity profiles under pulsatile flow, does have viscosity in the denominator, so under the pulsatile flow conditions there may have been an alteration in shear rate as well as shear stress on the addition of xanthan gum; because of the shear-thinning nature of the fluid, the exact change could not be calculated. However, it is expected to be smaller than the effect on shear stress mediated directly through increased viscosity and hence adding the gum also examined whether permeability responds to the shear rate – the velocity gradient

next to the wall, which would have remained roughly constant – or the shear stress, which is the near-wall velocity gradient multiplied by the viscosity.

Xanthan gum increases osmotic pressure as well as viscosity, so it was important that permeability was unaffected by the presence of xanthan gum under static conditions. That may reflect the absence of transmural flow in the unmodified bioreactor since oncotic pressure gradients directly influence transmural fluid flux. (Xanthan gum has a molecular weight in the $10^6 - 10^7$ Da range.)

Under both acute and chronic pulsatile conditions, the presence of xanthan gum lowered the permeability of endothelial cells to rhodamine-labelled albumin. Previous studies have shown that an increase in shear stress as opposed to shear rate has an effect on the calcium ion channels in the endothelial shear sensing interface, which could explain the result [125] .The increase in viscosity and shear stress could have been sensed by the ion channels, leading to tightening of the barrier and reduction in permeability. The increase in viscosity of the medium may also have had an effect on the remodelling of the endothelial cells, perhaps making it occur faster. The result emphasized the need for a more physiological environment in all two-dimensional and three-dimensional endothelial cell culture studies Possible future work would include studying the effects of the medium viscosity in microfluidic devices to visualize how the cells respond and remodel under the acute shear stress conditions.

4.3 The effect of flow waveform, transmural flow, and active transport on endothelial permeability in the hollow fibre bioreactor

4.3.1 The effect of flow waveform on transport across the monolayer

The next step in this project was to study the effects of different flow waveforms on endothelial cell permeability. The arrangement of the bioreactor flow circuit made it possible to dampen the flow by adding syringes filled with air. The addition of these syringes converted the pulsatile flow to nearly steady flow.

Chronic steady flow led to a statistically significant increase in cell permeability when compared to chronic pulsatile flow. These data suggest that the endothelial barrier may be tighter in regions of pulsatile flow than in those of steady flow (e.g. in arteries versus in the microcirculation), and also that within arteries, areas with more reverse flow might have tighter barriers. These inferences need to be tested further – for example by using a pump capable of generating more subtle differences in flow waveform, and by measuring permeability in real vessels perused *in situ* with different flow waveforms.

4.3.2 The effect of transmural flow on transport across the monolayer

Gradients of oncotic and hydrostatic pressure are important for driving fluid transport across the vessel wall. In the present study, transmural flow was achieved by lowering the hydrostatic pressure on the abluminal side of the endothelium. Although blood pressure acts perpendicularly to the frictional stresses sensed over the abluminal surface of endothelial cells, an increase in transmural flow does produce an increase in

shear stress on endothelial cells in the junctional regions. Increasing transmural flow is known to decrease hydraulic conductivity [126]. This known as the sealing effect. The reduction in transmural transport following an initial increase is an adaptive mechanism to protect the vasculature.

In the bioreactor system, the addition of transendothelial flow to chronic pulsatile axial flow increased transendothelial permeability to rhodamine-labelled albumin more than could be explained by the addition of the convective transport itself. This experimental series confirmed that the hollow fiber bioreactor system could be readily modified to replicate further aspects of the mechanical environment that endothelial cells experience *in vivo* but the result itself was surprising given that work by Tarbell and colleagues that has shown transendothelial flow to reduce transport across the endothelium [117, 126]. However, in one of these studies, it was shown that although effective permeability values were reduced and that there was a reduction in the small pore system for transport of water, this was not true for the transport of albumin or dextran [126].

4.3.3 The role of active transport in endothelial permeability

During experiments to investigate equilibrium conditions, by taking measurements after 24 hours of tracer circulation, a higher rhodamine-labelled albumin concentration was found in the cartridge (i.e. extra-capillary) space than in the capillary space. The excess was approximately 9% under steady flow conditions and 17% under pulsatile flow conditions. The result appears to be robust: a much smaller excess was observed in the absence of cells and the effect was also smaller (although not

significantly so) when using rhodamine-labelled dextran rather than rhodamine-labelled albumin as a tracer. (However, for reasons that are at present unknown, even the cell-free data were significantly different from zero excess.)

Currently, active transport across endothelium is not widely investigated. However, there have been earlier reports claiming, or consistent with, such a phenomenon. Breaks in tight junctions, vesicles, and leaky junctions are the main pathways that allow for the transport of macromolecules [88]. The paracellular pathway is more commonly studied but transcytosis via caveolae is a physiologically important process that is involved in the transport of albumin across the endothelium [127]. The work of Schnitzer strongly suggests that transendothelial albumin transport can occur through a vesicular pathway and it is hard to conceive of active paracellular transport [128]. They discovered that albondin enhanced albumin binding and transport across the endothelium and, as a result, increased capillary permeability. Low temperatures reduced the transport of albumin five-fold. At 37°C there was threefold greater transport of albumin than of maleic anhydride-treated albumin (which does not bind to albondin), but at low temperature this difference was eliminated. These data suggest that the transcellular pathway involves active transport [128].

Recently, it has been found that the coregulation of paracellular and transcellular pathways is important for a functional microvascular endothelium. Mice deficient in caveolin-1 do not perform transcytosis but have an increase in permeability. The reasons for this have been disputed. Schubert and colleagues[129] argue that the induction of paracellular leak is to compensate for the loss of transcytosis while others [130] claim that it is due to a change in capillary pressure or other functions of caveolin-1 in cell signalling and in the glycocalyx [82, 127].

To gain more understanding of this system, dynamin activity, which is essential for vesicle formation, was inhibited for 1 h and 24 h. It was the inhibition of dynamin and subsequent paracellular leak in work by Armstrong and colleagues that motivated this particular study [127]. In the bioreactor system there was an increase in 1-hour rhodamine-albumin transport after the dynasore, a dynamin inhibitor, was introduced, compared to vehicle control experiments. This strongly suggested that inhibiting vesicle formation disturbed the balance between transcellular and paracellular permeability, increasing the paracellular permeability and therefore overall permeability. In the 24-hour pulstatile flow experiments, dynasore lowered the percentage increase in the cartridge space from approximately 17% to 6.7%, further suggesting the importance of vesicles in active transport. The inconsistencies in some of the data mean that this topic requires further investigation.

4.3.4 Summary of findings on permeability

In summary, the unique advantages of the bioreactor system, as modified in the present study, have allowed the demonstration of the following: the lowest permeability was obtained under chronic pulsatile flow, and permeability was raised relative to this value by chronic application of steady flow, acute application of flow and the introduction of transmural flow. Additionally, evidence was found for the presence of active transport – presumably via a vesicular route – although some results were contradictory and therefore no firm conclusion could be drawn.

Permeability values in the bioreactor were higher than those obtained *in vivo*, but the monolayers responded to L-NAME and thrombin is a manner that has been observed under physiological conditions; the results may have relevance to properties of endothelium *in vivo*. Chronic pulsatile flow is the condition experienced by most endothelium in healthy arteries – low permeability, and hence low disease prevalence, might be expected. With increasing age, reverse flow diminishes due to the lowered elasticity of vessels, and therefore flow becomes more like steady flow, albeit not completely steady; raised permeability might therefore be expected. In regions of arteries prone to atherosclerosis, the flow tends to be complex – for example, its direction may alter substantially during the cardiac cycle. It could be argued that this is akin to the acute application of flow in the present study, which increased permeability. Finally, the permeability-raising effect of transmural flow, which would increase during endothelial dysfunction, has the interesting implication that once barrier function is impaired, there may be a tendency for it to remain impaired or even deteriorate.

4.4 Future work: the development of novel biomaterials using tissue engineering approaches

During the course of this PhD, bioprinting, microfluidic devices, and hollow fibres made from biomaterials were also investigated in attempts to create a more useful and reproducible alternative to the commercial bioreactor. All three are valuable areas for further work. For reasons of space, only the latter is discussed here: the preliminary

studies are reported, with a description of how they could be extended and successfully completed.

The aim of this part of the work was to create improved materials for the hollow fibers, with the objectives of:

(1) allowing the diameter of the tube to cyclically increase and decrease each pump cycle, as the pressure fluctuates, thus better mimicking the situation in arteries in vivo and providing a mechanical environment cue for the endothelial cells that is missing in the commercial device.

(2) Providing a material on which the cells may behave in a more natural fashion than when plated on the polymer used by the commercial manufacturer.

(3) Possibly permitting the microscopy of endothelial cells from outside the fibres, through the thickness of their walls,

(4) investigating permeability on the types of materials that might be used in tissue engineered constructs.

Approaches from tissue engineering were employed. Tissue engineering aims to create living arteries through the combination of cells and substrates *in vitro*, or by implanting cell free substrates *in vivo* for spontaneous repopulation of cells on the scaffolds.

4.4.1 The development of an acellular arterial matrix

In the field of tissue engineering, acellular/decellularized tissues have become a promising material for preclinical studies of transplants and grafting for multiple

organs including heart valve, bladder, tendon and arteries [131-135]. Their applications in a clinical setting highlight a potential use in disease modelling such as in the investigation of endothelial barrier dysfunction and atherosclerosis.

The approach requires all cellular and nuclear material to be removed from the tissue whilst disrupting the mechanical integrity, structure or biological activity of the extracellular matrix (ECM) as little as possible [131]. Once decellularized, cells can be seeded to the ECM for experimental studies. An arterial matrix can potentially provide a scaffold for culturing endothelial monolayers under physiological conditions. These bio-derived acellular arterial matrices can possess the native-like structure and geometry, and retain the arterial mechanical properties [132, 136]

The most robust and effective decellularization protocols that have been developed require a combination of physical, enzymatic and chemical methods. Following an extensive literature research [131, 132, 137-142] and some pilot experiments, a reproducible protocol outlined by Negiahi et al. was used and modified for these studies [142].

The protocol requires the non-ionic detergent Triton-X 100 (tert-octylphenylpolyoxyethylen) and the ionic detergent sodium deoxycholate (SDC) combined with mechanical stimulation. Triton X-100 functions by disrupting lipid-lipid and lipid-protein interations while leaving protein-protein interactions intact. Sodium deoxycholate is a more effective decellularization agent than the commonly used ionic detergent sodium dodecyl sulphate (SDS) [137]. It decellularizes the tissue by solubilising cytoplasmic, nuclear and cellular membranes, denatures proteins and removes nuclear remnants. Mechanical agitation increases the effectiveness of decellularization [137]. The

final stage is removal of cellular debris from the tissue by means of washing over a 72-hour period in medium. The protocol is time critical because too prolonged an exposure to the decellularizing agents can result in destruction of the extracellular matrix [137].

Carotid arteries were selected as potential scaffolds for the bioreactor because they lack significant side branches and have smaller dimensions than the aorta, as required for replacing narrow artificial fibres in a bioreactor. However, porcine aortas were used for method development because they are readily available from the abattoir.

Preliminary studies involved assessing the effects of the standard decellularization agents, Triton-X 100 and SDS, on porcine aortas.

Figure 36 demonstrates that the decellularization agents were capable of disrupting and removing most cells attached to the lumen of the aorta following 12 h of exposure. These preliminary method development studies highlighted the requirement for increased exposure to the decellularization agents as some cells remained attached.

Image A in **Figure 36** demonstrates two aortic segments; the lower section has been decellularized (A). The following images are the SEM micrographs of a control (B), a sample treated for 12 h with 0.25% Triton-X 100 (C) and a sample treated for 12 h with 0.25% sodium dodecyl sulphate *(*SDS) (D). In the control image (B) the cells have the cobblestone morphology of endothelial cells. Comparison with the control has shown that the agents used for decellularization (C-D) had started to remove cellular

material. Extracellular Matrix (ECM) fibres can be seen beneath the cells. In images C and D, the cells form bright circular balls, indicating that the cells are dying and becoming disconnected from the ECM. It is obvious from these results that the agents had a decellularizing effect but the tissue required additional exposure time.
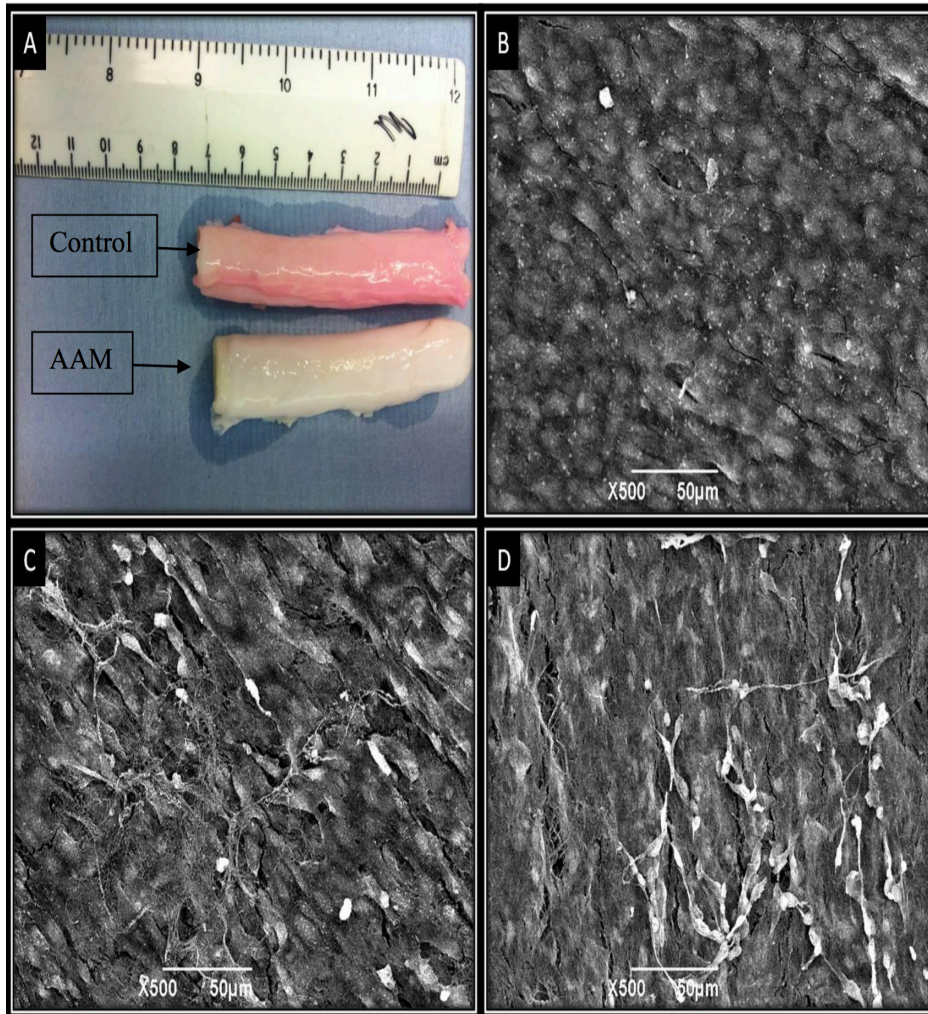
Figure 36 Assessment of decellularization materials

[A] An image of a control porcine aorta and one decellularized using the protocol outlined by Negishi et al [120]. The lower segment of aorta has undergone decellularization. [B] Scanning Electron Microscopy (SEM) micrographs of a control aorta sample. Note the cobblestone morphology of endothelial cells. [C] SEM of aortic tissue exposed to 0.25% Triton-X 100 for 12 h. The cellular material was beginning to be stripped from the lumen. [D] SEM of aortic tissue exposed to 0.25% SDS for 12 h. More of the ECM was exposed.

Carotid arteries were used in subsequent studies, using the decellularization protocol outlined in [142]. The increase in time improved decellularization. The effects of decellularization were studied in greater detail for the carotid arteries and included mechanical mixing using an orbital shaker for 72 h. In the SEM micrographs of **Figure 37,** the endothelial surface of the control aorta was intact and followed the direction of blood flow. Increasing magnifications were used to confirm that the cells were attached to the ECM. (The particles present on the surface of cells seem to be gold particle debris from the coating protocol prior to SEM imaging.)
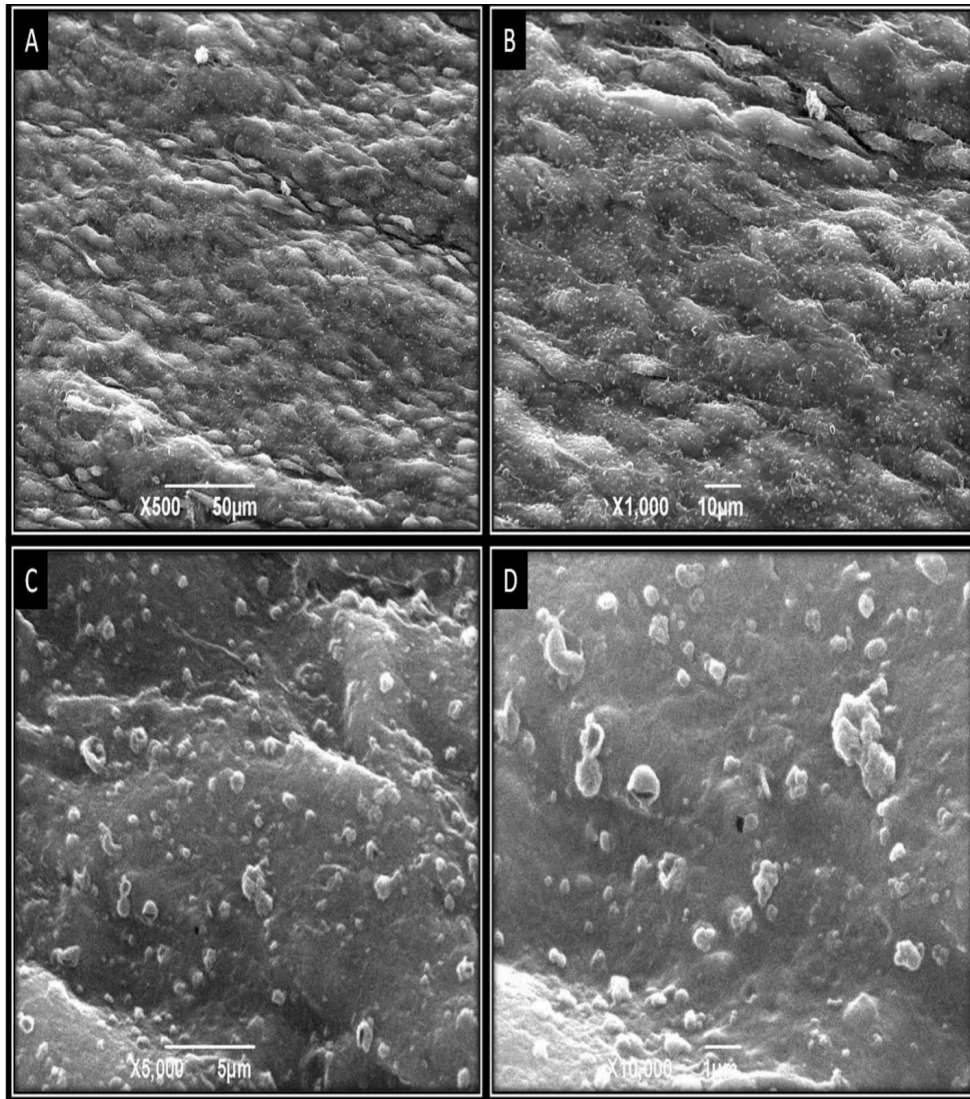
Figure 37 Scanning Electron Micrographs of a control carotid artery

[A-D] Scanning electron micrographs at increasing magnification (x500 - x10,000) of the lumen of control carotid artery. Note the cobblestone morphology of the endothelial cells and their alignment with the general direction of blood flow. In [C-D], the increased magnifications confirm that the cells are intact with no gaps exposing ECM. The particles deposited on the surface of the cells could be vesicles but could also be excess gold particles.

Each stage of decellularization was assessed with SEM because the technique provides a clear picture of cell removal. The first assessment was carried out after 24 h decellularization prior to the 72 h washing step. It is evident from the SEM micrographs in **Figure 38** that a great deal of cellular material has been destroyed. The endothelial cell layer appears to have been removed and the smooth muscle cells were destroyed, exposing the ECM.
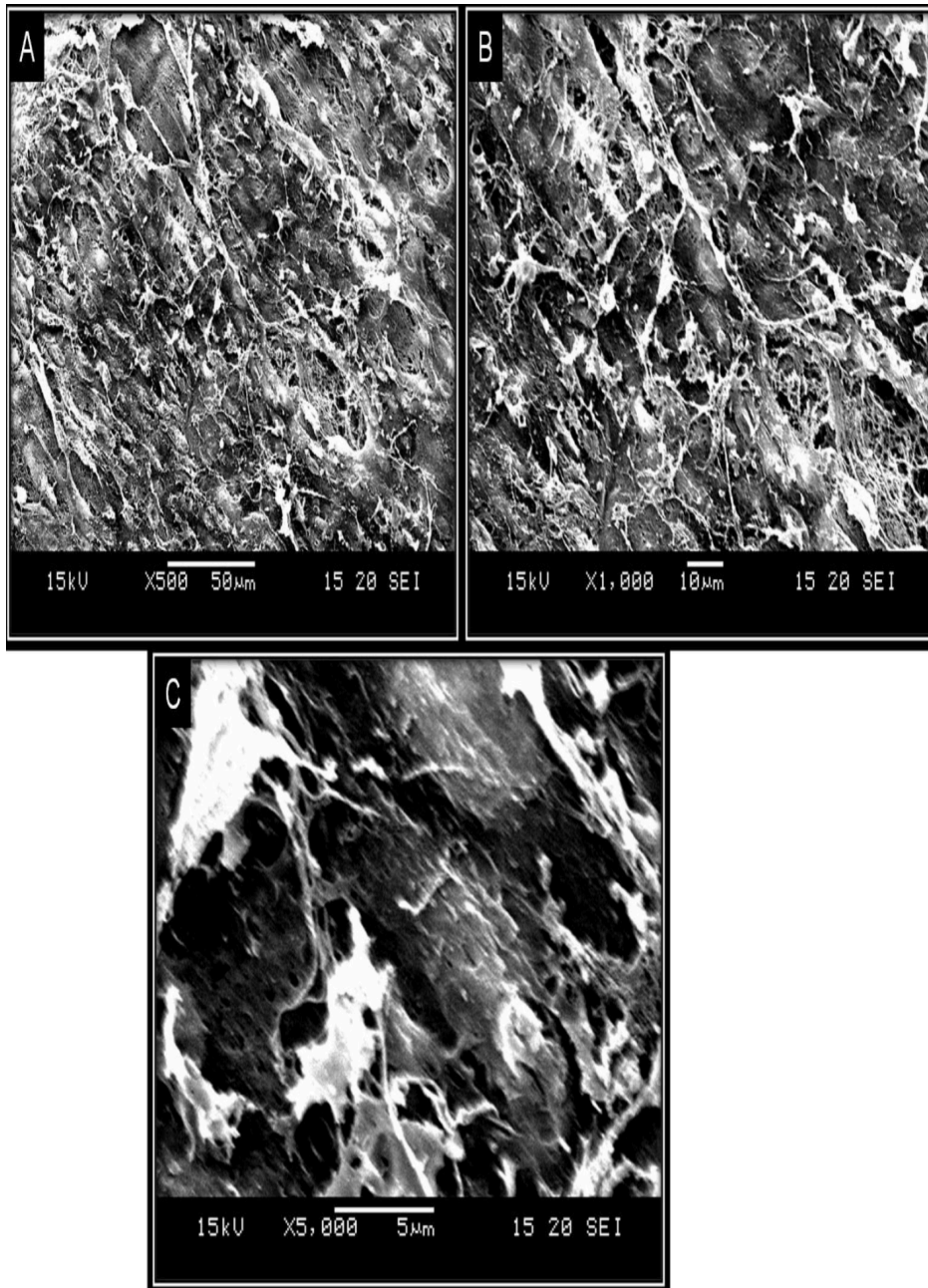
Figure 38 Scanning Electron Micrograph of carotid artery following 24h decellularization

SEM micrographs at increasing magnifications (x500 - x5,000) of the lumen of a carotid artery following decellularization for 24 h. The cells have been stripped away exposing the ECM components. There was still a great deal of cell debris following the first stage. It is evident from these images that the decellularization agents act better in a combinatory manner for cell removal.

After the 72-hour wash, samples were taken again and imaged with SEM (**Figure 39**). It is evident that all cellular material has been stripped, exposing the components of the ECM. Increasing magnifications demonstrated what appeared to be disruption to the native ECM following the decellularization protocol.

Time did not allow for full investigation into the recellularization of these scaffolds. In future work, it would be possible to seed these tissues with PAEC's. There is also the potential for combining the decellularized materials with methods involving 3D bioprinters. Possible protocols involve the ability to bioprint cells into exact locations of the decellularized tissue scaffolds or to crush up the decellularized tissue and merge it with endothelial cells and vascular smooth muscle cells printed using CAD scans of an aortic segment.
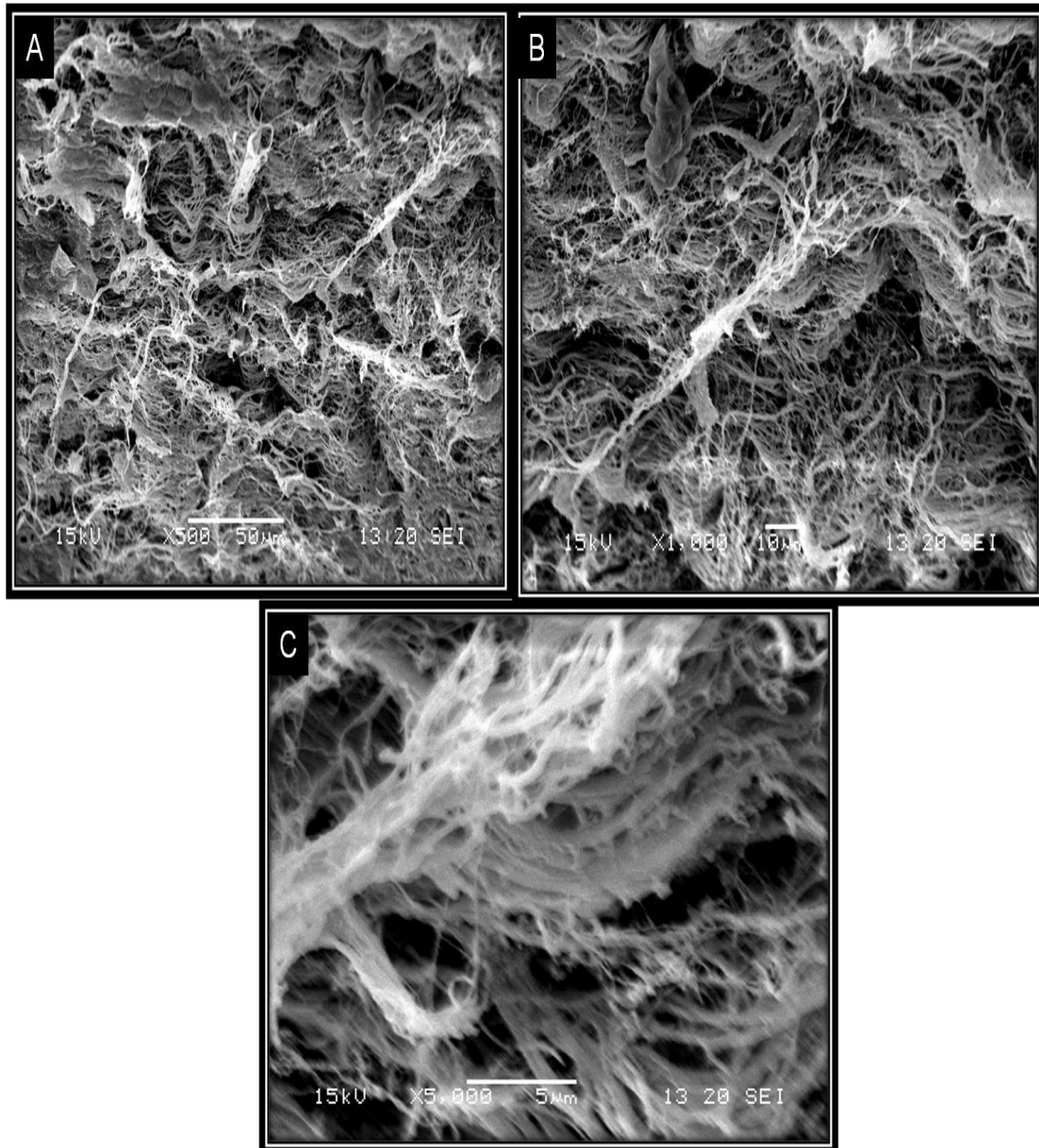
**Figure 39 Scanning electron micrograph of carotid artery following 24 h decellularization and 72 h wash cycle**

[A-C] SEM micrographs at increasing magnifications (x500 - x5,000) of the inner wall of carotid artery following the entire protocol. The images demonstrate complete removal of the cellular material, exposing the complex composition of the highly porous and interconnected collage/elastin fibres of the ECM.

4.4.2 The Development of Novel Synthetic Biomaterials for Bioreactor Fibres

Advances in natural and synthetic polymers for tissue engineering also provide a potential scaffold for the culture of endothelial monolayers under more physiological conditions. The alignment of extracellular matrix fibres in blood vessels contributes to their overall ability to withstand the repetitive force and pressure generated from blood flow. Electrospinning of scaffolds is the best approach to the construction of a vascular scaffold as it provides the means to control fibre alignment and randomization based on equipment or parameter modifications [143]

The majority of scaffolds are created from bioresorbable poly (lactic acid) (PLA), poly (glycolic acid) (PGA), polydioxanone (PDO), and poly (caprolactone) (PCL), along with natural polymers like collagen and elastin [144-149]. However, there have been problems with some of the polymers. The synthetic polymers PGA and PDO degrade rapidly under physiological conditions and PLA has high stiffness that makes it undesirable for an arterial substitute [143]

Electrospining was used to determine whether it might provide a viable option for establishing a scaffold for the bioreactor fibres. Dense Disorganized Collagen Constructs (DDCC) and electrospun Polycaprolactone PCL vascular scaffolds were successfully generated. Low magnification SEM micrographs from each scaffold are shown in **Figure 40**. From left to right the samples are as follows: collagen film (A), aligned PCL (B), randomly aligned PCL (C) and PCL and collagen (D). The first set of experiments required the polymerization and dialysis of collagen type 1 to form a thin

film. Initial results suggest that it might not be suitable for a bioreactor (although it may prove beneficial for other endothelial stretch studies once optimized).
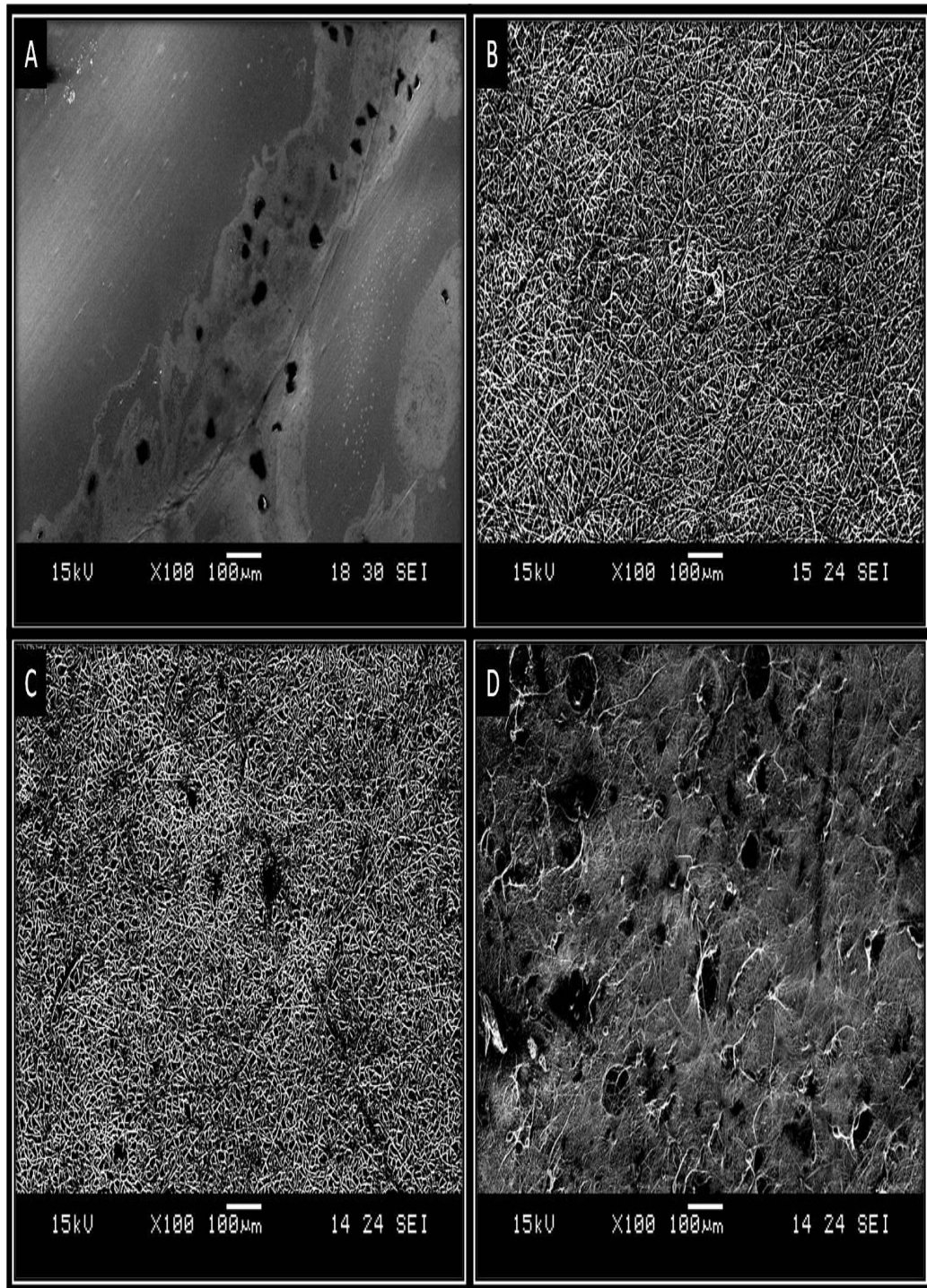
Figure 40 Scanning Electron Micrographs of individual synthetic scaffolds

Low magnification (x100) SEM micrographs were taken for each scaffold. [A] Disorganized Collagen Construct (DDCC); [B] Aligned Polycaprolactone PCL scaffold; [C] randomly aligned PCL scaffold; [D] PCL and collagen scaffold

The collagen film was brittle, and not uniform in shape; it snapped into pieces once removed from the dialysis cassette. Further investigation by SEM (**Figure 41 [A-D]**) demonstrated the weak structural integrity of the film and showed that it may not be very porous. Future work should focus on improving the polymerization and dialysis of this collagen gel for stretch experiments.
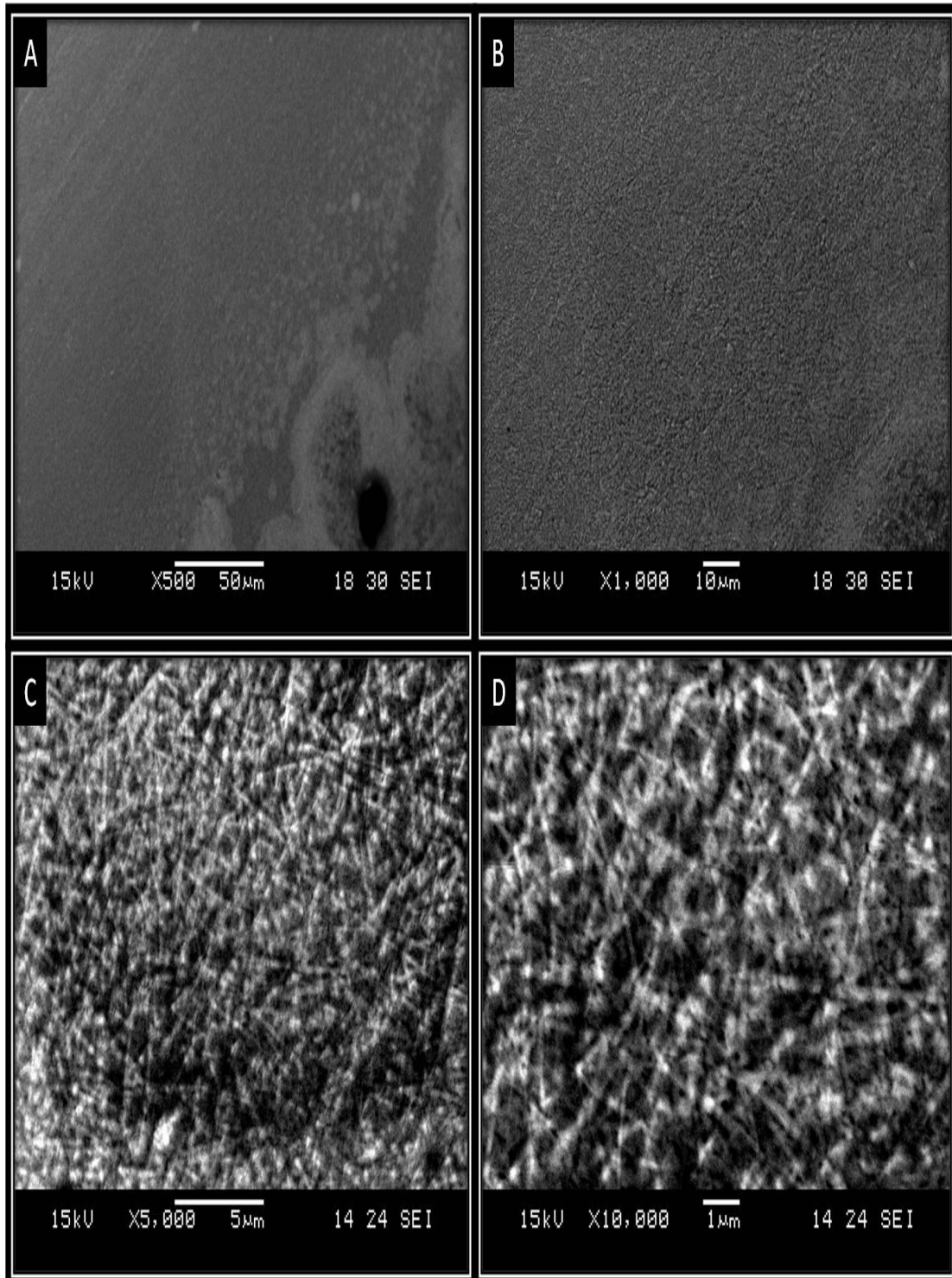
Figure 41 Scanning electron micrographs of dense disorganized collagen construct (DDCC)

[A-D] The DDCC scaffold was imaged at increasing magnifications (x500 - x10,000). It seemed to lack any porous structures. The film itself was very brittle.

The alternate route – electrospinning – for constructing a scaffold proved more successful. Tubular scaffolds were created on a mandrel for all three samples outlined in **Table 12**. It is evident from SEM micrographs in **Figures 42-44** that the original starting material/concentrations and rotation speed of the mandrel affect the fibre alignment and porosity of the scaffold.

Table 12 Electrospinning materials and parameters

This table outlines the differences between the types of poolycaprolactone scaffolds. The highlighted sections are the main factors that differ between scaffold fabrication via electrospinning.

Scaffold	PCL(%w/v)	Collagen (mg/mL)	Mandrel rotation Speed (rpm)
A	12	0	3,000
B	12	0	100
C	6	2	100

In the scaffolds produced at a higher rpm (**Figure 42**) the fibres become more aligned but maintained porosity. From inspection of multiple SEM micrographs the individual fibre diameters ranged from 100 nm to 4 μm. The scaffold contained many interconnected pores of various sizes (500 nm - 10 μm). Future modifications could be made to the protocol to generate scaffolds with an ideal pore size similar to that of the bioreactor system for permeability experiments.
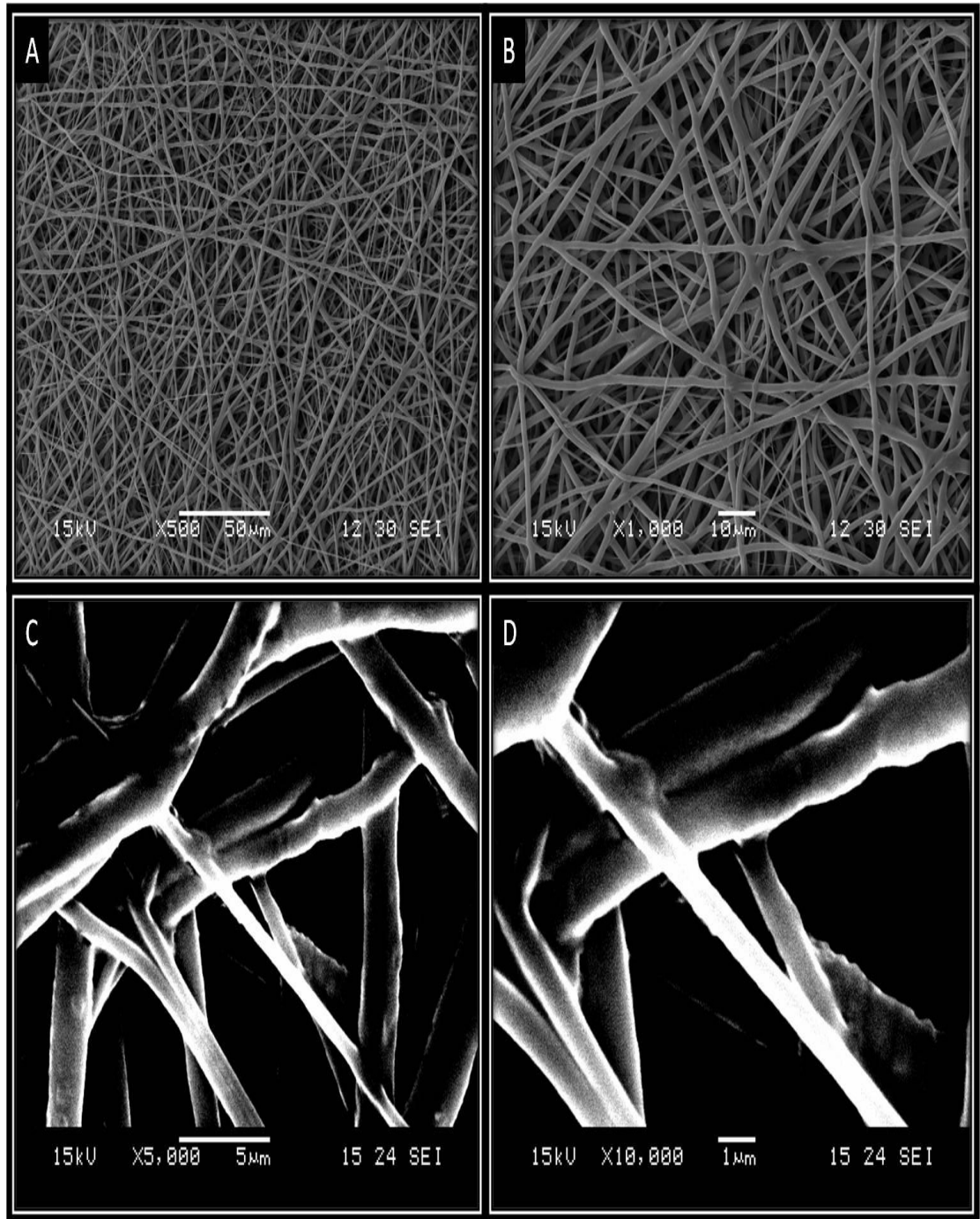
Figure 42 Scanning Electron Micrograph of aligned Polycaprolactone (PCL) scaffold

[A-D] The highly aligned Polycaprolactone (PCL) scaffold was imaged at increasing magnifications (x500 - x10,000). It was highly porous and the fibres formed a structured multilayered pattern.

In the randomly aligned scaffolds (**Figure 43**), the final material was approximately 100 -150 μm thick. Here the SEM micrographs demonstrated that the fibres were dispersed with less of a structured pattern than the aligned scaffold in **Figure 42**. The fibres were thicker in diameter (200 nm - 5 μm) and arranged in a random pattern. Similarly to the highly aligned scaffold, it contained many interconnected pores with varied sizes (200 nm - 1 0μm). The low magnification images of the randomly aligned scaffolds demonstrated greater discrepancies in structural integrity than the highly aligned scaffolds. Holes formed in some areas of the gel. Although the holes did not penetrate the entire gel they could prove problematic for studies of permeability under pressure. The defects may be improved by marginally increasing the rpm or creating a thicker gel with increase in volume of starting material.
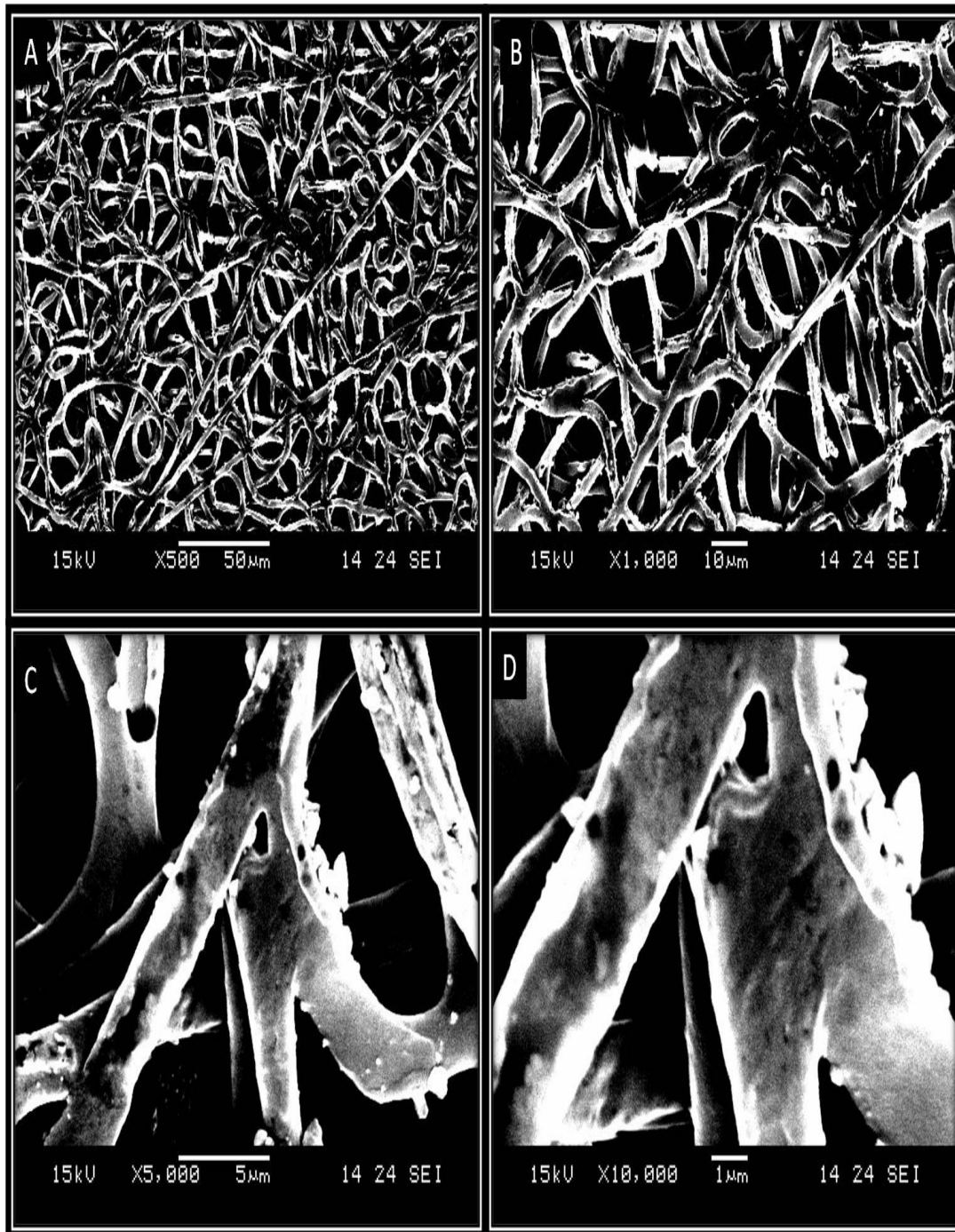
Figure 43 Scanning Electron Micrograph of randomly aligned PCL scaffold

[A-D] The randomly aligned PCL scaffold was imaged at increasing magnifications (x500 – x10,000). It was highly porous but lacked the compact pattern of the aligned scaffold. It also did not appear as complex as the layers of the aligned scaffold.

In order to construct the fourth scaffold with 2 mg/mL of freeze dried collagen content, a reduced Polycaprolactone PCL w/v of 6% was used for the initial studies. The obvious problems with this decreased PCL fraction are evident in **Figure 44** below, with random bead formation on the gel and an increase in hole formation. However, the presence of randomly aligned collagen fibres does make it more closely resemble the ECM visualized in the decellularization experiments. The scaffold has randomly dispersed thinner fibres with a maximum diameter of approximately 1 μm. Like the other scaffolds, it is highly porous. The collagen fibres are interconnected with PCL but they require additional strengthening via crosslinking to prevent solubility in water.
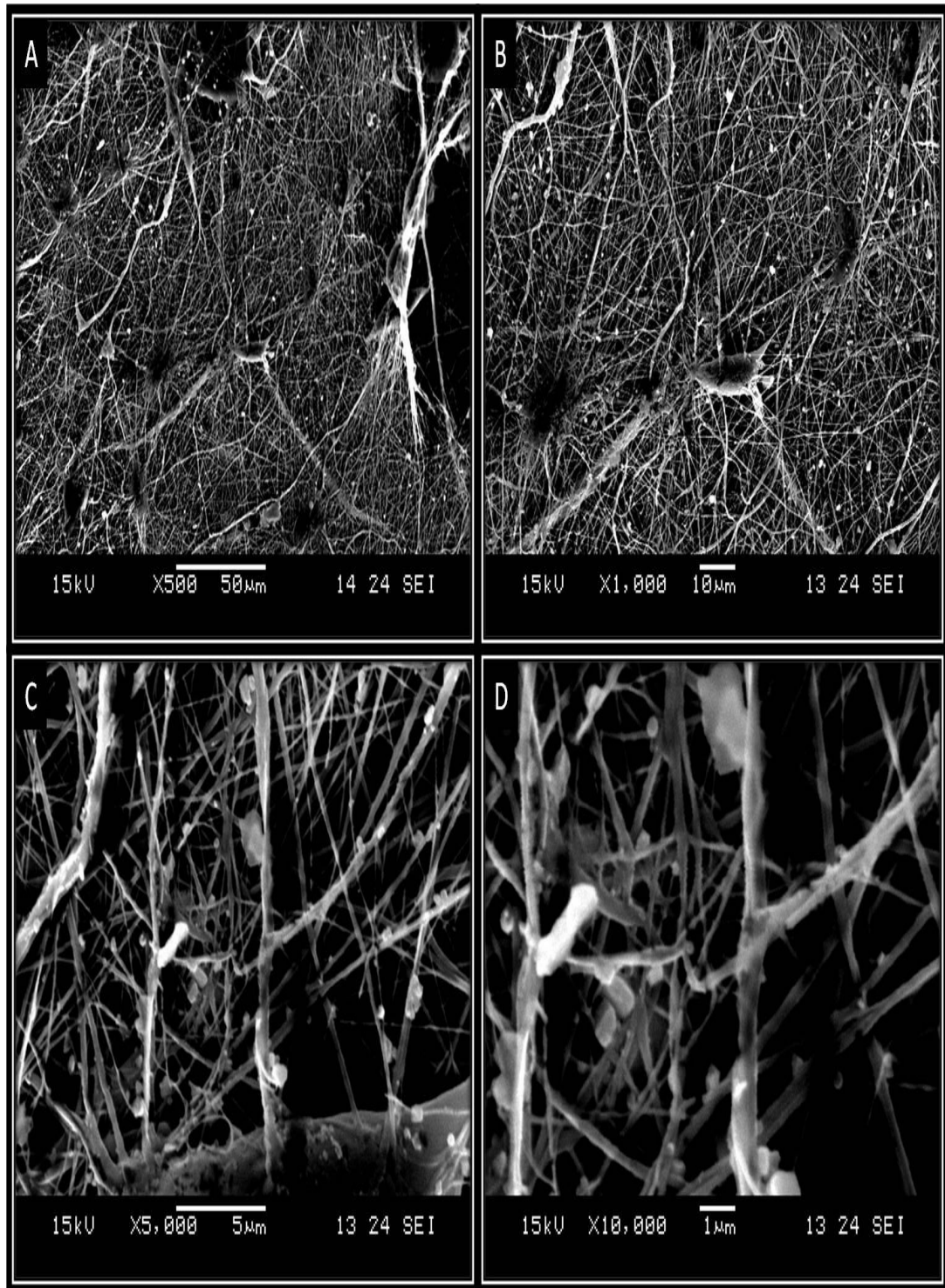
Figure 44 Scanning Electron Micrograph of PCL-Collagen scaffold

[A-D] The PCL scaffold electrospun with collagen was imaged at increasing magnifications (x500 - x10,000). It was a highly porous structure that resembled the basement membrane of an artery. However, it contained many holes and showed bead formation due to the lower percentage of PCL used.

It is evident from SEM imaging of different techniques processes and biomaterial combinations that the electrospinning process is efficient, highly reproducible, and easy to modify. Optimization is a necessity at this point and the first step of future studies would be to construct a smaller mandrel in order to create a tubular scaffold with the desired dimensions for the bioreactor. In the experiments that generated the results shown above, the diameter of the mandrel (10 cm) was too great to make tubular scaffolds appropriate for a bioreactor. Studies of the permeability of the scaffold itself will be required. Further literature research and experimentation is also required to determine which protocol, and hence fibre alignment, is optimal for endothelial cell monolayer seeding. Along with being highly reproducible, the system could prove to be more cost effective without the need to crosslink with collagen, as PCL is relatively affordable. This would require further cell studies before a decision is made.

The randomly aligned scaffold was used for preliminary research into the seeding of endothelial cells. The efficiency of cell seeding was initially determined by hematoxylin staining (**Figure 45**) The images were taken the day after cell seeding. This staining protocol demonstrated the presence of cell nuclei (purple) which suggested that cells had successfully seeded to the scaffold. In order to substantiate that cells were indeed seeded, they were stained with DAPI (nuclei) and rhodamine phalloidin (actin filaments) and imaged via fluorescence microscopy, as shown in **Figure 46** [A-I]. The DAPI stain demonstrated the presence of nuclei on the scaffold. The nuclei were circular in shape and had not fragmented which meant that the cells were still viable. The extended actin filaments (red) on the scaffolds suggested that the cells had seeded to the fibres of the scaffold. The hydrophobic nature of the PCL

scaffold may prevent complete seeding of cells or require multiple seedings with cells of the same passage number. There is some autofluorescence from the gels but the results do indicate that with further work the PCL electrospun scaffolds are likely to be a viable option for a scaffold for the novel bioreactor.
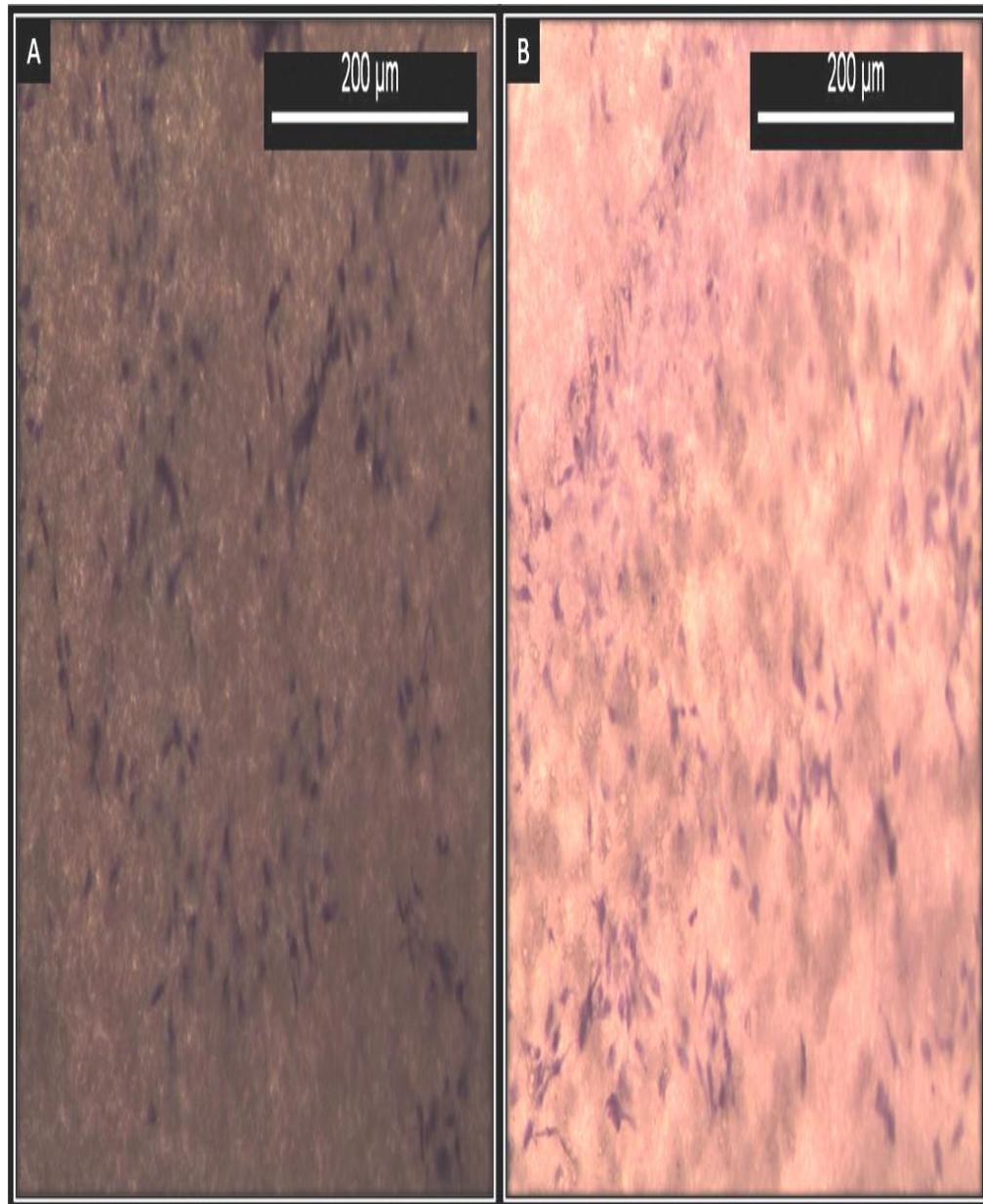
Figure 45 Assessment of cell seeding to PCL scaffold

[A-B] Hematoxylin staining was carried out to determine whether cells (nuclei stained purple) were seeded to the scaffold.
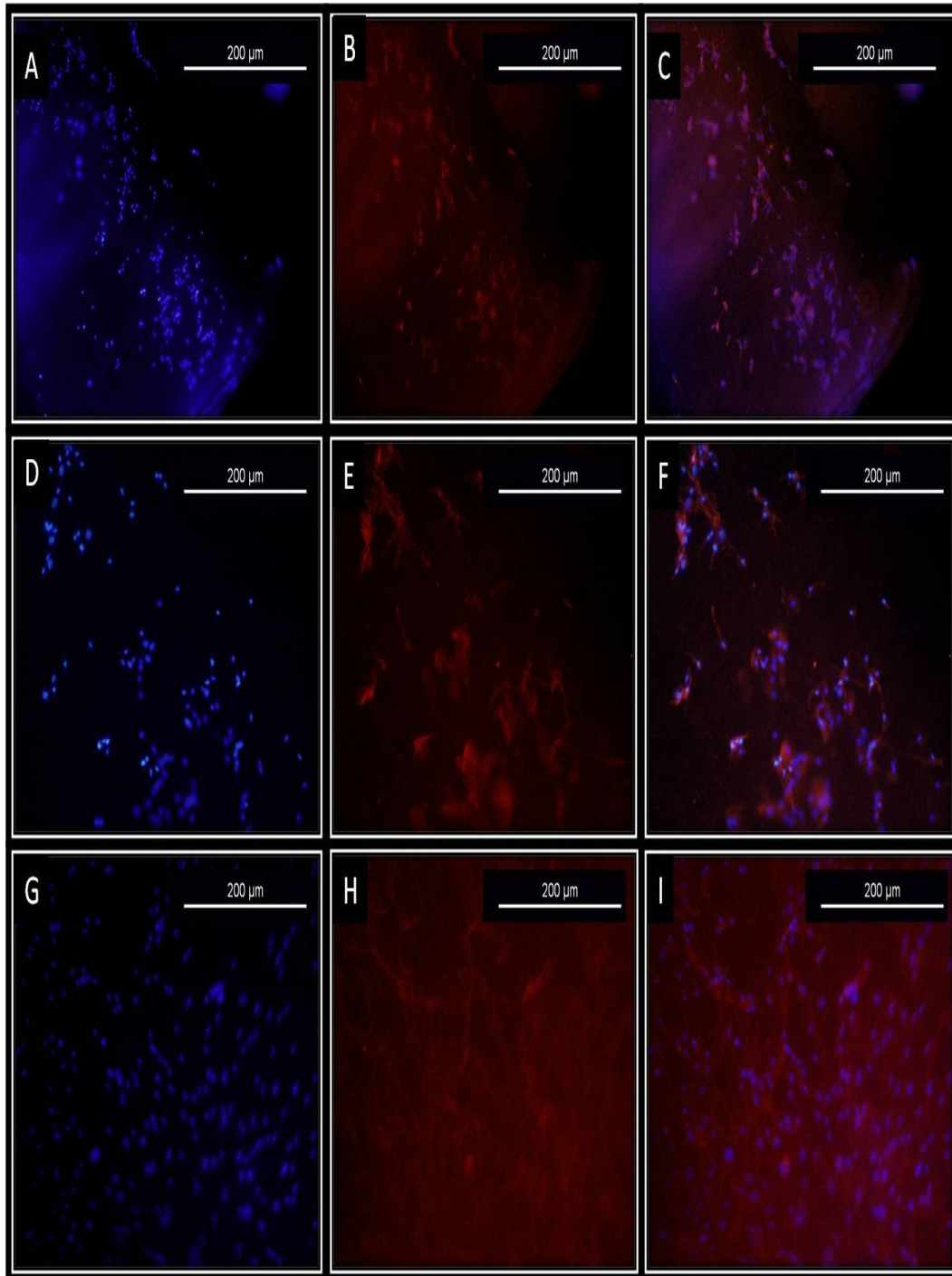
Figure 46 Fluorescent evaluation of endothelial cells seeded to electrospun PCL scaffold

EC were stained with DAPI (A, D, G, blue) to detect nuclei and Rhodamine Phalloidin (B, E, H, red) to detect actin filaments. The EC were examined with a fluorescence microscope at different magnifications. The first scaffold was imaged at x5 [A-C]. An increased magnification to x10 was then used for this scaffold [D-F]. An additional scaffold was imaged at x10 magnification [G-I] for cellular F-actin filaments. Composite images were created of both stains[C, F, I]

An additional step was carried out to determine whether the cells that seeded to the scaffolds might indeed be viable on the scaffold. A cytotoxicity assessment of the PCL scaffold was carried out by means of the Live/Dead assay (with the help of Molly Stevens' research group) to determine whether the cells seeded to the scaffold were alive or dead. The cells were seeded to the PCL scaffold at the same density as those seeded for the previous fluorescence studies. The live/dead assay stains live cells green and dead cells red. The green luminescence from cells demonstrated that the PAECs were alive on the scaffold (**Figure 47**).

This was a positive result, but it is important to note that the cells were not present at a high density throughout the scaffold. A higher seeding density or additional culturing may be required for monolayer formation. In images obtained at increasing magnifications, the PAECs appeared to seed along the fibres of the PCL scaffold. There was some background autofluoresence from the electrospun scaffold. The autofluoresence was not as intense as the hollow fiber membranes which means that the material could be the desired alternative with the right production modifications. It is highly likely that the scaffold requires additional priming prior to seeding to eliminate any residual hydrophobicity. These studies, too, should be carried out in future research.
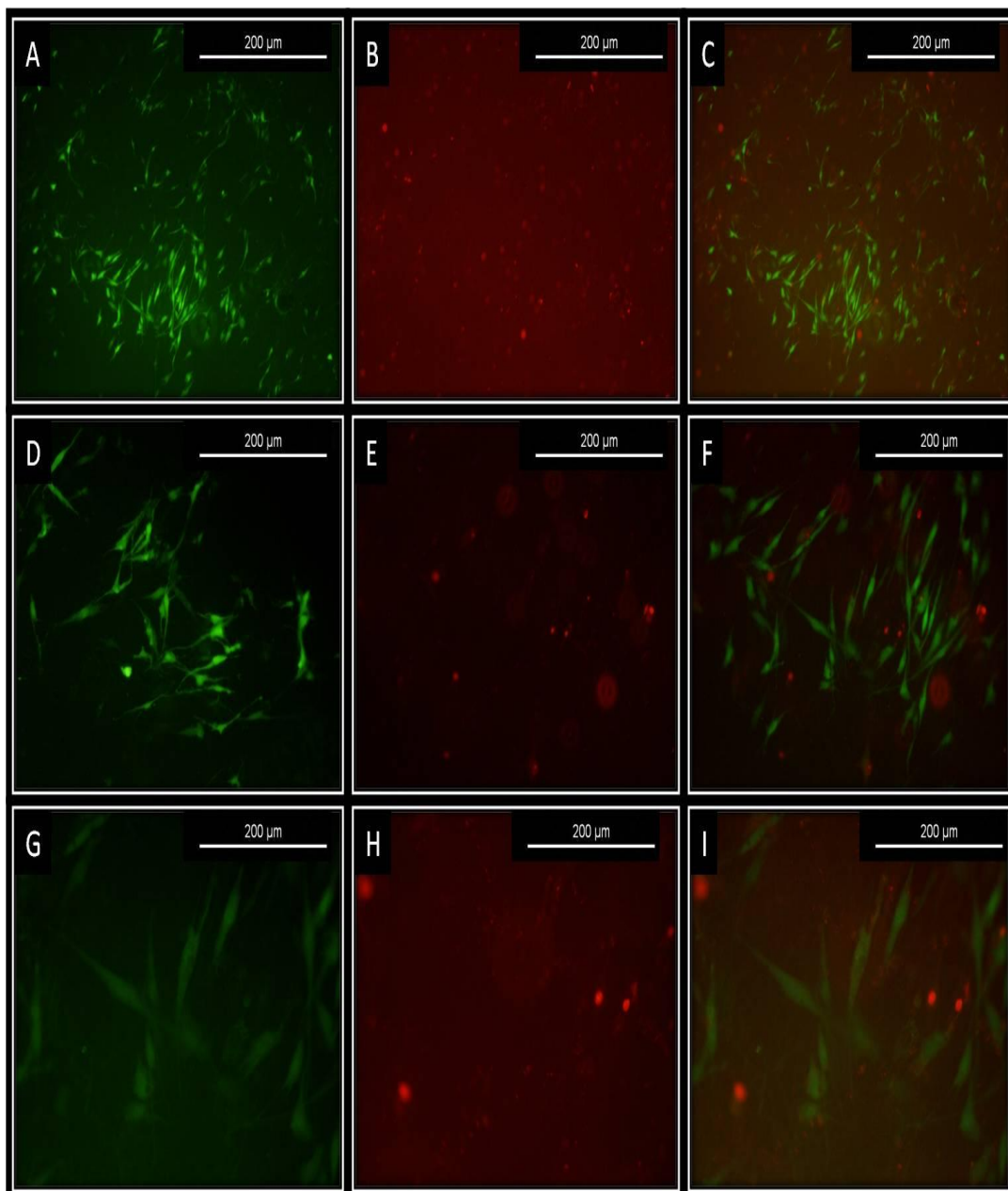
Figure 47 Cytotoxicity assessment of cells on an electrospun PCL scaffold

Live EC were stained with Calcein AM (A, D, G, green) and dead EC with EthD-1(B, E, H, red). They were examined with a fluorescence microscope at different magnifications. The first scaffold was imaged at x5 [A-C]. An increased magnification of x10 was then used for this scaffold [D-F]. An additional image was acquired at x20 magnification [G-I]. Composite images of both stains were created [C, F, I]. Following two days in culture it is evident that the scaffold is non-toxic as live cells populate the scaffold.

Due to the limitations associated with existing biomaterials and electrospinning technologies (e.g. lack of structural integrity, issues with seeding cells) for creating a satisfactory 3D structure for studying endothelial permeability *in vitro*, further work was started to develop 3D bioprinting hardware, with the long-term aim of printing suitable substrates. This work is described in narrative form in Appendix 1.

4.5 Conclusion

Overall the bioreactor system proved useful for investigating the biomechanical determinants of endothelial permeability under 3D cell culture conditions. The system was successfully employed and modified to investigate endothelial cell permeability under different patterns of mechanical stress with and without the introduction of pharmacological agents. It was possible to gain an understanding of the sensitivity of permeability to the presence and temporal pattern of shear stress, flow waveform, transmural flow, and active transport processes.

Its main limitation was in preventing the imaging of endothelial cell junctions and live imaging of transport across the membrane. The research and development of novel 3D materials, machines and methods for studying effects of cyclic strain on endothelial permeability was successfully initiated. The tissue engineered approach provided viable candidates for a novel bioreactor but further evaluation would be required in biomechanical testing and permeability studies with different types of PCL scaffold prior to creating a novel tubular scaffold for the bioreactor system.

APPENDIX 1

An excursion into the development of novel 3D bioprinting hardware and methods to develop the ideal scaffold for a hollow fibre bioreactor

The following text describes an excursion into the development and commercialization of new technologies for making appropriate scaffolds, in collaboration with others.

Due to the limitations associated with existing biomaterials, molding of 3D vessels, and electrospinning technologies (e.g. lack of structural integrity, issues with seeding cells) for creating satisfactory 3D structure for studying endothelial permeability *in vitro*, I started to develop 3D bioprinting hardware with the long-term aim of printing suitable substrates. I took what I learned in building and using electrospinning device technology and also building 3D printing technology and worked on the extrusion of 3D biological materials with a mix of different designs and drafts of more advanced multiplexed machines. The first piece of 3D bioprinting hardware I developed (in 2012/2013) was based upon the open-sourced RepRap 3D printers that led to a community of people developing new hardware based upon the machine parts[150]. Briefly, RepRap was an initiative started in 2005 by Dr. Adrian Boyer from the University of Bath that released all information surrounding the development of 3D printing technology. The device was capable of a build for layers of fluid material with one manual and later pump extrusion printhead and further experiments were conducted with the electodes used for the electrospinning part of my research work at imperial college to determine If possible to create improved resolution during 3D printing process 2011-2016. The work on electrospinning was what inspired the ideas for 3D bioprinting but also the multiplexing of different additive manufacturing process by attaching low voltage to the single extrusion head to determine if multiple processes could be implemented in one device. This was the first prototype that led me to form a start-up in 3D Bioprinting which would later connect with the work of Jemma Redmond

and our co-founding of advanced 3D bioprinting robotics and regenerative medicine start-up Ourobotics.

At that time, 3D bioprinting hardware retailed at over $200,000 and the market was small. I believed that it was technically possible to create an affordable desktop version with similar capabilities due to the availability of open source material from the RepRap initiative. Affordable desktop bioprinting would later disrupt the market of regenerative medicine by causing growth of a market that was approximately 100 million USD in 2014/2015 and is expected to become 1,647.4 million by 2024 [151]. I hypothesized that one of the open-source 3D printing machines could be suitably modified to extrude biomaterials with the right 3D structures, thereby creating an affordable desktop bioprinter. The first basic bioprinting device was developed when I modified a normal 3D RepRap device with a paste extruder. In 2013 it was further developed by a group of students who experimented with multiple bioprinting extrusion techniques and electrical bioinks, co-supervised by myself and Dr. Dominic Southgate as a project for the Rio Tinto Sports Innovation Programme at Imperial College.

Further work was done with other students interested in 3D Bioprinting for multiple applications during 2015 when I gave lectures on entrepreneurship or implementation of bioengineering technologies like electrospinning and 3D bioprinting on the Innovation Design Engineering masters between Imperial College London and Royal College of Art. Projects ranged from advanced textiles, architecture, sustainability, transforming materials into new projects or devices. One robotic project for implantation of bioprinted devices with Dr. Ravi Vaidyanathan and his biomechatronics group, a grant was proposed on these novel advanced biorobotic

projects that required different advanced manufacturing technologies like other 3D bioreactor or bioprocessing devices that I designed and co-developed with others. One Ourobotics project with Dr. Vaidyanathan was on the development of a Cybernetic Human-Robot Interface System and Bioprinted Organoid Biorobotics, Bioelectronics & Bionics but it was never funded despite the innovation potential for an idea like this in 2015. Dr. Southgate and Prof. Childs made the introduction of Jemma Redmond and I to Dr. Vaidyanathan and we had some amazing discusssions about the potential for 3D Bioprinting technology in the field of Biomechatronics, Human Machine Interfaces and Novel 3D Bionic devices.

The final "affordable" bioprinter included Richard Horn's open source Universal Paste Extruder design[152] with modifications. The design used the NEMA17 stepper motor, which is normally used for extruding solid material in the RepRap, to compress a syringe filled with biomaterial. The extra steps, started in 2013, are illustrated by videos on Richard Horn's tutorials[152, 153]. The wiring for the paste extruder was almost identical to the normal RepRap; the main difference is that the extruder wires are interchanged on the RepRap circuit board to swap the direction of extrusion so that the stepper motor presses down on the syringe plunger without having to change any of the default settings on the software. The fan and thermistor were no longer needed as the heat bed and thermistor temperatures were set to zero. The fan was still required; it was attached to the top of the frame to ensure it was out of the way.

The extrusion settings on the Pronterface software were established by trial and error for the different materials that were extruded, the environmental conditions, and the desired nozzle diameters (which were changed by using Luer Lock-compatible needles). As a guide, the initial experiments used a highly viscous conductive bioink at a temperature of 21°C, with a nozzle diameter of 2.1mm. Subsequent experiments were carried out with basic collagen and gelatin biomaterials, but the device (**Figure A1**) proved to have limitations and it would have required a great deal of work to establish what was needed to produce a 3D vasculature for a bioreactor. Experimentation was carried out with the single extruder and high voltages like those used for electrospinning or electrohydrodynamic printing but the final materials were not suitable and there were issues with the materials and short circuiting of the device when X,Y,Z bioprinting was coupled to the device without appropriate grounding.
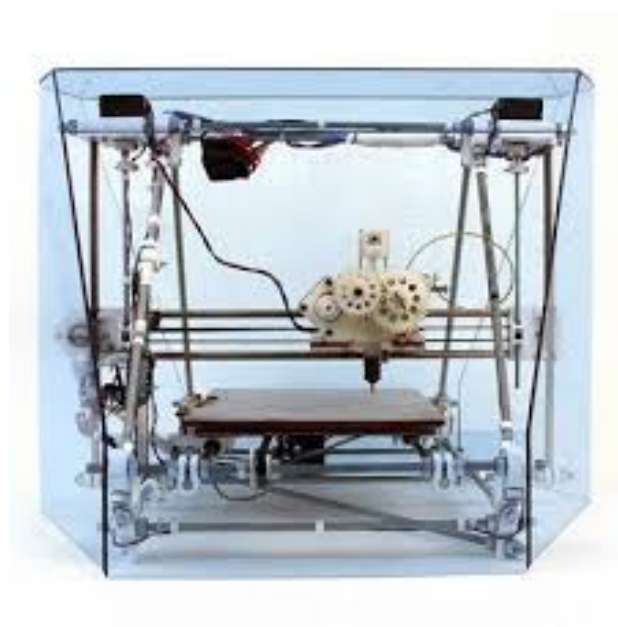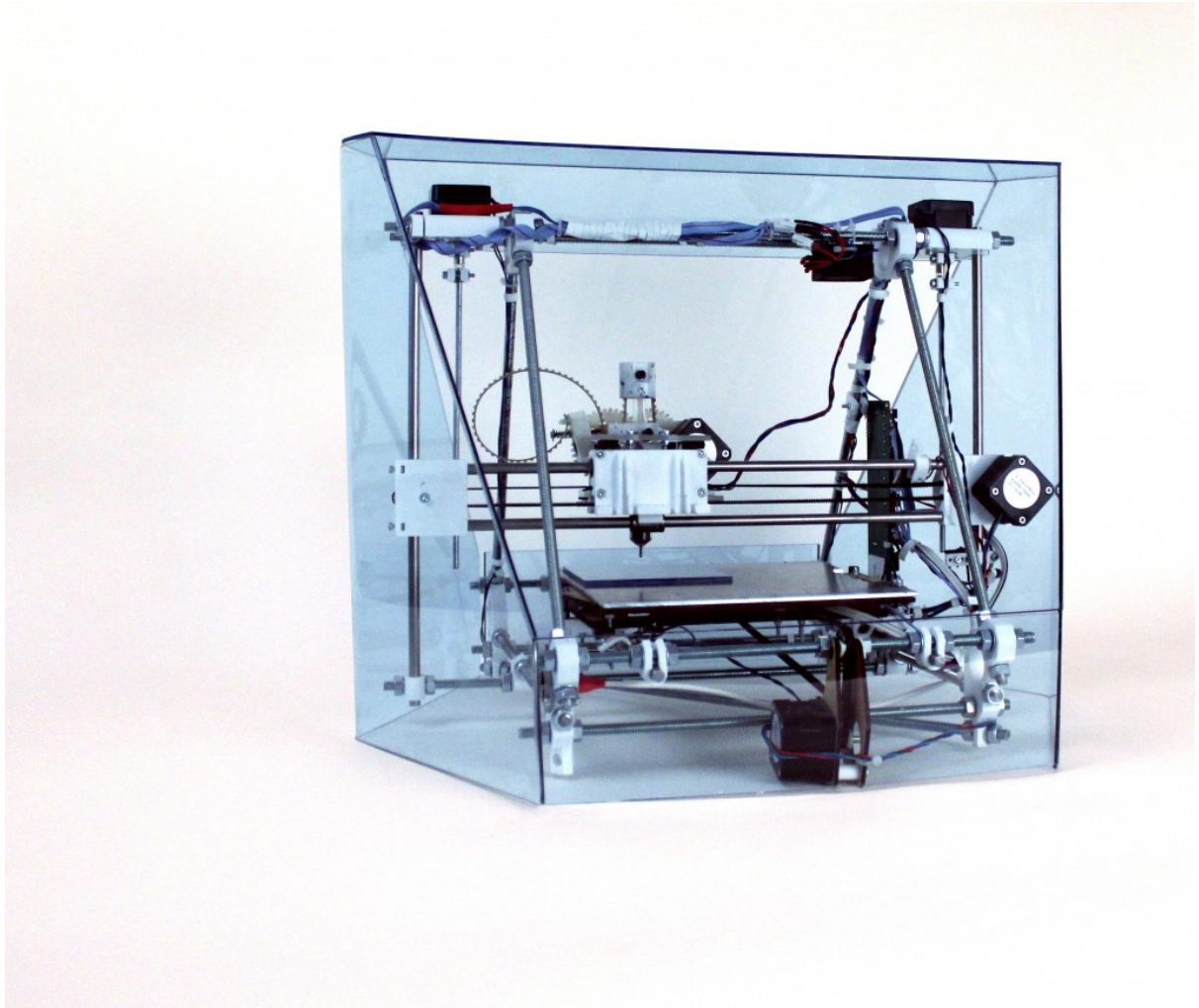
Figure A1 The basic 3D Bioprinting device without any additional attachments

It was clear that more advanced and affordable hardware was needed. As a result, I started to work with entrepreneurial engineer Jemma Redmond: together we co-developed more advanced robotic machines. This led to us co-founding our start-up company called Ourobotics based upon both ventures activities in 3D bioprinting. In 2015 its main office and lab in Cork, Ireland and some research and development at Imperial College London, following Jemma obtaining seed funding from SOSVentures and the Hardware accelerator HAX. The purpose of the bioprinting start-up company was to develop advanced and affordable hardware based upon the existing technology within the emerging field of 3D bioprinting. Jemma and I designed and developed the advanced "Revolution" bioprinter and a more advanced Medusa system with multiple

bioprinting technologies (shown with further developments in **Figure A2**). Prof Alexander Sefilaian and Hana Salussolia provided a great deal of collaborative support for all of Ourobotic's 3D Bioprinting ventures via their innovative novel graphene biomaterial company NanoRegMed.

Additional systems were designed by me at Imperial College and prototyped to include an electrohydrodynamic component, electrospinning component, or bioelectrospraying component, based upon my work with electrospun materials during my PhD. Electrohydrodynamic printing, Bioelectrospraying, and Cell electrospinning are forms of additive manufacturing that uses and electric field to deposit a material and was first developed by Prof. Jayasinghe for tissue engineering applications [154-156]. The design and development of the advanced 3d biofabrication machine with these novel attachments, the "Medusa system," started following a conversation with Prof. Suwan Jayasinghe in 2015. Jemma and I started to examine ways of implementing bioelectrospraying and other components; the designs were based upon multiple print heads with different advanced manufacturing functionalities. Briefly, a high voltage source was applied to all printheads; my father, Gerard Gray and colleague Aidan Hickey, provided electrical engineering insight on grounding of materials and the original setup needed for one syringe. Simple modifications were made to one syringe of the basic open-source 3D bioprinter, allowing the use of a pump rather than the screwhead-based extrusion. In parallel, further versions of the Medusa system were co-designed by Jemma Redmond, Gerard Gray and me. Jemma implemented a closed loop control of the high voltage and additional electrodes to focus the beams of deposited materials, similar to electrospinnning or Prof. Jayasinghe's bioelectrospraying and cell electrospinning devices, but with an X,Y, and Z axis. Basic materials were fabricated.

Dr. Andrew Comerford came on board as a co-founder and Chief Technology Officer with Jemma and I in 2015 and co-developed innovative software and gave feedback on the designs of advanced machines.

Briefly a high voltage source was applied to all printheads based upon insight that Prof. Jayasinghe gave to Jemma Redmond and my father Gerard Gray provided electrical engineering insights on grounding of components and the use of the voltage materials for material deposition in the X,Y, Z axis of the basic 3D Bioprinter and singular print head but experiments would fail and at times the machines had to be reassembled with new parts. The addition of the high voltage to the basic machine came from my experience on work with electrospinning which was discussed in the future work chapter. Simple addition modifications were made to one syringe of the basic open sourced 3D bioprinter with the use of a pizoelectric pump rather than the screw head-based extrusion. In parallel more designs of the second Medusa system were co designed by Jemma Redmond, Gerard Gray and I while she was assisting some of the Innovation Design Engineering student projects I was co supervising for 3D bioprinting or other bioengineering technologies. We copyrighted our ideas and designs as no funding was available for patents. Jemma implemented a closed loop control of the high voltage and additional electrodes to focus the beams of deposited materials similar to electrospoinnning or Prof. Jayasinghes bioelectrospraying and cell electrospinning devices but with an X,Y, and Z axis. Dr. Dominic Southgate provided some insight on the advanced machines potential as did the discussions with Prof. Jordon miller following his extrusion of 3d printed sugar material and nature publication[157].

Other needs for ultrasonic calibration, movement of electrode beneath the print bead for true 3D structures, precise deposition of materials during the extrusion process, or use of electrode to focus the electric jet of extruded materials were noted but not implemented prior to me finishing my work at Imperial College in late 2015. Basic materials were fabricated using the combination of the basic technology experiments at Imperial College, the more advanced experiments with the high voltage and 10 materials robotic arm bioprinter. Issues appeared in relation to the voltage control and the connection of certain chemicals or biomaterials with the right components for high voltage extrusion were difficult. Voltage waveforms were experimented with using the basic, and advanced 3D bioprinting devices but the experimentation required more advanced work and was put on hold until 2016.

In 2016 I started a postdoctoral position at Massachusetts Institute of Technology and the Singapore MIT Alliance, so I had limited time for the development of anything in 3D Bioprinting as I was focused on the development of organ on a chip technology for blood brain barrier vasculature. During that time I designed multiple revisions for a modular machine and during the startup we revisited the development and further design of the "medusa system" to include not only multi materials and different types of extrusion print heads rather than general extrusion bioprinting along with bioreactor and incubator enclosures and machine vision technology. More advanced camera calibration was introduced but never completed. Together we explored the issue of grounding the print bed with Gerard Gray to improve the deposition of the materials using the electrical fields within incubator setting so that materials could be extruded and form 3d biological components within the right environment, but issues appeared with humidity and the final 3d biological material. The needles were also grounded, or

negative voltage was experimented with also further work was done all lower voltage as published by Professor Jayasinghe[158], but it failed during experiments with the basic machine at Imperial College and lower voltages were attempted with the more complex devices. The temperature of the reservoirs and the materials can be controlled but did not influence the final device performance and were increasingly difficult with the robotic arm which would malfunction when we tried to implement new bioprinting technologies

The first commercially available machine developed by our start-up Ourobotics "The Revolution" had 10 printheads controlled by a robotic arm with the ability to build. Surface or materials with or without electrostatic charge was first featured in a news article in 3D Printing Industry Magazine in 2015 and retailed at under $12,000-20,000[159] .The machine itself was one of the world's first affordable multi-material 3D bioprinter with robotic arm functions rather than the traditional modified 3D printer approach of other desktop bioprinters that were created at that time. The machine that we co-developed and other future machines that we documented proved to be suitable for the development of the vascular scaffolds required but time did not permit the further development of the scaffolds for this thesis. The first machine that I developed from the RepRap model was later open sourced and published in 3D Printing Industry Magazine in 2016 as the "Renegade" model retailing at $900[160]. The combination of electrospinning or high voltage technologies electrohydrodynamic printing, bioelectrospraying, and cell electrospinning was used in the further development of the device but too complex to be open sourced information.

The machine that Jemma and I co-developed was featured in "The top 10 3D Bioprinter's" for 3D Printing Industry Magazine in 2015[161] . The hardware developed by Ourobotics, Cellink and others disrupted the existing market dominated by companies such as Envisontec and Organovo. They created a new market segment of affordable 3D bioprinting hardware technology. "Disruptive Technology" was first coined by Clayton Christensen in 1997 and makes reference to a new market segment being established with the ability to act as a new channel of products for early adopters in competition with established products on the market or by introducing high performance products without the higher priced products[162].Ourobotics also follows the Knowledge Intensive Entrepeneurship phenomenon of startups and entrepreneurial companies being created on the basis of different types of knowledge amongst founders, sources, financial, or the societal impact of the startup[163].

From the hardware development perspective, the core technology functioned as an intelligent robot with multi-biomaterial capabilities and artificial intelligence retooling software to build complex 3D biological structures. Dr. Comerford created some innovative software platform designs like an online database of 3D organ designs that could be readily used and implemented like printable organs with the click of a button. The machine's robotic arm could be operated remotely and print up to 10 different biomaterials at once. Jemma and I drafted plans and grant applications with Professor Jimmy Moore on a use of the start-up developing a GMP/GLP 3D Bioprinting Facility for "Lymph Node Replacement Implant for Prevention and Treatment of Lymphoedema". We had collaboration discussions with Dr. Ravi Valiathank via Dr. Dominic Southgate. The machines originally used the extrusion bioprinting technology, but the novel retooling system allowed for the incorporation of other bioprinting

technologies like 3D bioelectrospraying, cell electrospinning, and electrohydrodynamic bioprinting. We also developed upgrades for incubator/bioreactor enclosure systems, part of which is partially shown as an enclosure in in the Figures.
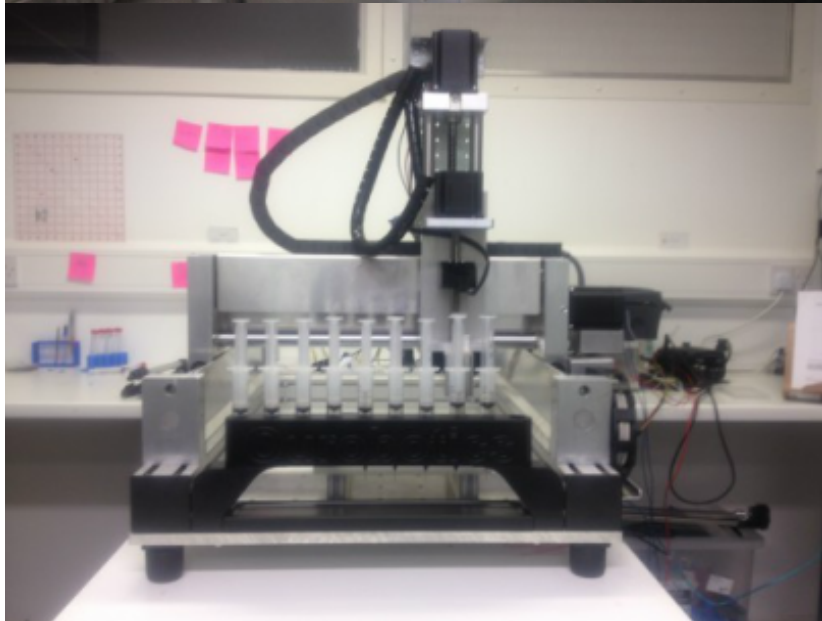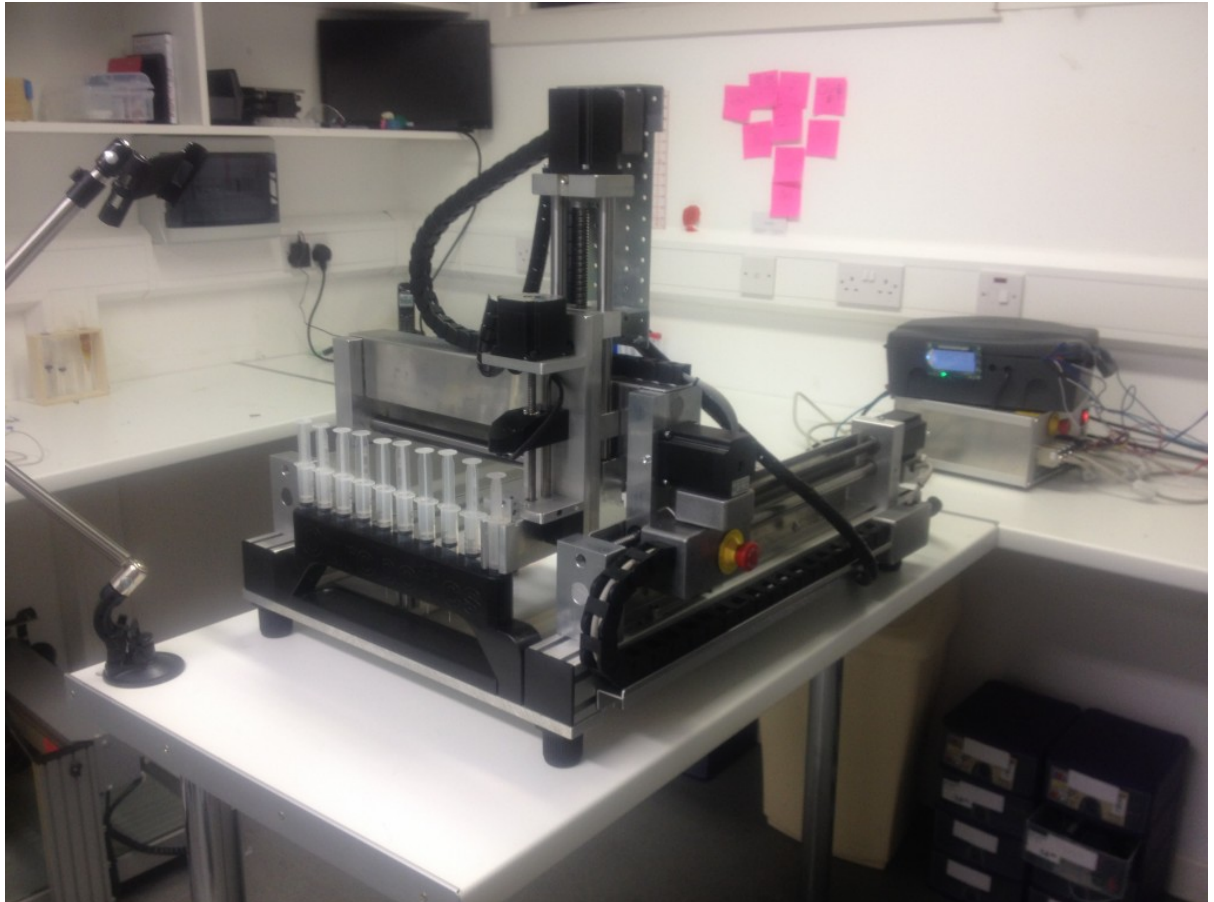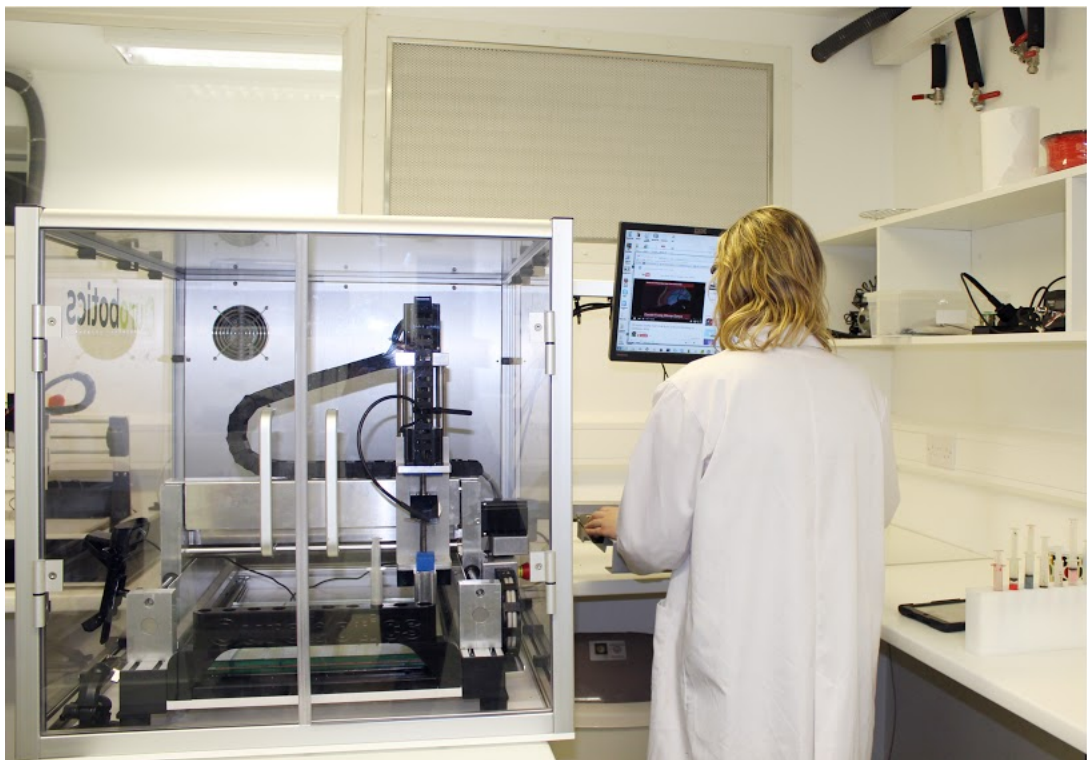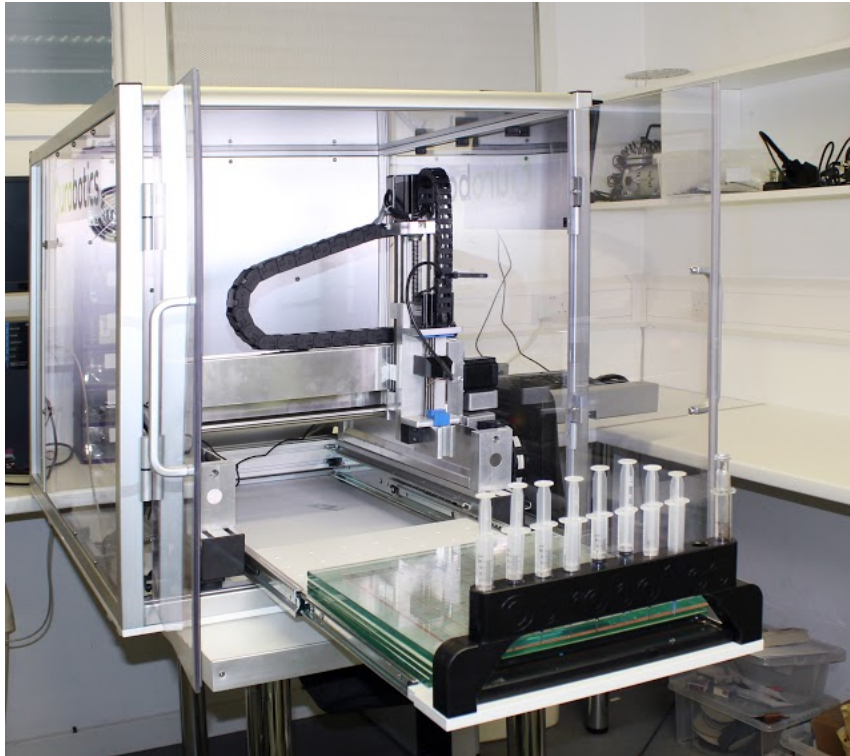
Figure A2 The advanced machine co-developed with start-up Ourobotics to include multiple bioprinting functionality methods and processes

Some images of attempted bioprinting using multiple techniques and methods with alginate and gelatin can be found in Figure A3. Sadly work on the devices did not continue with Jemma Redmond while I was working as a postdoctoral researcher at MIT as she passed away in September 2016[164].

The first commercially available machines and A.I. software's and platforms I co-developed with Jemma Redmond and others at Imperial College has since been featured in a number of scientific publications on bioink development, new biofabrication techniques, pharmaceutical drug development and other experiments for regenerative medicine or tissue engineering applications[165-170]. Our ideas, 20+ patent designs, documents, and novel bioprinting experimental method, logos, business models were all copyrighted and some research and development information, designs and documentation. Some images of attempted 3D bioprinting

with and without electrodes and high voltages using multiple techniques and methods with alginate and gelatin can be found in **Figure A3**.

During my PhD I also co-founded a. second start-up organization- Research DynamiX[171] with some individuals and colleagues mentioned in the acknowledgements to provide free data analytics-based strategy consultancy advice and solutions to advance the potential of international biotechnology, life science, & deep technology companies from start-up to scale-up. Copyrights surrounding multiple ideas were protected under the names Research Dynamix, Biochanges, and Ourobotics. The group of co-founders have revolutionized international start-up and scale-up company potential with free data driven strategy assistance and solutions with advanced software platform tools and access to individual co-founder skillsets. The team of co-founders used data analytics, trend forecasting, market/industry evaluation, machine learning, financial engineering, and business intelligence tooling to advance a start-up stability and scalability.

Originally co-founded in 2011-2016 by a group of 10 entrepreneurs, business professionals, PhD/postdoctoral scientists and engineers working at Imperial College London, and Massachusetts Institute of Technology. A number of the original team members or co-founders joined over the years and most have gone on to form award winning start-up companies within the fields of regenerative medicine, deep technology, 3D bioprinting robotics, organ on a chip technology, artificial intelligence, fintech, and synthetic biology. The team has previously used the data analytic approach and tools or internal expertise available to freely advise a number of start-ups and scale-ups on strategic solutions for pipeline and corporate expansion,

corporate restructuring or change in revenue distribution, new revenue models, business development strategies, private investment, mergers and acquisitions, funding strategies and opportunities, pitch deck, business plans, business case, guided entry into UK, EU or USA markets, and location of talent or innovative technologies within high ranking universities. In addition to this we have provided free data driven strategies for scale ups by pin pointing optimal valuation, preparation of winning pitch decks, business cases, business plans, negotiation of technology acquisition terms, due diligence, and connections to high profile talent, and novel technology developers and innovators in the different industries. The group hosted events at Imperial College London, MIT Media Lab, and the Royal College of Art during my time as a visiting lecturer for the master's Course Innovation Design Engineering.

Overall the 3D bioprinting technologies that were developed during my research at Imperial College London from 2011-2016 made an impact on the sector, created a new industry, and our ideas and 37 patent designs went beyond bioprinting.
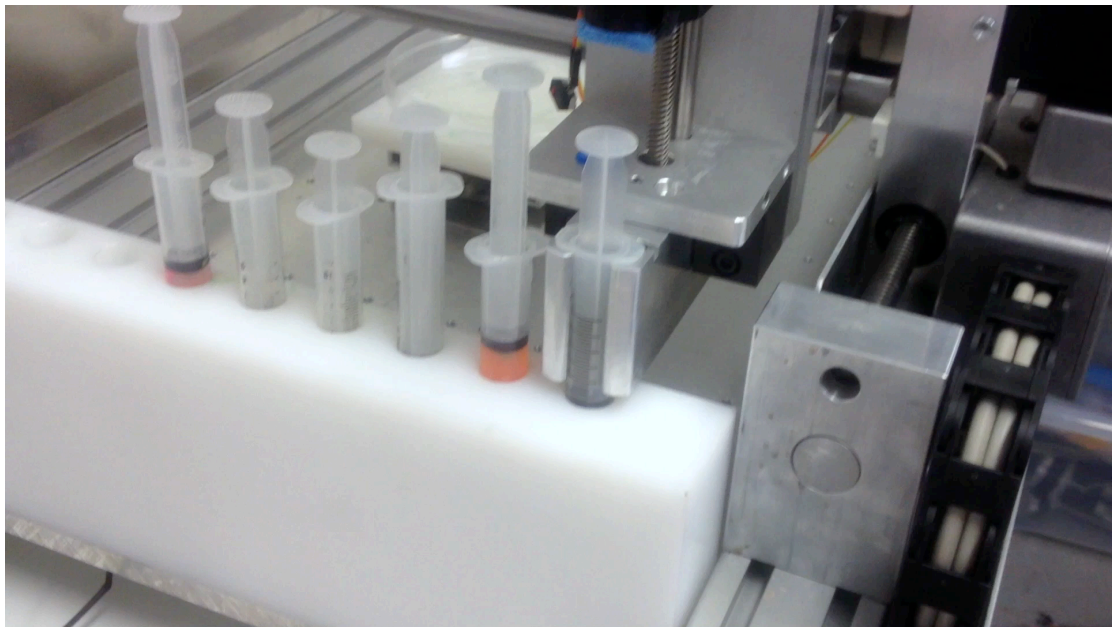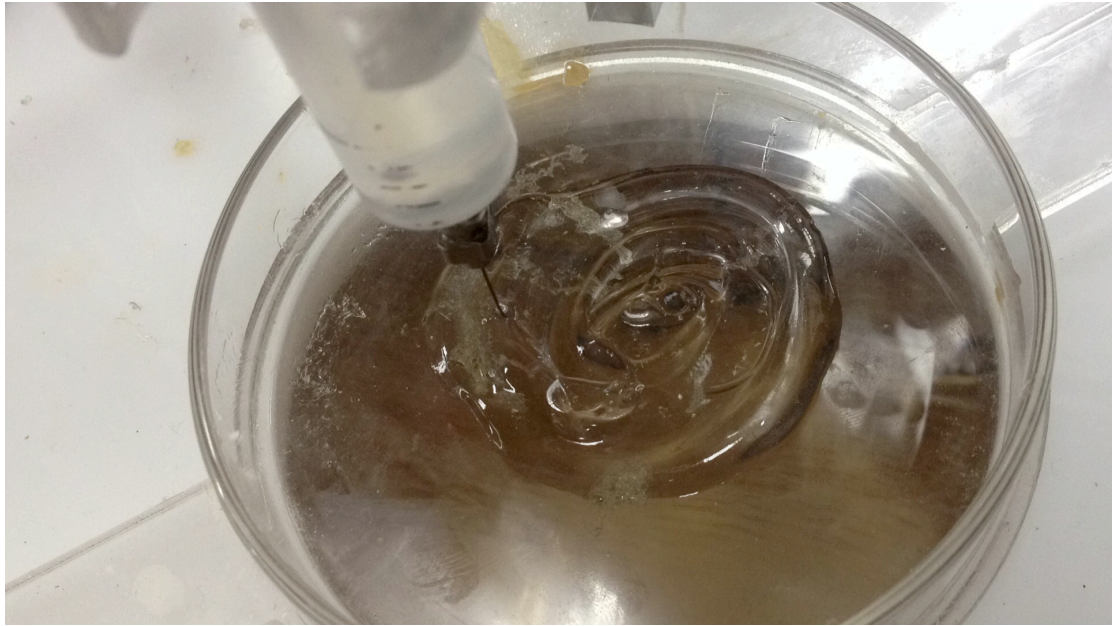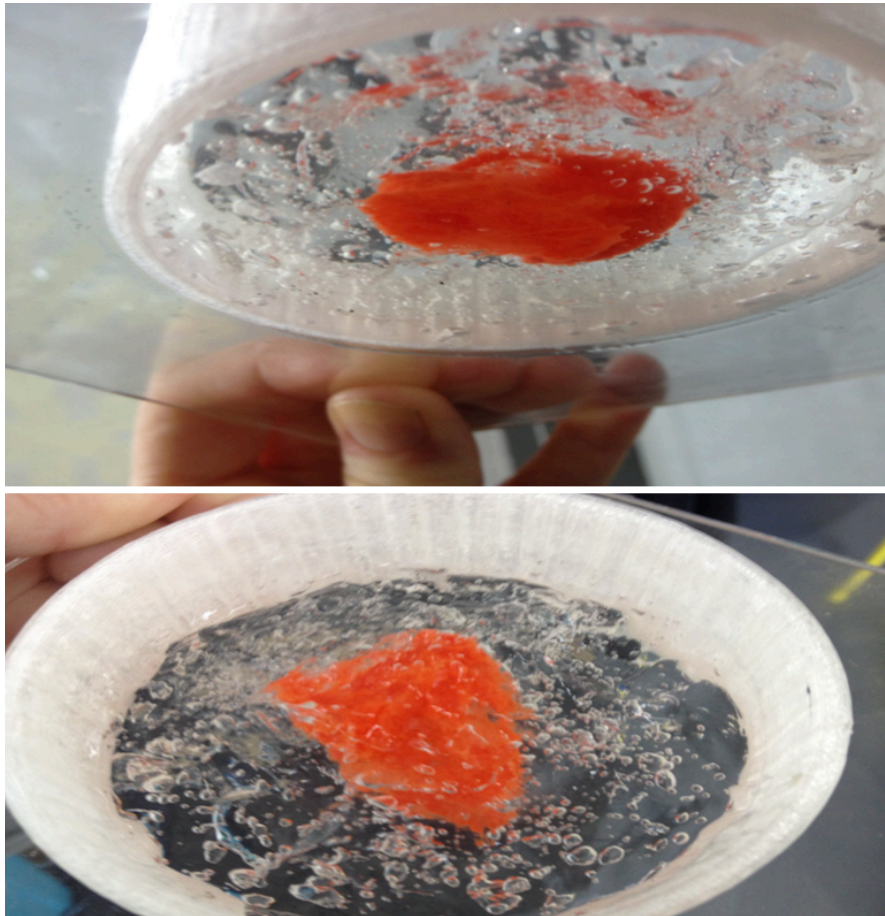
Figure A3   3D bioprinted collagen, gelatin, and alginate

References

1. Weinberg, P.D. Rate-Limiting Steps in the Development of Atherosclerosis: The Response-to-Influx Theory. *Journal of Vascular Research* **41**, 1-17 (2004).
2. Staughton, T.J., Lever, M.J. & Weinberg, P.D. Effect of altered flow on the pattern of permeability around rabbit aortic branches. *American Journal of Physiology - Heart and Circulatory Physiology* **281**, H53-H59 (2001).
3. Weinbaum, S., Tzeghai, G., Ganatos, P., Pfeffer, R. & Chien, S. Effect of cell turnover and leaky junctions on arterial macromolecular transport. *American Journal of Physiology - Heart and Circulatory Physiology* **248**, H945-H960 (1985).
4. Hammoudeh, A.J. *et al.* Prevalence of conventional risk factors in Jordanians with coronary heart disease: The Jordan Hyperlipidemia and Related Targets Study (JoHARTS). *International Journal of Cardiology* **110**, 179-183 (2006).
5. Ndiaye, N.C., Azimi Nehzad, M., El Shamieh, S., Stathopoulou, M.G. & Visvikis-Siest, S. Cardiovascular diseases and genome-wide association studies. *Clinica Chimica Acta* **412**, 1697-1701 (2011).
6. Nordestgaard, B.G. & Zacho, J. Lipids, atherosclerosis and CVD risk: Is CRP an innocent bystander? *Nutrition, Metabolism and Cardiovascular Diseases* **19**, 521-524 (2009).
7. Liu, P., Zhou, B., Gu, D., Zhang, L. & Han, Z. Endothelial progenitor cell therapy in atherosclerosis: A double-edged sword? *Ageing Research Reviews* **8**, 83-93 (2009).
8. Mendis, S., Nordet, P., Fernandez-Britto, J.E. & Sternby, N. Atherosclerosis in children and young adults: An overview of the World Health Organization and International Society and Federation of Cardiology study on Pathobiological Determinants of Atherosclerosis in Youth study (1985–1995). *Prevention and Control* **1**, 3-15 (2005).
9. O'Donnell Jr, T.F. Pulsatile flow and atherosclerosis in the human carotid bifurcation: Positive correlation between plaque location and low and oscillating shear stress: Ku DN, Giddens DP, Zarins CK, et al. Arteriosclerosis 1985; 5: 293–302. *Journal of Vascular Surgery* **3**, 944 (1986).
10. Kritchevsky, D. Fatty acids, triglyceride structure, and lipid metabolism. *The Journal of Nutritional Biochemistry* **6**, 172-178 (1995).
11. Caro CG, F., Schroter RC Atheroma and arterial wall shear. Observation, correlation and proposal of a shear dependent mass transfer mechanism for atherogenesis. *Proceedings of the Royal Society of London Series Biological Sciences* **177**, 109- (1971).
12. Peiffer, V., Sherwin, S.J. & Weinberg, P.D. Does low and oscillatory wall shear stress correlate spatially with early atherosclerosis? A systematic review. *Cardiovascular Research* (2013).
13. Gotto, A.M. Introduction. *Circulation* **109**, III-1-III-1 (2004).

14.   Vita, J.A. & Mitchell, G.F. Effects of shear stress and flow pulsatility on endothelial function: Insights gleaned from external counterpulsation therapy*. *Journal of the American College of Cardiology* **42**, 2096-2098 (2003).

15.   Traub, O. & Berk, B.C. Laminar shear stress: mechanisms by which endothelial cells transduce an atheroprotective force. *Arterioscler Thromb Vasc Biol* **18**, 677-685 (1998).

16.   Ross , R. Atherosclerosis — An Inflammatory Disease. *New England Journal of Medicine* **340**, 115-126 (1999).

17.   Gimbrone, M.A., Topper, J.N., Nagel, T., Anderson, K.R. & Garcia-CardeÑA, G. Endothelial Dysfunction, Hemodynamic Forces, and Atherogenesisa. *Annals of the New York Academy of Sciences* **902**, 230-240 (2000).

18.   Davies, P.F. Flow-mediated endothelial mechanotransduction. *Physiol Rev* **75**, 519-560 (1995).

19.   Resnick, N. *et al.* Fluid shear stress and the vascular endothelium: for better and for worse. *Progress in Biophysics and Molecular Biology* **81**, 177-199 (2003).

20.   Ballermann, B.J., Dardik A Fau - Eng, E., Eng E Fau - Liu, A. & Liu, A. Shear stress and the endothelium. (1998).

21.   Chatzizisis, Y.S. *et al.* Role of Endothelial Shear Stress in the Natural History of Coronary Atherosclerosis and Vascular Remodeling: Molecular, Cellular, and Vascular Behavior. *Journal of the American College of Cardiology* **49**, 2379-2393 (2007).

22.   Yamaguchi, T., Kikkawa, S., Yoshikawa, T., Tanishita, K. & Sugawara, M. Measurement of turbulence intensity in the center of the canine ascending aorta with a hot-film anemometer. *J Biomech Eng* **105**, 177-187 (1983).

23.   Weinberg, P.D. & Ross Ethier, C. Twenty-fold difference in hemodynamic wall shear stress between murine and human aortas. *J Biomech* **40**, 1594-1598 (2007).

24.   Hahn, C., Orr, A.W., Sanders, J.M., Jhaveri, K.A. & Schwartz, M.A. The subendothelial extracellular matrix modulates JNK activation by flow. *Circ Res* **104**, 995-1003 (2009).

25.   Ingber, D.E. Tensegrity: the architectural basis of cellular mechanotransduction. *Annual review of physiology* **59**, 575-599 (1997).

26.   Helmke, B.P., Rosen, A.B. & Davies, P.F. Mapping Mechanical Strain of an Endogenous Cytoskeletal Network in Living Endothelial Cells. *Biophysical Journal* **84**, 2691-2699 (2003).

27.   Davies, P.F. Hemodynamic shear stress and the endothelium in cardiovascular pathophysiology. (2009).

28.   Muller, J.M., Chilian, W.M. & Davis, M.J. Integrin signaling transduces shear stress--dependent vasodilation of coronary arterioles. *Circulation research* **80**, 320-326 (1997).

29.   Mehta, D. & Malik, A.B. Signaling Mechanisms Regulating Endothelial Permeability. *Physiological Reviews* **86**, 279-367 (2005).

30.   Mestel, A.J., Mokady, A.J., Parker, K.H. & Winlove, C.P. Effects of the glycocalyx on the electrophoretic mobility of red cells and on streaming potentials in blood vessels: predictions of a structurally-based model. *Biorheology* **35**, 365-381 (1998).

31. Iomini, C., Tejada, K., Mo, W., Vaananen, H. & Piperno, G. Primary cilia of human endothelial cells disassemble under laminar shear stress. *The Journal of cell biology* **164**, 811-817 (2004).
32. Lu, D. & Kassab, G.S. Role of shear stress and stretch in vascular mechanobiology. *Journal of the Royal Society Interface* **8**, 1379-1385 (2011).
33. Dalby, M.J. *et al.* Nanomechanotransduction and interphase nuclear organization influence on genomic control. *Journal of cellular biochemistry* **102**, 1234-1244 (2007).
34. Komarova, Y. & Malik, A.B. Regulation of Endothelial Permeability via Paracellular and Transcellular Transport Pathways. *Annual Review of Physiology* **72**, 463-493 (2010).
35. R.J. Levick, H.A. An Introduction to Cardiovascular Physiology (5th edition). *An Introduction to Cardiovascular Physiology (5th edition)* (2010).
36. Mehta, D. & Malik, A.B. Signaling Mechanisms Regulating Endothelial Permeability. *Physiological Reviews* **86**, 279-367 (2006).
37. van den Broek, C.N. *et al.* Medium with blood-analog mechanical properties for cardiovascular tissue culturing. *Biorheology* **45**, 651-661 (2008).
38. Adriani, G., Ma, D., Pavesi, A., Goh, E.L.K. & Kamm, R.D. in 2015 37th Annual International Conference of the IEEE Engineering in Medicine and Biology Society (EMBC) 338-341 (2015).
39. Radeva, M.Y. & Waschke, J. Mind the gap: mechanisms regulating the endothelial barrier. *Acta Physiologica* **222**, e12860 (2018).
40. Soon, A.S., Chua, J.W. & Becker, D.L. Connexins in endothelial barrier function - novel therapeutic targets countering vascular hyperpermeability. *Thromb Haemost* **116**, 852-867 (2016).
41. Simionescu, N. *Cellular aspects of transcapillary exchange*, Vol. 63. (1983).
42. Pappenheimer, J.R., Renkin, E.M. & Borrero, L.M. Filtration, diffusion and molecular sieving through peripheral capillary membranes; a contribution to the pore theory of capillary permeability. *Am J Physiol* **167**, 13-46 (1951).
43. Tuma, P. & Hubbard, A.L. Transcytosis: crossing cellular barriers. *Physiol Rev* **83**, 871-932 (2003).
44. Palade, G.E. *Fine Structure of Blood Capillaries*, Vol. 24. (J Appl Phys., 1953).
45. Yamada, E. The fine structure of the gall bladder epithelium of the mouse. *J Biophys Biochem Cytol* **1**, 445-458 (1955).
46. Razani, B.L., Michael The Role of Caveolae and the Caveolins in Mammalian Physiology. *Revies in Undergraduate Research* **1**, 44-50 (2002).
47. Frank, P.G., Woodman, S.E., Park, D.S. & Lisanti, M.P. Caveolin, caveolae, and endothelial cell function. *Arteriosclerosis Thrombosis and Vascular Biology* **23**, 1161-1168 (2003).
48. Predescu, S.A., Predescu, D.N. & Malik, A.B. Molecular determinants of endothelial transcytosis and their role in endothelial permeability. *American Journal of Physiology - Lung Cellular and Molecular Physiology* **293**, L823-L842 (2007).
49. Frank, P.G. & Lisanti, M.P. Caveolin-1 and caveolae in atherosclerosis: differential roles in fatty streak formation and neointimal hyperplasia. *Curr Opin Lipidol* **15**, 523-529 (2004).

50. Shelton, S.E. & Kamm, R.D. Chapter 13 - In vitro, primarily microfluidic models for atherosclerosis, in *Biomechanics of Coronary Atherosclerotic Plaque*, Vol. 4. (eds. J. Ohayon, G. Finet & R.I. Pettigrew) 303-319 (Academic Press, 2020).

51. Hajal, C., Ibrahim, L., Serrano, J.C., Offeddu, G.S. & Kamm, R.D. The effects of luminal and trans-endothelial fluid flows on the extravasation and tissue invasion of tumor cells in a 3D in vitro microvascular platform. *bioRxiv*, 2020.2009.2023.309872 (2020).

52. Al-Hilal, T.A. *et al.* Pulmonary-arterial-hypertension (PAH)-on-a-chip: fabrication, validation and application. *Lab on a Chip* **20**, 3334-3345 (2020).

53. Tiruppathi, C., Song, W., Bergenfeldt, M., Sass, P. & Malik, A.B. Gp60 activation mediates albumin transcytosis in endothelial cells by tyrosine kinase-dependent pathway. *J Biol Chem* **272**, 25968-25975 (1997).

54. Tiruppathi, C. *et al.* Albumin mediates the transcytosis of myeloperoxidase by means of caveolae in endothelial cells. *Proceedings of the National Academy of Sciences of the United States of America* **101**, 7699-7704 (2004).

55. Mehta, D. & Malik, A.B. Signaling mechanisms regulating endothelial permeability. *Physiol Rev* **86**, 279-367 (2006).

56. Kraehling, J.R. *et al.* Genome-wide RNAi screen reveals ALK1 mediates LDL uptake and transcytosis in endothelial cells. *Nature Communications* **7**, 13516 (2016).

57. Zhang, X., Sessa, W.C. & Fernández-Hernando, C. Endothelial Transcytosis of Lipoproteins in Atherosclerosis. *Frontiers in Cardiovascular Medicine* **5** (2018).

58. Ghim, M. *et al.* Visualization of three pathways for macromolecule transport across cultured endothelium and their modification by flow. *American Journal of Physiology-Heart and Circulatory Physiology* **313**, H959-H973 (2017).

59. Dubrovskyi, O., Birukova, A.A. & Birukov, K.G. Measurement of local permeability at subcellular level in cell models of agonist- and ventilator-induced lung injury. *Lab Invest* **93**, 254-263 (2013).

60. Ghim, M., Mohamied, Y. & Weinberg, P.D. The Role of Tricellular Junctions in the Transport of Macromolecules Across Endothelium. *Cardiovascular Engineering and Technology* (2020).

61. Claesson-Welsh, L. Vascular permeability—the essentials. *Upsala Journal of Medical Sciences* **120**, 135-143 (2015).

62. Montermini, D., Winlove, C.P. & Michel, C.C. Effects of Perfusion Rate on Permeability of Frog and Rat Mesenteric Microvessels to Sodium Fluorescein. *The Journal of Physiology* **543**, 959-975 (2002).

63. Kajimura, M., Head, S.D. & Michel, C.C. The effects of flow on the transport of potassium ions through the walls of single perfused frog mesenteric capillaries. *The Journal of Physiology* **511**, 707-718 (1998).

64. Curry, F.E. & Clough, G.F. Flow-Dependent Changes in Microvascular Permeability - an Important Adaptive Phenomenon. *The Journal of Physiology* **543**, 729-729 (2002).

65. Adamson, R.H. *et al.* Microvascular permeability to water is independent of shear stress, but dependent on flow direction. *American Journal of Physiology - Heart and Circulatory Physiology* **304**, H1077-H1084 (2013).

66. Williams, D.A. Ramp acceleration and hydraulic conductivity (Lp) of living capillaries. *Microvascular Research* **79**, 114-120 (2010).

67. Berceli, S.A. *et al.* Hemodynamics and low density lipoprotein metabolism. Rates of low density lipoprotein incorporation and degradation along medial and lateral walls of the rabbit aorto-iliac bifurcation. *Arteriosclerosis* **10**, 686-694 (1990).

68. Carew, T.E. & Patel, D.J. Effect of tensile and shear stress on intimal permeability of the left coronary artery in dogs. *Atherosclerosis* **18**, 179-189 (1973).

69. Forster, B.A. & Weinberg, P.D. Evans' blue dye abolishes endothelium-dependent relaxation of rabbit aortic rings. *Atherosclerosis* **129**, 129-131 (1997).

70. Staughton, T.J., Lever, M.J. & Weinberg, P.D. Effect of altered flow on the pattern of permeability around rabbit aortic branches. *Am J Physiol Heart Circ Physiol* **281**, H53-59 (2001).

71. Jo, H., Dull, R.O., Hollis, T.M. & Tarbell, J.M. Endothelial albumin permeability is shear dependent, time dependent, and reversible. *Am J Physiol* **260**, H1992-1996 (1991).

72. Sill, H.W. *et al.* Shear stress increases hydraulic conductivity of cultured endothelial monolayers. *Am J Physiol* **268**, H535-543 (1995).

73. Kang, H., Cancel, L.M. & Tarbell, J.M. Effect of shear stress on water and LDL transport through cultured endothelial cell monolayers. *Atherosclerosis* **233**, 682-690 (2014).

74. Warboys, C.M., Eric Berson, R., Mann, G.E., Pearson, J.D. & Weinberg, P.D. Acute and chronic exposure to shear stress have opposite effects on endothelial permeability to macromolecules. *American Journal of Physiology - Heart and Circulatory Physiology* **298**, H1850-H1856 (2010).

75. Warboys, C.M., Overby, D.R. & Weinberg, P.D. Dendritic Cells Lower the Permeability of Endothelial Monolayers. *Cellular and Molecular Bioengineering* **5**, 184-193 (2012).

76. Tzeghai, G., Ganatos, P., Pfeffer, R., Weinbaum, S. & Nir, A. A theoretical model to study the effect of convection and leaky junctions on macromolecule transport in artery walls. *Journal of Theoretical Biology* **121**, 141-162 (1986).

77. Kopincová, J., Púzserová, A. & Bernátová, I. L-NAME in the cardiovascular system – nitric oxide synthase activator? *Pharmacological Reports* **64**, 511-520 (2012).

78. Pfeiffer, S., Leopold, E., Schmidt, K., Brunner, F. & Mayer, B. Inhibition of nitric oxide synthesis by NG-nitro-L-arginine methyl ester (L-NAME): requirement for bioactivation to the free acid, NG-nitro-L-arginine. *British Journal of Pharmacology* **118**, 1433-1440 (1996).

79. Hinder, F., Booke, M., Traber, L.D. & Traber, D.L. Nitric oxide and endothelial permeability. *Journal of Applied Physiology* **83**, 1941-1946 (1997).

80. Kubes, P. & Granger, D.N. Nitric oxide modulates microvascular permeability. *American Journal of Physiology - Heart and Circulatory Physiology* **262**, H611-H615 (1992).

81. Draijer, R., Atsma, D.E., van der Laarse, A. & van Hinsbergh, V.W.M. cGMP and Nitric Oxide Modulate Thrombin-Induced Endothelial Permeability.

Regulation via Different Pathways in Human Aortic and Umbilical Vein Endothelial Cells **76**, 199-208 (1995).

82. Schubert, W. *et al.* Microvascular Hyperpermeability in Caveolin-1 (−/−) Knock-out Mice: TREATMENT WITH A SPECIFIC NITRIC-OXIDE SYNTHASE INHIBITOR,l-NAME, RESTORES NORMAL MICROVASCULAR PERMEABILITY IN Cav-1 NULL MICE. *Journal of Biological Chemistry* **277**, 40091-40098 (2002).

83. Fukumura, D. *et al.* Predominant role of endothelial nitric oxide synthase in vascular endothelial growth factor-induced angiogenesis and vascular permeability. *Proceedings of the National Academy of Sciences* **98**, 2604-2609 (2001).

84. Yang, B. *et al.* Nitric Oxide Increases Arterial Endotheial Permeability through Mediating VE-Cadherin Expression during Arteriogenesis. *PLOS ONE* **10**, e0127931 (2015).

85. Rabiet, M.-J. *et al.* Thrombin-Induced Increase in Endothelial Permeability Is Associated With Changes in Cell-to-Cell Junction Organization. *Arteriosclerosis, Thrombosis, and Vascular Biology* **16**, 488-496 (1996).

86. Sukriti, S., Tauseef, M., Yazbeck, P. & Mehta, D. Mechanisms regulating endothelial permeability. *Pulmonary Circulation* **4**, 535-551 (2014).

87. Bevan, H.S. *et al.* Acute laminar shear stress reversibly increases human glomerular endothelial cell permeability via activation of endothelial nitric oxide synthase. *American Journal of Physiology - Renal Physiology* **301**, F733-F742 (2011).

88. Tarbell, J.M. Shear stress and the endothelial transport barrier. *Cardiovascular Research* **87**, 320-330 (2010).

89. Cancel, L.M. & Tarbell, J.M. The role of mitosis in LDL transport through cultured endothelial cell monolayers. *American Journal of Physiology - Heart and Circulatory Physiology* **300**, H769-776 (2011).

90. Harmon Lewis, W. Experimental evidence in support of the theory of outgrowth of the axis cylinder. *American Journal of Anatomy* **6**, 461-471 (1906).

91. Storm, M.P. *et al.* Hollow Fiber Bioreactors for In Vivo-like Mammalian Tissue Culture. *Journal of Visualized Experiments : JoVE*, 53431 (2016).

92. Knazek, R.A., Gullino, P.M., Kohler, P.O. & Dedrick, R.L. Cell Culture on Artificial Capillaries: An Approach to Tissue Growth in vitro. *Science* **178**, 65-67 (1972).

93. Eghbali, H., Nava, M.M., Mohebbi-Kalhori, D. & Raimondi, M.T. Hollow fiber bioreactor technology for tissue engineering applications. *The International Journal of Artificial Organs* **39**, 1-15 (2016).

94. Ott, M.J. & Ballermann, B.J. Shear stress-conditioned, endothelial cell-seeded vascular grafts: Improved cell adherence in response to in vitro shear stress. *Surgery* **117**, 334-339 (1995).

95. Westmuckett, A.D. *et al.* Fluid Flow Induces Upregulation of Synthesis and Release of Tissue Factor Pathway Inhibitor In Vitro. *Arteriosclerosis, Thrombosis, and Vascular Biology* **20**, 2474-2482 (2000).

96. Ott, M.J., Olson, J.L. & Ballermann, B.J. Chronic In Vitro Flow Promotes Ultrastructural Differentiation of Endothelial Cells. *Endothelium* **3**, 21-30 (1995).

97. O, S.K.A.N.F.S.T.J.G.G.A.E.A.M.D. A new model of the blood--brain barrier: co-culture of neuronal, endothelial and glial cells under dynamic conditions. *Neuroreport* **10**, 3725-3731 (1999).

98. Neuhaus, W. *et al.* A novel flow based hollow-fiber blood–brain barrier in vitro model with immortalised cell line PBMEC/C1–2. *Journal of Biotechnology* **125**, 127-141 (2006).

99. Salvetti, F. *et al.* Insulin Permeability Across an in Vitro Dynamic Model of Endothelium. *Pharmaceutical Research* **19**, 445-450 (2002).

100. Milton, S.G. & Knutson, V.P. Comparison of the function of the tight junctions of endothelial cells and epithelial cells in regulating the movement of electrolytes and macromolecules across the cell monolayer. *Journal of Cellular Physiology* **144**, 498-504 (1990).

101. Oliver, J.A. Endothelium-derived relaxing factor contributes to the regulation of endothelial permeability. *Journal of Cellular Physiology* **151**, 506-511 (1992).

102. Milovanova, T. *et al.* Endothelial Cell Proliferation Associated with Abrupt Reduction in Shear Stress Is Dependent on Reactive Oxygen Species. *Antioxidants & Redox Signaling* **6**, 245-258 (2004).

103. Walsby, E. *et al.* Development and characterization of a physiologically relevant model of lymphocyte migration in chronic lymphocytic leukemia. *Blood* **123**, 3607-3617 (2014).

104. Bogle, R.G., Baydoun, A.R., Pearson, J.D. & Mann, G.E. Regulation of L-arginine transport and nitric oxide release in superfused porcine aortic endothelial cells. *The Journal of Physiology* **490**, 229-241 (1996).

105. Baker, S.M., Kim, N., Gumpert, A.M., Segretain, D. & Falk, M.M. Acute internalization of gap junctions in vascular endothelial cells in response to inflammatory mediator-induced G-protein coupled receptor activation. *FEBS letters* **582**, 4039-4046 (2008).

106. Levin, E.G., Marzec, U., Anderson, J. & Harker, L.A. Thrombin stimulates tissue plasminogen activator release from cultured human endothelial cells. *Journal of Clinical Investigation* **74**, 1988-1995 (1984).

107. Suttorp, N. *et al.* Bacterial exotoxins and endothelial permeability for water and albumin in vitro. *American Journal of Physiology - Cell Physiology* **255**, C368-C376 (1988).

108. Bowman, P.D., Ennis, S.R., Rarey, K.E., Lorris Betz, A. & Goldstein, G.W. Brain microvessel endothelial cells in tissue culture: A model for study of blood-brain barrier permeability. *Annals of Neurology* **14**, 396-402 (1983).

109. S. M. Albelda, P.M.S., F. R. Haselton Permeability characteristics of cultured endothelial cell monolayers. *Journal of Applied Physiology* **64**, 308-322 (1988).

110. Chang, Y.S. *et al.* Effect of Vascular Endothelial Growth Factor on Cultured Endothelial Cell Monolayer Transport Properties. *Microvascular Research* **59**, 265-277 (2000).

111. DeMaio, L., Antonetti, D.A., Scaduto, R.C., Gardner, T.W. & Tarbell, J.M. VEGF increases paracellular transport without altering the solvent-drag reflection coefficient. *Microvascular Research* **68**, 295-302 (2004).

112. Nan, Y.-S. *et al.* Neuropeptide Y enhances permeability across a rat aortic endothelial cell monolayer. *American Journal of Physiology-Heart and Circulatory Physiology* **286**, H1027-H1033 (2004).

113. Sebkhi, A. & Weinberg, P.D. Effect of Age on the Pattern of Short-term Albumin Uptake by the Rabbit Aortic Wall Near Intercostal Branch Ostia. *Arteriosclerosis, Thrombosis, and Vascular Biology* **16**, 317-327 (1996).

114. Tedgui, A. & Lever, M.J. Filtration through damaged and undamaged rabbit thoracic aorta. *American Journal of Physiology-Heart and Circulatory Physiology* **247**, H784-H791 (1984).

115. Turner, M.R. Flows of liquid and electrical current through monolayers of cultured bovine arterial endothelium. *The Journal of Physiology* **449**, 1-20 (1992).

116. Dull, R.O., Jo, H., Sill, H., Hollis, T.M. & Tarbell, J.M. The effect of varying albumin concentration and hydrostatic pressure on hydraulic conductivity and albumin permeability of cultured endothelial monolayers. *Microvascular Research* **41**, 390-407 (1991).

117. Kim, M.-h., Harris, N.R. & Tarbell, J.M. Regulation of hydraulic conductivity in response to sustained changes in pressure. *American Journal of Physiology - Heart and Circulatory Physiology* **289**, H2551-H2558 (2005).

118. Zhang, Y. *et al.* In vitro study of directly bioprinted perfusable vasculature conduits. *Biomaterials Science* **3**, 134-143 (2015).

119. Datta, P., Ayan, B. & Ozbolat, I.T. Bioprinting for vascular and vascularized tissue biofabrication. *Acta Biomaterialia* **51**, 1-20 (2017).

120. Li, Y.-S.J., Haga, J.H. & Chien, S. Molecular basis of the effects of shear stress on vascular endothelial cells. *Journal of Biomechanics* **38**, 1949-1971 (2005).

121. Olesen, S.-P., Claphamt, D. & Davies, P. Haemodynamic shear stress activates a K+ current in vascular endothelial cells. *Nature* **331**, 168-170 (1988).

122. Helmlinger, G., Berk, B.C. & Nerem, R.M. Pulsatile and Steady Flow-Induced Calcium Oscillations in Single Cultured Endothelial Cells. *Journal of Vascular Research* **33**, 360-369 (1996).

123. Di Lorenzo, A. *et al.* eNOS-derived nitric oxide regulates endothelial barrier function through VE-cadherin and Rho GTPases. *Journal of Cell Science* **126**, 5541-5552 (2013).

124. Privratsky, J.R. & Newman, P.J. PECAM-1: regulator of endothelial junctional integrity. *Cell and Tissue Research* **355**, 607-619 (2014).

125. Ando, J., Ohtsuka, A., Korenaga, R., Kawamura, T. & Kamiya, A. Wall Shear Stress Rather Than Shear Rate Regulates Cytoplasmic Ca++ Responses to Flow in Vascular Endothelial Cells. *Biochemical and Biophysical Research Communications* **190**, 716-723 (1993).

126. DeMaio, L., Tarbell, J.M., Scaduto, R.C., Gardner, T.W. & Antonetti, D.A. A transmural pressure gradient induces mechanical and biological adaptive responses in endothelial cells. *American Journal of Physiology - Heart and Circulatory Physiology* **286**, H731-H741 (2004).

127. Armstrong, S.M. *et al.* Co-Regulation of Transcellular and Paracellular Leak Across Microvascular Endothelium by Dynamin and Rac. *The American Journal of Pathology* **180**, 1308-1323 (2012).

128. Schnitzer, J.E. & Oh, P. Albondin-mediated capillary permeability to albumin. Differential role of receptors in endothelial transcytosis and endocytosis of native and modified albumins. *Journal of Biological Chemistry* **269**, 6072-6082 (1994).

129. Schubert, W. *et al.* Microvascular hyperpermeability in caveolin-1 (-/-) knock-out mice. Treatment with a specific nitric-oxide synthase inhibitor, L-NAME, restores normal microvascular permeability in Cav-1 null mice. *J Biol Chem* **277**, 40091-40098 (2002).

130. Rosengren, B.-I. *et al.* Transvascular protein transport in mice lacking endothelial caveolae. *American Journal of Physiology - Heart and Circulatory Physiology* **291**, H1371-H1377 (2006).

131. Zou, Y. & Zhang, Y. Mechanical Evaluation of Decellularized Porcine Thoracic Aorta. *Journal of Surgical Research* **175**, 359-368.

132. Bouten, C.V.C. *et al.* Substrates for cardiovascular tissue engineering. *Advanced Drug Delivery Reviews* **63**, 221-241 (2011).

133. Uchimura, E. *et al.* Novel method of preparing acellular cardiovascular grafts by decellularization with poly(ethylene glycol). *Journal of Biomedical Materials Research Part A* **67A**, 834-837 (2003).

134. Narita, Y. *et al.* Decellularized ureter for tissue-engineered small-caliber vascular graft. *Journal of Artificial Organs* **11**, 91-99 (2008).

135. Martin, N.D. *et al.* In Vivo Behavior of Decellularized Vein Allograft[1,2]. *Journal of Surgical Research* **129**, 17-23.

136. Dong, J.-D., Huang, J.-H., Gao, F., Zhu, Z.-H. & Zhang, J. Mesenchymal stem cell-based tissue engineering of small-diameter blood vessels. *Vascular* **19**, 206-213 (2011).

137. Gilbert, T.W., Sellaro, T.L. & Badylak, S.F. Decellularization of tissues and organs. *Biomaterials* **27**, 3675-3683 (2006).

138. Allaire, E., Bruneval, P., Mandet, C., Becquemin, J.-P. & Michel, J.-B. The immunogenicity of the extracellular matrix in arterial xenografts. *Surgery* **122**, 73-81 (1997).

139. Henderson, P.W. *et al.* Development of an Acellular Bioengineered Matrix with a Dominant Vascular Pedicle1. *Journal of Surgical Research* **164**, 1-5 (2010).

140. Böer, U. *et al.* The effect of detergent-based decellularization procedures on cellular proteins and immunogenicity in equine carotid artery grafts. *Biomaterials* **32**, 9730-9737 (2011).

141. Lehr, E.J. *et al.* Decellularization reduces immunogenicity of sheep pulmonary artery vascular patches. *The Journal of Thoracic and Cardiovascular Surgery* **141**, 1056-1062 (2011).

142. Negishi, J. *et al.* Effect of treatment temperature on collagen structures of the decellularized carotid artery using high hydrostatic pressure. *Journal of Artificial Organs* **14**, 223-231 (2011).

143. McClure, M.J., Sell, S.A., Ayres, C.E., Simpson, D.G. & Bowlin, G.L. Electrospinning-aligned and random polydioxanone–polycaprolactone–silk fibroin-blended scaffolds: geometry for a vascular matrix. *Biomedical Materials* **4**, 055010 (2009).

144. Ayres, C. *et al.* Modulation of anisotropy in electrospun tissue-engineering scaffolds: Analysis of fiber alignment by the fast Fourier transform. *Biomaterials* **27**, 5524-5534 (2006).

145. Buttafoco, L. *et al.* Electrospinning of collagen and elastin for tissue engineering applications. *Biomaterials* **27**, 724-734 (2006).

146. Daamen, W.F., Veerkamp, J.H., van Hest, J.C.M. & van Kuppevelt, T.H. Elastin as a biomaterial for tissue engineering. *Biomaterials* **28**, 4378-4398 (2007).

147. Del Gaudio, C., Bianco, A., Folin, M., Baiguera, S. & Grigioni, M. Structural characterization and cell response evaluation of electrospun PCL membranes: Micrometric versus submicrometric fibers. *Journal of Biomedical Materials Research Part A* **89A**, 1028-1039 (2009).

148. Zhang, Y., Ouyang, H., Lim, C.T., Ramakrishna, S. & Huang, Z.-M. Electrospinning of gelatin fibers and gelatin/PCL composite fibrous scaffolds. *Journal of Biomedical Materials Research Part B: Applied Biomaterials* **72B**, 156-165 (2005).

149. Katsogiannis, K.A.G., Vladisavljević, G.T. & Georgiadou, S. Porous electrospun polycaprolactone (PCL) fibres by phase separation. *European Polymer Journal* **69**, 284-295 (2015).

150. RepRap https://reprap.org/wiki/RepRap. (2005).

151. Markets, M.a. 3D bioprinting market. *https://www.marketsandmarkets.com/Market-Reports/3d-bioprinting-market-170201787.html?gclid=EAIaIQobChMI36K8lpf_6QIVSsKyCh2GiQPTEAAYASAAEgKZSvD_BwE* (2019).

152. Horne, R. Universal Paste Extruder. *https://www.youtube.com/watch?v=Moiyvq8P2Vs* (2012).

153. Horne, R. 3D printing designs. *https://www.youmagine.com/richrap/designs https://www.youtube.com/channel/UCvGQ-pMFD1C5HShRin8RVDA?feature=emb_ch_name_ex* (2013).

154. Townsend-Nicholson, A. & Jayasinghe, S.N. Cell electrospinning: a unique biotechnique for encapsulating living organisms for generating active biological microthreads/scaffolds. *Biomacromolecules* **7**, 3364-3369 (2006).

155. Jayasinghe, S.N., Qureshi, A.N. & Eagles, P.A. Electrohydrodynamic jet processing: an advanced electric-field-driven jetting phenomenon for processing living cells. *Small* **2**, 216-219 (2006).

156. Sampson, S.L., Saraiva, L., Gustafsson, K., Jayasinghe, S.N. & Robertson, B.D. Cell electrospinning: an in vitro and in vivo study. *Small* **10**, 78-82 (2014).

157. Miller, J.S. *et al.* Rapid casting of patterned vascular networks for perfusable engineered three-dimensional tissues. *Nat Mater* **11**, 768-774 (2012).

158. Townsend-Nicholson, A. & Jayasinghe, S.N. Cell Electrospinning: a Unique Biotechnique for Encapsulating Living Organisms for Generating Active Biological Microthreads/Scaffolds. *Biomacromolecules* **7**, 3364-3369 (2006).

159. Industry, D.P. Ourobotics Low Cost 3D bioprinter does 10 materials and more. *https://3dprintingindustry.com/news/jemma-redmonds-ourobotics-low-cost-3d-bioprinter-does-10-materials-and-more-63237/* (2015).

160. Magazine, D.P.I. Ourobotics releases fully open source renegade bioprinter built for 900. *https://3dprintingindustry.com/news/ourobotics-releases-fully-open-source-renegade-bioprinter-built-for-900-66271/* (2016).

161. Industry, D.P. Top 3D Bioprinters of 2015. *https://3dprintingindustry.com/news/top-10-bioprinters-55699/* (2015).

162. Christensen, C.M. The Innovator's Dilemma: When New Technologies Cause Great Firms to Fail. *Harvard Business Press* **https://www.hbs.edu/faculty/Pages/item.aspx?num=46** (1997).

163. Maureen McKelvey (Author, E., Astrid Heidemann Lassen (Author, Editor) How Entrepreneurs Do What They Do: Case Studies in Knowledge Intensive Entrepreneurship. *https://www.amazon.com/How-Entrepreneurs-What-They-Entrepreneurship/dp/1781005494* (2013).

164. Guardian Jemma Redmond. *https://www.theguardian.com/technology/2016/sep/20/jemma-redmond-obituary* (2016).

165. Choudhury, D., Anand, S. & Naing, M.W. The Arrival of Commercial Bioprinters - Towards 3D Bioprinting Revolution! *2018* **4** (2018).

166. Li, H., Tan, C. & Li, L. Review of 3D printable hydrogels and constructs. *Materials & Design* **159**, 20-38 (2018).

167. DOINA DRĂGĂNESCU 1, D.L., GEORGE TRAIAN ALEXANDRU BURCEA DRAGOMIROIU 3, ADRIAN COSMIN ROŞCA 4, LUCIAN HÎNCU 5*, DANIELA CIOACĂ 3D PRINTING PHARMACEUTICAL FORMULATION OF DRUGS IN PERSONALIZED THERAPY. *Official Journal of Romanian Society for Pharmaceutical Sciences* (2019).

168. Stratton, S. *et al.* Polymeric 3D printed structures for soft-tissue engineering. *Journal of Applied Polymer Science* **135**, 45569 (2018).

169. Hölzl, K. *et al.* Bioink properties before, during and after 3D bioprinting. *Biofabrication* **8**, 032002 (2016).

170. Gill, A.S., Deol, P.K. & Kaur, I.P. An Update on the Use of Alginate in Additive Biofabrication Techniques. *Curr Pharm Des* **25**, 1249-1264 (2019).

171. Dynamix, R. in https://www.researchdynamix.org/ (2012).